ADA053252

AFML-TR-77-101

TITANIUM DAMAGE TOLERANT DESIGN DATA FOR PROPULSION SYSTEMS

James R. Beyer
David L. Sims
Raymond M. Wallace
United Technologies Corporation
Pratt & Whitney Aircraft Group
Government Products Division
West Palm Beach, Florida 33402

20080815 258

June 1977
Final Report for Period 1 June 1975 Through 30 April 1977

Prepared for:
Air Force Materials Laboratory
Air Force Systems Command
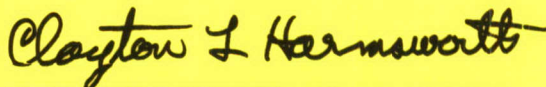Wright-Patterson Air Force Base, Ohio 45433

NOTICE

When Government drawings, specifications, or other data are used for any purpose other than in connection with a definitely related Government procurement operation, the United States Government thereby incurs no responsibility nor any obligation whatsoever; and the fact that the Government may have formulated, furnished, or in any way supplied the said drawings, specifications, or other data, is not to be regarded by implication or otherwise as in any manner licensing the holder or any other person or corporation, or conveying any rights or permission to manufacture, use, or sell any patented invention that may in any way be related thereto.

This report has been reviewed by the Information Office (IO) and is releasable to the National Technical Information Service (NTIS). At NTIS, it will be releasable to the general public, including foreign nations.

This technical report has been reviewed and is approved for publication.
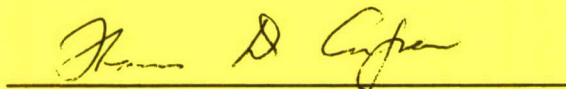
Allan W. Gunderson
Engineering & Design Data
Materials Integrity Branch

Clayton L. Harmsworth
Technical Manager
Engineering and Design Data
Materials Integrity Branch

FOR THE COMMANDER

Thomas D. Cooper
Chief, Materials Integrity Branch
Systems Support Division

Copies of this report should not be returned unless return is required by security considerations, contractual obligations, or notice on a specific document.

REPORT DOCUMENTATION PAGE		READ INSTRUCTIONS BEFORE COMPLETING FORM
1. REPORT NUMBER AFML-TR-77-101	2. GOVT ACCESSION NO.	3. RECIPIENT'S CATALOG NUMBER
4. TITLE (and Subtitle) TITANIUM DAMAGE TOLERANT DESIGN DATA FOR PROPULSION SYSTEMS		5. TYPE OF REPORT & PERIOD COVERED Final 1 June 75 through 30 April 77
		6. PERFORMING ORG. REPORT NUMBER FR-8480
7. AUTHOR(s) James R. Beyer, David L. Sims, Raymond M. Wallace		8. CONTRACT OR GRANT NUMBER(s) F33615-75-C-5130
9. PERFORMING ORGANIZATION NAME AND ADDRESS Pratt & Whitney Aircraft Group Government Products Division West Palm Beach, Florida 33402		10. PROGRAM ELEMENT, PROJECT, TASK AREA & WORK UNIT NUMBERS
11. CONTROLLING OFFICE NAME AND ADDRESS Air Force Materials Laboratory Air Force Systems Command Wright-Patterson Air Force Base, Ohio 45433		12. REPORT DATE August 1977
		13. NUMBER OF PAGES 91
14. MONITORING AGENCY NAME & ADDRESS(if different from Controlling Office)		15. SECURITY CLASS. (of this report) Unclassified
		15a. DECLASSIFICATION/DOWNGRADING SCHEDULE

16. DISTRIBUTION STATEMENT (of this Report)

Approved for public release, distribution unlimited

17. DISTRIBUTION STATEMENT (of the abstract entered in Block 20, if different from Report)

18. SUPPLEMENTARY NOTES

19. KEY WORDS (Continue on reverse side if necessary and identify by block number)

Fracture Mechanics,
Titanium,
Ti 8-1-1,
Ti 6-2-4-2,
Ti 6-2-4-6,
Crack Propagation
Low Cycle Fatigue
Hyperbolic Sine Model

20. ABSTRACT (Continue on reverse side if necessary and identify by block number)

Fracture mechanics design properties have been determined under Air Force Materials Laboratory Contract, F33615-75-C-5130, for three titanium alloys, Ti 8-1-1, Ti 6-2-4-2, and Ti 6-2-4-6. The program consisted of crack growth threshold, crack growth rate, and fracture toughness testing for each alloy plus strain controlled low cycle fatigue crack initiation testing on Ti 8-1-1. The effects of stress ratio, cyclic frequency, and temperature were determined, providing a broad data base for damage tolerant design of titanium gas turbine engine components.

PREFACE

CONTENTS

ILLUSTRATIONS

ILLUSTRATIONS (Continued)

ILLUSTRATIONS (Continued)

ILLUSTRATIONS (Continued)

TABLES

SUMMARY

This report describes work conducted under Contract F33615-75-C-5130, an Air Force Materials Laboratory program to determine the fracture mechanics design properties for three titanium alloys, Ti 6-2-4-6, Ti 6-2-4-2, and Ti 8-1-1. The material testing and evaluation was accomplished in five broad areas:

1. Basic tensile property characterization was completed.

2. Stress intensity thresholds were determined.

3. The effects of temperature, stress ratio, and frequency on fatigue crack propagation were established.

4. Critical stress intensities (fracture toughnesses) were measured for three specimen thicknesses for each alloy.

5. Crack initiation on Ti 8-1-1 was studied under strain-controlled conditions.

This program provides data which can be used in an integrated methodology for damage tolerant design of titanium gas turbine engine components.

SECTION I

INTRODUCTION

Damage tolerant design is accomplished through the use of fracture mechanics analysis of component life by predicting crack propagation from an initial, inspectable flaw size to a critical crack length. This program provides data useable in an integrated methodology for the design of titanium gas turbine engine components commonly life limited by thermal and mechanical fatigue.

Three advanced titanium alloys, Ti 6Al-2Sn-4Zr-6Mo, Ti 8Al-1Mo-1V, and Ti 6Al-2Sn-4Zr-2Mo (Ti 6-2-4-6, Ti 8-1-1, and Ti 6-2-4-2, respectively) were tested at room temperature and two elevated temperatures to provide fracture mechanics data. Stress intensity thresholds and slow crack growth rates were determined for positive stress ratios (R) in Region I (da/dn $<10^{-6}$ inch/cycle). In Region II (da/dn $>10^{-6}$ inch/cycle) the effects of frequency and positive and negative stress ratios were determined. Region III fracture toughness testing included three specimen thicknesses. Low-cycle fatigue crack initiation time under constant cyclic strain was determined for the Ti 8-1-1 alloy at two elevated temperatures under two different test cycles. Life curves relating strain range, mean strain, and stabilized mean stress have been constructed for strain ratios of zero, -1, and $-\infty$.

The materials forgings were microstructurally characterized and tensile and creep properties measured.

1

SECTION II

MATERIALS

The three alloys being tested in this program were Ti 6Al-2Sn-4Zr-6Mo (Ti 6-2-4-6), Ti 8Al-1Mo-1V (Ti 8-1-1), and Ti 6Al-2Sn-4Zr-2Mo (Ti 6-2-4-2). The forgings were heat treated to the following specifications:

Alloy	*Nominal Heat Treatment*
Ti 8-1-1	1830°F/1 hr, Water Quench + 1100°F/8 hr, Air Cool
Ti 6-2-4-2	($\beta^* - 25°F$)/1 hr, Air Cool + 1100°F/8 hr, Air Cool
Ti 6-2-4-6	1690°F/2 hr, Air Cool + 1550°F/2 hr, Oil Quench + 1100°F/8 hr, Air Cool

*Beta Transus Temperature

The selection of a heat treatment entails a balancing of properties to meet the particular requirements of a gas turbine component. Pratt & Whitney Aircraft Group selected heat treatments which produce a set of properties it believes results in optimum use of these alloys. However, the materials also can be used in other heat-treat conditions.

The Ti 8-1-1 alloy is classified as a "near alpha" or alpha-rich titanium alloy which is heat treatable for moderate tensile and creep strength in the 500 to 900°F range. In addition, its low density (0.158 lb/in.^{3}) relatively high modulus (17×10^6 psi) combine to give it an exceptionally high specific modulus compared to other alloys. These features make it most attractive for stiffness limited components at lower temperatures. Currently, this alloy is extensively used in military gas turbine compressor disks, blades, and vanes.

Normal heat treatment for Ti 8-1-1 consists of a duplex cycle with a solution anneal within the range of 1625 to 1875°F (1 hour) followed by air cooling or quenching. The precipitation (aging) treatment consists of an 1100°F (8 hour) air cool cycle. Solution treating at the higher end of the range of 1775 to 1875°F, generally enhances elevated temperature tensile strength, creep capability, and notched toughness properties with only a slight decrease in room temperature tensile ductility. Data reveal that material with a higher primary alpha content resulting from relatively low solution temperature has improved low temperature properties with decreased toughness. Therefore, the higher solution temperature has the net result of producing the best balance of properties for gas turbine application.

The heat treatment used in this program for Ti 8-1-1 yields a microstructure of 40 to 50 percent primary equiaxed alpha phase in a transformed beta matrix as shown in Figure 1. In the lower magnification photomicrograph a slight amount of elongated alpha phase can be observed.

The Ti 6-2-4-2 alloy is, like Ti 8-1-1, a near alpha alloy which was heat treated to produce a good combination of high creep and tensile strengths in the 800 to 1000°F range. This alloy is superior in creep strength to Ti 8-1-1 and Ti 6-2-4-6 above 900°F and has excellent metallurgical and surface stability up to approximately 1050°F depending on length of service. Current military applications include high compressor disks and blades.

The heat treatment used in this program for the Ti 6-2-4-2 alloy is one chosen for a good combination of creep and low-cycle fatigue strength, as well as creep strength stability. It produces a microstructure of 20 to 40 percent primary equiaxed alpha phase in a transformed beta platelet matrix as shown in Figure 2. The prior beta grain size is generally comparable to the Ti 8-1-1 alloy.
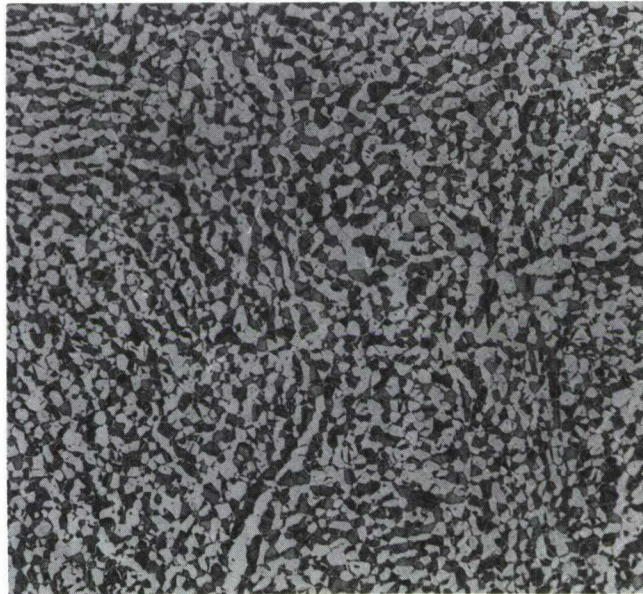
Mag: 100X
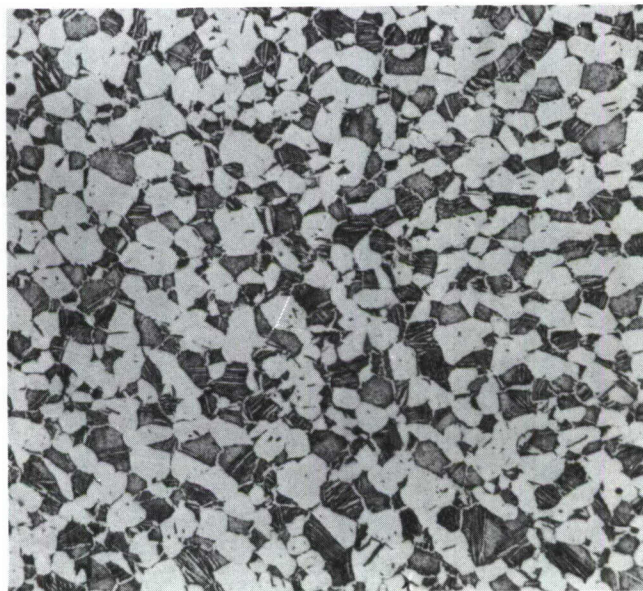
Mag: 250X

FD 121057

Figure 1. Microstructure of Ti 8-1-1 Alloy Forging LYSJ-8438, Krolls Etch

3
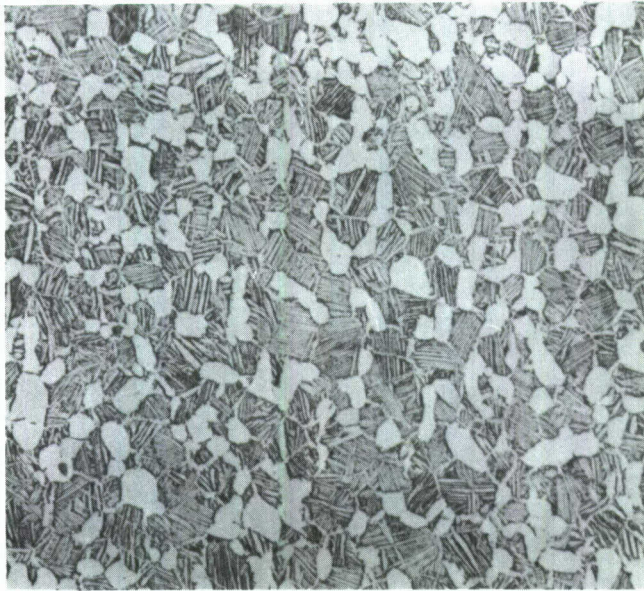
Mag: 250X

a Forging LWDD-2001 Rim Region
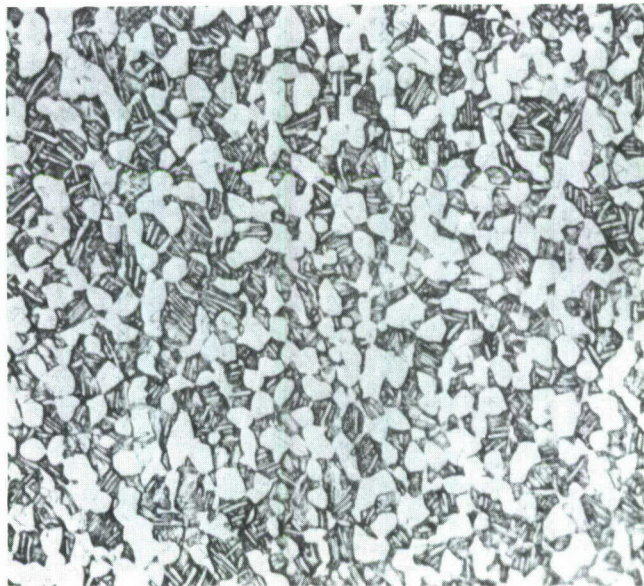
Mag: 250X

b Forging LWCC-2003 Rim Region

FD 121058

Figure 2. Microstructure of Ti 6-2-4-2 Alloy Forging, Krolls Etch

The Ti 6-2-4-6 alloy is a high strength heat treatable alpha-beta alloy which exhibits high tensile and creep strength up to 800°F with good fatigue properties. The alloy is currently used in military engine compressor disks and blades.

The Ti-6-2-4-6 alloy is a solid solution and precipitation strengthened alloy which strongly responds to heat treatment due to the beta stabilizing effect of 6 percent molybdenum. The beta stabilizers are isomorphous and do not induce precipitation of brittle phases as a result of conventional heat treatments. However, the alloy can exhibit wide ranging strengths, ductilities and fracture toughness depending upon heat treatment. Solution temperature and the cooling rate from high solution heat-treatment temperature appear to be especially critical in relation to plane-strain fracture toughness and tensile properties. These characteristics indicate the alloy is more sensitive to microstructural variations caused by heat treatment than the lower strength Ti 8-1-1 and Ti 6-2-4-2 alloys. Consequently, different heat treatment specifications and resultant microstructures are used depending on the particular application. The heat treatment evaluated in this program produces exceptionally high tensile and fatigue strength which is used in production Air Force engines.

The heat treatment utilized in this program was chosen to produce a good high temperature tensile yield and creep strengths, along with acceptable fracture toughness. Representative microstructures in the test forging (Figure 3) consist of approximately 10 to 20 percent primary alpha with secondary acicular alpha resulting from the 1550°F cycle. The morphology of the secondary alpha has been found to correlate with toughness change. It should be noted that the Ti 6-2-4-6 alloy microstructure is somewhat finer than the other two alloys.

The following fully heat treated forgings were utilized for test material.

Alloy	Forging Designation (Heat Code)	OD (inch)	Thickness (inch)
Ti 8-1-1	LULS, LYSJ, LZDH, LZBF	24	1.0
Ti 6-2-4-2	LWDD, LWCC	24	2.0
Ti 6-2-4-6	LYKD	22	2.8
	LYNC	24	1.8

Each forging was from a different heat code and therefore is identified by that designation only. Test specimens were identified by inclusion of the forging/heat code letters from which they were obtained.

The forgings were found to conform to production requirements by measuring mechanical properties, chemistry, and microstructure. These data are presented in Tables 1 through 4.

For each alloy and temperature at which crack growth data were obtained, a tensile test was conducted. The tensile test specimens were cylindrical round specimens (Figure 4) with extensometer ridges. These were tested at a strain rate of 0.005 inches per inch per minute. Stress-strain curves, reduction in area, yield strength, ultimate strength, and modulus of elasticity were determined. Figure 5 shows the 0.2 percent offset yield strength, Figure 6 shows the tensile elongation, and Figure 7 shows the modulus of elasticity as a function of temperature for each alloy. The Ti 6-2-4-6 alloy has the highest yield strength, lowest ductility, and an average modulus for the three alloys being investigated. The Ti 6-2-4-2 alloy has the highest ductility, lowest yield strength and lowest modulus of these alloys. The Ti 8-1-1 alloy has the highest modulus, yield strength about the same as Ti 6-2-4-2, and ductility slightly higher than Ti 6-2-4-6 alloy.

Table 5 gives a summary of the tensile test data for each alloy at those temperatures for which crack propagation tests were conducted. The data given in Tables 1 through 4 was for qualification of the selected heat codes of each alloy and does not appear on the above mentioned figures.
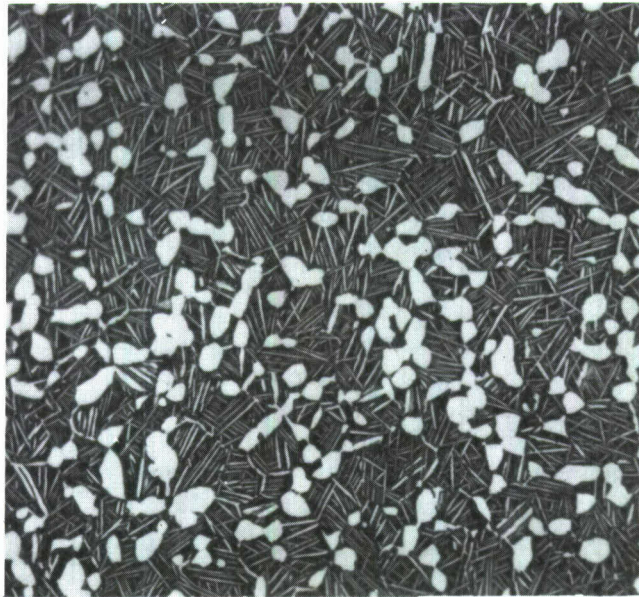
Mag: 500X

a Outer Rim Region
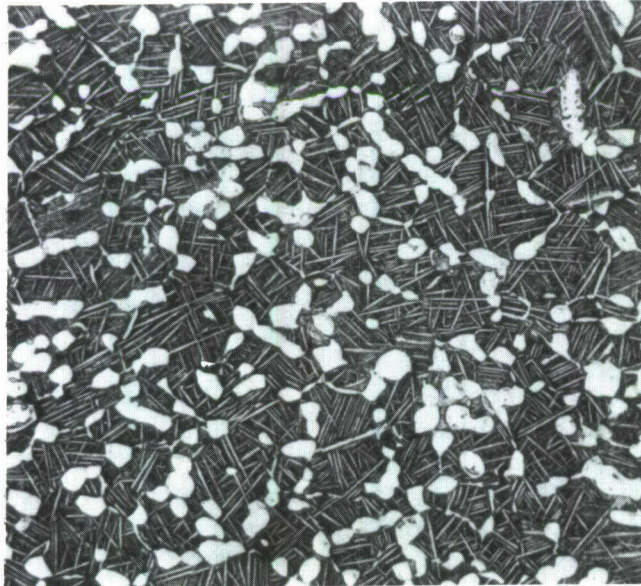
Mag: 500X

b Inner Bore or Hub Region

FD 121059

Figure 3. Microstructure of Ti 6-2-4-6 Alloy Forging
LYKD-2019, Krolls Etch

6

TABLE 1. QUALIFICATION DATA FOR Ti 8-1-1 ALLOY FORGINGS

Tensile

Heat Code	Temperature (°F)	YS (ksi)	UTS (ksi)	EL (%)	RA (%)
LYSJ	70	149	161	15	38
		146	158	15	42
		136	149	18	42
		137	150	13	28
	800	92	113	17	48
		89	112	19	55
		79	105	20	51
		81	103	16	47
LULS	70	151	165	16	40
		150	163	10	41
		140	154	20	39
		142	155	16	37
	800	93	119	16	52
		91	115	12	50
		90	117	18	51
		87	111	18	51
LZDH	70	141	154	14	33
		137	149	14	42
		134	149	16	42
		130	142	13	42
	800	82	106	20	61
		78	102	18	49
		77	102	20	49
		77	102	20	48
LZBF	70	145	160	16	46
		140	155	18	49
		132	150	16	46
		133	148	18	44
	800	82	105	20	60
		82	105	19	59
		72	102	20	50
		80	104	20	53

Note: Materials control data obtained in qualifying this alloy

V-Notch Stress Rupture

Heat Code	Temperature (°F)	Stress (ksi)	Time (hr)	Fracture Observed
LYSJ	70	150	5.0	None
			5.0	None
			5.0	None
LULS	70	150	5.2	None
			5.2	None
			5.2	None
LZDH	70	150	5.1	None
			5.0	None
			5.1	None
LZBF	70	150	5.0	None
			5.1	None
			5.1	None

Creep Elongation

Heat Code	Temperature (°F)	Stress (ksi)	Time (hr)	Creep (%)
LYSJ	850	40	23	0.07
			23	0.06
LULS	850	40	23	0.03
			23	0.04
LZDH	850	40	23	0.04
			23	0.06
LZBF	850	40	23	0.05
			23	0.05

Note: Materials control data obtained in qualifying this alloy.

7

TABLE 2. QUALIFICATION DATA FOR Ti 6-2-4-6 ALLOY FORGINGS

Tensile

Heat Code	Temperature (°F)	YS (ksi)	UTS (ksi)	EL (%)	RA (%)
LYKD	70	164	180	13	30
		161	177	10	28
		168	184	14	34
		171	188	12	19
	400	129	156	14	40
		128	154	14	36
		135	162	14	40
		134	161	14	42
LUNC	70	165	180	12	28
		158	173	11	30
		161	176	14	28
		167	183	12	31
		168	184	11	29
		174	189	12	32
	400	128	157	16	39
		132	162	14	44
		131	158	16	45
		132	160	15	43
		133	162	15	44
		128	157	16	52

V-Notch Stress Rupture

Heat Code	Temperature (°F)	Stress (ksi)	Time (hr)	Fracture Observed
LYKD	70	190	5.0	None
			5.0	None
LUNC	70	190	5.0	None
			5.5	None

Note: Materials control data obtained in qualifying this alloy.

TABLE 3. QUALIFICATION DATA FOR Ti 6-2-4-2 ALLOY FORGINGS

Tensile

Heat Code	Temperature (°F)	YS (ksi)	UTS (ksi)	EL (%)	RA (%)
LWDD	70	147	161	14	35
		138	150	13	38
		142	152	15	33
		140	151	14	37
		137	151	13	35
		136	145	15	36
		136	151	15	39
	900	84	111	16	46
		80	103	18	50
		84	107	18	43
		80	105	18	50
		82	105	18	46
		79	104	18	48
		79	101	18	50
LWCC	70	144	153	14	32
		137	149	14	38
		138	148	14	34
		153	163	14	46
		136	149	14	34
		138	150	14	36
		140	154	15	40
	900	81	107	19	47
		78	102	20	56
		80	103	18	50
		81	107	20	58
		80	102	19	51
		80	104	19	51

Note: Materials control data obtained in qualifying this alloy

V-Notch Stress Rupture

Heat Code	Temperature (°F)	Stress (ksi)	Time (hr)	Fracture Observed
LWDD	70	170	5.0	None
			5.0	None
			5.0	None
LWCC	70	170	5.0	None
			5.0	None
			5.0	None

Creep

Heat Code	Temperature (°F)	Stress (ksi)	Time (hr)	Creep (%)
LWDD	950	35	35	0.08
			35	0.10
			35	0.06
LWCC	950	35	35	0.08
			23	0.10
			35	0.05

Note: Material control data obtained in qualifying this alloy

TABLE 4. COMPOSITION OF ALLOYS UTILIZED IN PROGRAM

Composition-Weight %

Heat Code	Ti	C	Si	N	B	O	Mo	V	Sn	Al	Fe	Cu	Zr	H
Ti 8-1-1														
LYSJ	Bal	0.01	-	0.02	-	0.08	1.05	1.10	0.01	8.09	0.14	<0.01		0.006
LULS	Bal	0.01	-	0.01	-	0.07	1.05	0.98	<0.01	8.12	0.09	<0.01		0.006
LZDH	Bal	0.01	<0.01	0.01	<0.001	0.07	1.20	0.97	<0.01	7.94	0.06	<0.01		0.007
LZBF	Bal	0.01	<0.01	0.01	<0.001	0.07	1.21	0.96	<0.01	7.92	0.06	<0.01		0.006
Ti 6-2-4-6														
LYKD	Bal	0.01	-	0.01	<0.001	0.09	5.64		2.06	6.34	0.09		3.92	0.0068
LUNC	Bal	0.01	0.01	0.01		0.08	5.77		2.01	6.22	0.10		3.90	0.0076
Ti 6-2-4-2														
LWDD	Bal	0.008		0.01		0.08	1.94		2.0	6.14	0.17		4.21	0.0066
LWCC	Bal	0.010		0.01		0.08	1.89		2.12	6.12	0.10		4.24	0.0057

10
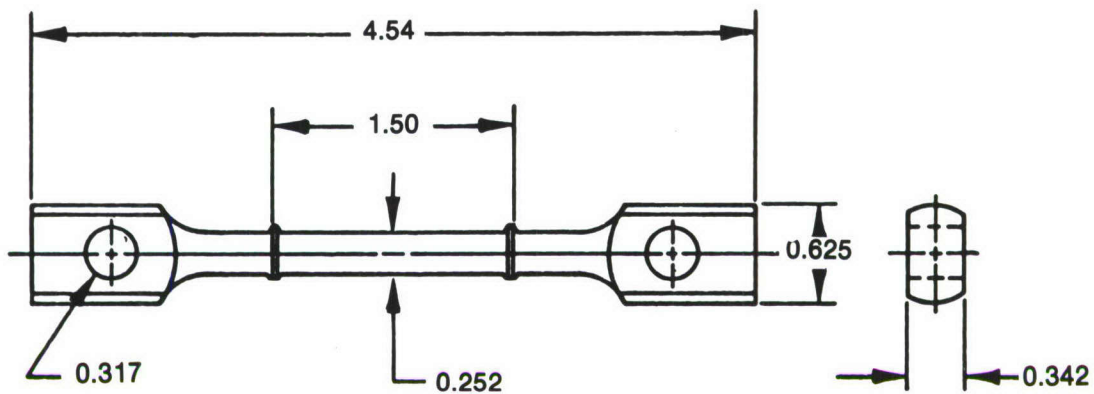
Dimensions in Inches

FD 121060

Figure 4. Standard Round Flat-End Tensile Specimen
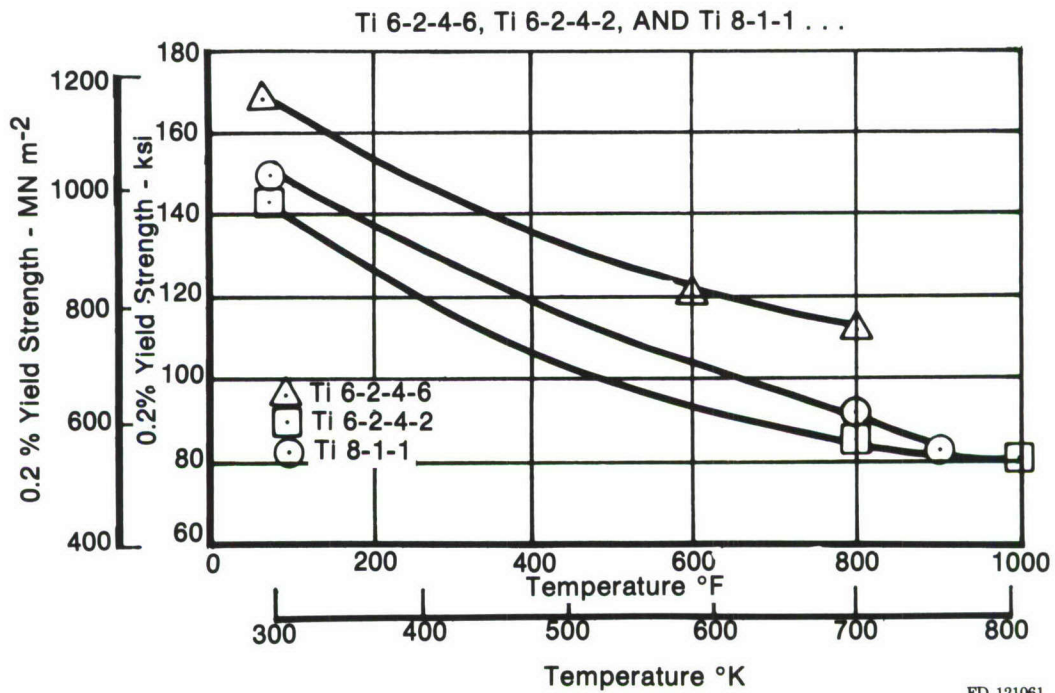
FD 121061

Figure 5. The Effect of Temperature on Yield Strength for Ti 6-2-4-6, Ti 6-2-4-2, and Ti 8-1-1

11
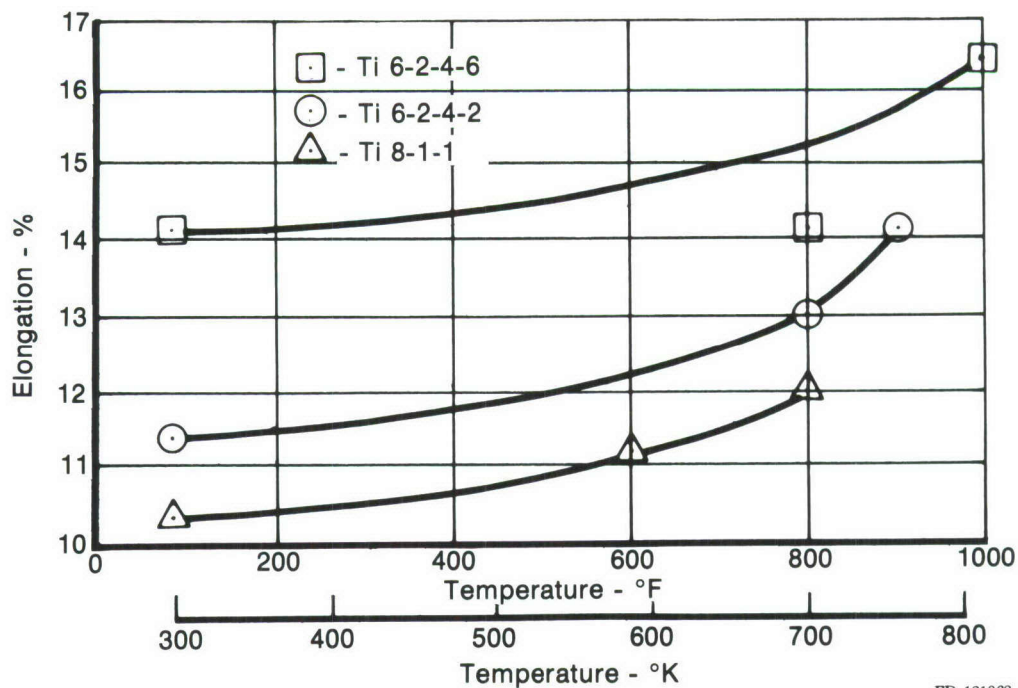
Figure 6. The Effect of Temperature on Percent Elongation for Ti 6-2-4-6, Ti 6-2-4-2, and Ti 8-1-1
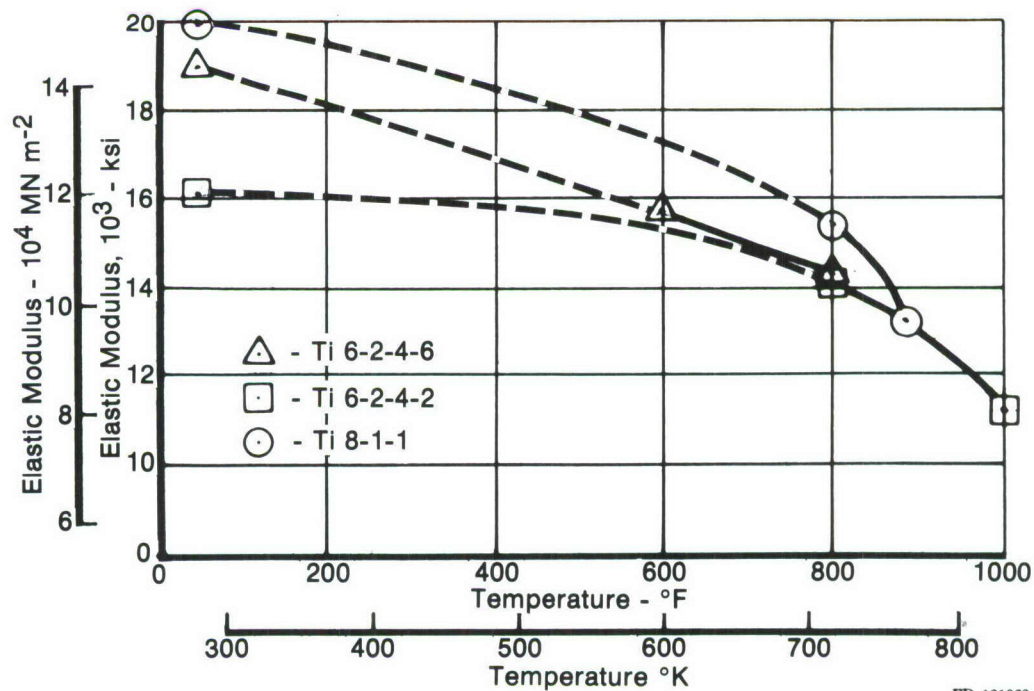
Figure 7. The Effect of Temperature on Elastic Modulus for Ti 6-2-4-6, Ti 6-2-4-2, and Ti 8-1-1

12

TABLE 5. TENSILE TEST DATA FROM TITANIUM ALLOY FORGINGS

Alloy	Heat Code	Temperature (F)	Modulus of Elasticity (ksi)	0.2% YS (ksi)	UTS (ksi)	EL (%)	RA (%)
Ti 8-1-1	LULS	70	20.0×10^3	145.7	159.3	11.4	41.4
		800	15.3×10^3	87.5	112.1	13.0	40.8
		900	13.2×10^3	83.4	106.3	14.0	47.7
Ti 6-2-4-2	LWCC	70	16.2×10^3	143.2	152.1	14.1	31.4
		800	14.2×10^3	84.2	109.6	14.0	29.1
		1000	11.2×10^3	82.0	104.5	16.3	40.4
Ti 6-2-4-6	LYKD	70	18.9×10^3	169.0	182.0	10.3	28.1
		600	15.5×10^3	121.0	150.2	11.1	30.8
		800	14.5×10^3	114.2	149.0	12.0	34.6

[1]Strain rate was 0.005 in./in./min
[2]Single test results plotted on Figures 5 through 7.

SECTION III

FRACTURE MECHANICS

EXPERIMENTAL PROCEDURES

All positive stress ratio tests were conducted in accordance with the test methods given in Reference 1. Center-cracked specimens, shown in Figures 8 and 9, were used for threshold determination, Region I crack propagation testing, and plane stress (K_c) fracture toughness testing. A modified compact tension specimen (Figure 10) was used for plane strain (K_{I_c}) fracture toughness testing.

Threshold tests were conducted using a high frequency (1000 Hz) magnetostrictive machine. Here, both alternating and static loads are controlled by a closed-loop system and are automatically maintained constant as specimen compliance changes. Region II crack propagation tests were performed using hydraulic test equipment for the 10 cpm and 2-minute dwell tests and a Sonntag SF-1-U fatigue testing machine for the 30 Hz tests. All tests were load controlled. Load accuracy for this frequency range was better than 2%.

Crack lengths for the threshold and 30 Hz tests were measured using cellulose acetate tape replicas with an accuracy of 0.001 in. (0.0025 mm) for changes in crack length. All other tests were monitored with a 50X traveling telescope at intervals of approximately 0.01 to 0.02 in. The accuracy of this method is approximately 0.002 to 0.004 in.

Data reduction methods are described in the Fatigue Crack Propagation Section.

Negative stress ratio tests were conducted using the specimen shown in Figure 11. This specimen was designed at the Pratt & Whitney Aircraft's Commercial Products Division and the K-calibration was obtained in Reference 2. The specimen has been used extensively at P&WA for the design of turbine airfoil and disk components. Crack lengths were monitored with the traveling telescope and verified with cellulose acetate tape replicas. Testing was performed in load control on servo-hydraulic test machines.

Specimen heating was accomplished using induction methods for all Region I 1000 Hz tests, while resistance furnaces were used for region II crack propagation and fracture toughness tests. LCF crack initiation tests were heated with a resistance furnace.

All optical crack length measurements were made at temperature, without stopping the actual cycling, through windows in the resistance furnaces or through the induction coil.

The specimen thicknesses were determined to maintain elastic conditions in the specimen as well as to simulate typical gas turbine engine hardware.

THRESHOLD

Both the stress intensity threshold (ΔK_{TH}) and low crack growth rate were determined at a test frequency of 1000 Hz. The threshold values were determined at three high stress ratios for each test temperature, using the center crack tension specimen design shown previously in Figure 8.
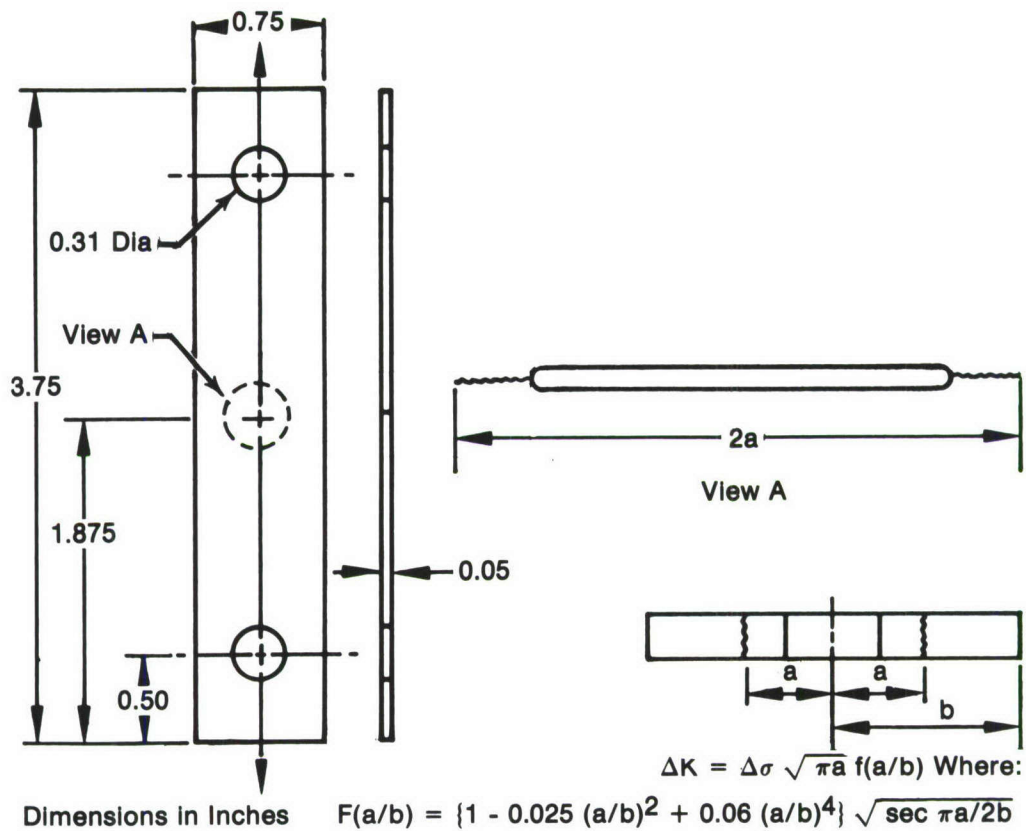
Figure 8. *Standard Fatigue Threshold and Crack Propagation Sheet Specimen*

$$\Delta K = \Delta \sigma \sqrt{\pi a}\; f(a/b) \quad \text{Where:}$$

$$F(a/b) = \{1 - 0.025\,(a/b)^2 + 0.06\,(a/b)^4\}\;\sqrt{\sec\,\pi a/2b}$$
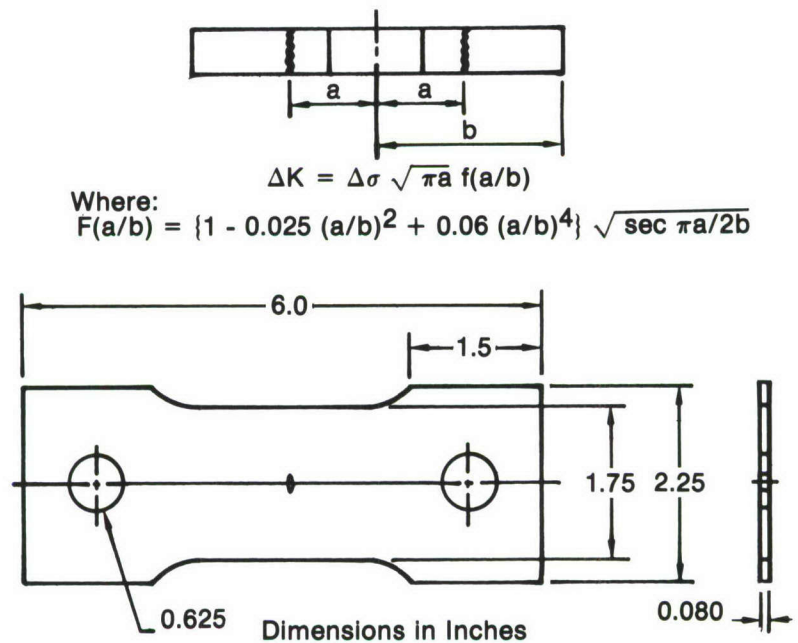
Figure 9. *Center Flaw Fatigue Crack Propagation Specimen for Positive Stress Ratio Testing*

15
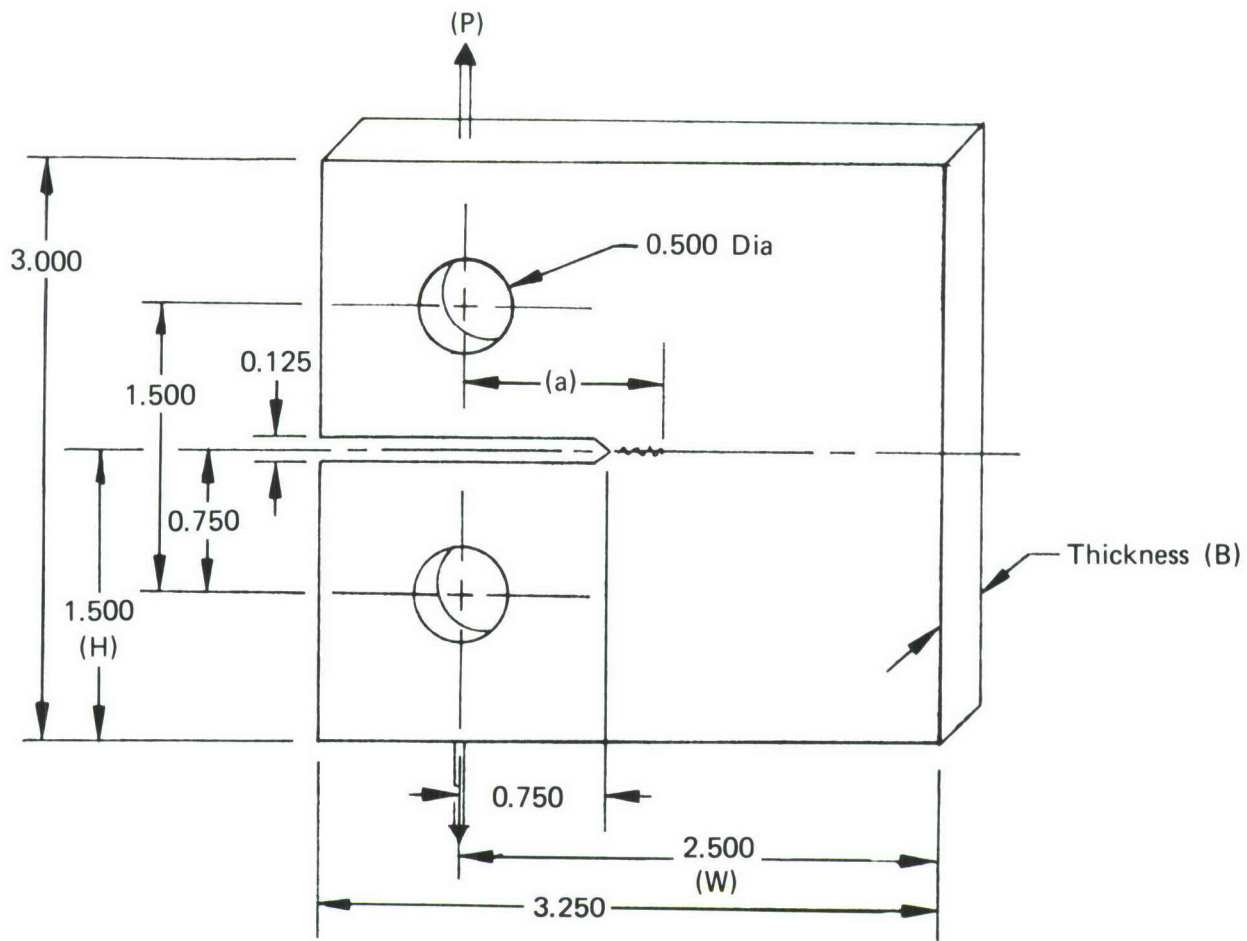
K Calibration:

$$K = Y \frac{P}{BW} \sqrt{a}$$

for a/w = 0.3 - 0.7; H/W - H/W = 0.6

$$Y = f\,(a/w) = [0.2960 - 1.855\,(a/w) + 6.557\,(a/w)^2 - 10.17\,(a/w)^3 + 6.389\,(a/w)^4]\,10^2$$

Accuracy: 0.5%

Net Section Stress:

$$\sigma_{Net} = \frac{KW^{1/2}}{f\,(a/w)\,(w\text{-}a)} \left[1 + \frac{3(w+a)}{(w\text{-}a)}\right]$$

FD 82803A

Figure 10. Modified Compact Tension Fatigue Crack Propagation Specimen

16

$$\Delta K = \Delta\sigma \sqrt{\pi a}\, G(a/rt)$$

$$G(a/rt) = 1 + 0.0574 \left[\frac{a}{(rt)^{1/2}} \right] + 0.0455 \frac{a^2}{rt} - 0.00308 \frac{a^3}{(rt)^{3/2}}$$

Figure 11. Fatigue Crack Propagation Tubular Specimen for Negative Stress Ratio Testing

The final stage of precracking was done at the test temperature, with a stress ratio of 0.1, and a maximum stress intensity equal to or less than the mean stress intensity of the high stress ratio test condition. This procedure minimizes both planar change in the crack front and retardation effects (Reference 3). Changes in crack length of less than 0.001 in. (25 μm) were detectable by taking cellulose acetate replicas of the specimen and examining them under an optical microscope. The specimen was examined every 10^7 cycles, and if no growth was detected, the range in stress intensity was raised by 0.2 ksi $\sqrt{\text{in}}$. (0.22 MN/m$^{3/2}$) keeping the stress ratio constant. This periodic increase was continued until the crack was observed to grow. The ΔK_{TH} value reported here is the last increment before crack growth was measured, and represents a growth rate of less than 10^{-10} in. per cycle (2.5 $\times$ 10^{-9} mm per cycle).
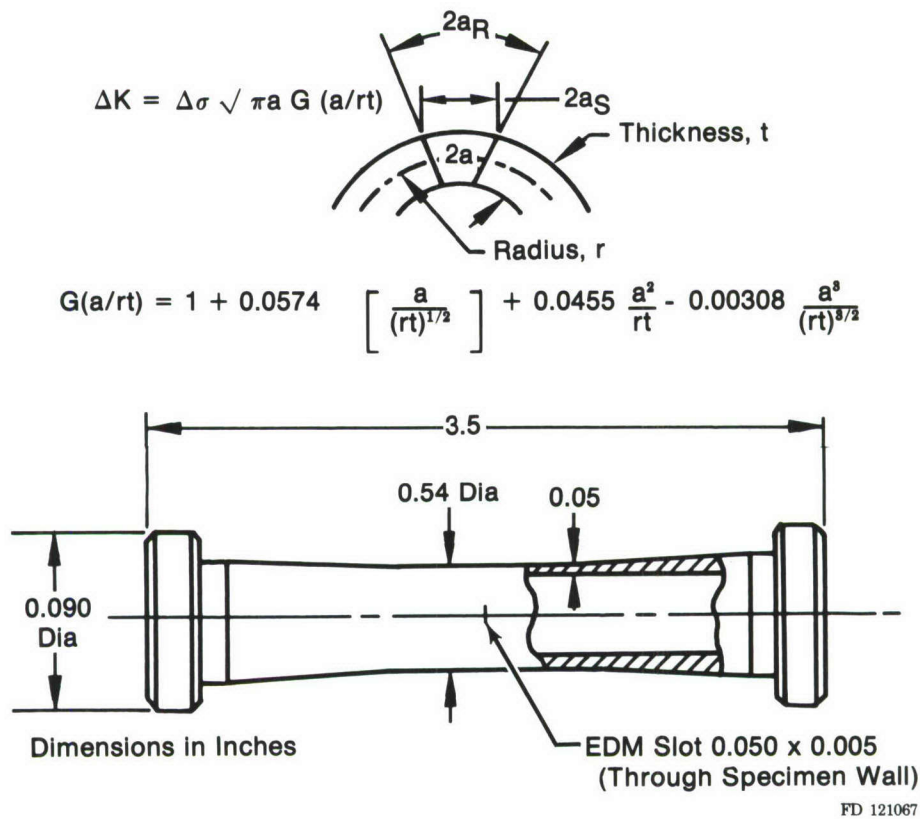
The results of the ΔK_{TH} tests on Ti 8-1-1, Ti 6-2-4-2, and Ti 6-2-4-6 are given in Table 6. A comparison of these values shows Ti 6-2-4-2 to be superior at room temperature and Ti 8-1-1 to be superior at 800°F (700°K), a common test temperature for each alloy.

The ΔK_{TH} results for Ti 8-1-1, Ti 6-2-4-2, and Ti 6-2-4-6 are shown in Figures 12 through 14, respectively. All three alloys show a decrease in ΔK_{TH} with increasing stress ratio.

Figures 12 and 14 show that ΔK_{TH} for R = 0.5 increases with increasing temperature; however, this trend does not hold at the higher stress ratios. The 900°F (755°K) data drop below that obtained at 800°F (700°K), probably due to an increasingly important role of K_{max} at the higher temperatures where creep and oxidation effects become controlling factors in the fracture process.

17

TABLE 6. THRESHOLD STRESS INTENSITY LEVELS FOR TITANIUM ALLOY FORGINGS

Alloy	Heat Code	Temperature (F)	R - Ratio ($\sigma_{min}/\sigma_{max}$)	Threshold Stress Intensity Range (ksi $\sqrt{in.}$)
Ti 8-1-1	LULS-16B	70	0.5	2.2
	LULS-16A	70	0.7	2.0
	LULS-16C	70	0.9	1.6
	LULS-17B	800	0.5	2.6
	LULS-17A	800	0.7	2.4
	LULS-17C	800	0.9	2.2
	LULS-18A	900	0.5	2.8
	LULS-18B	900	0.7	2.4
	LULS-19C	900	0.9	1.8
Ti 6-2-4-2	LWDD-6A	70	0.5	2.6
	LWDD-6C	70	0.7	<2.2
	LWDD-6H	70	0.9	1.6
	LWDD-6E	800	0.5	2.2
	LWCC-11B	800	0.7	1.8
	LWCC-6J	800	0.9	<1.4
	LWCC-11E	1000	0.5	2.8
	LWCC-11C	1000	0.7	2.0
	LWCC-11D	1000	0.9	1.2*
Ti 6-2-4-6	LYKD-1A	70	0.5	2.2
	LYKD-1C	70	0.7	1.6
	LYKD-1B	70	0.9	1.4
	LYKD-1G	600	0.5	2.4
	LYKD-1D	600	0.7	2.2
	LYKD-1M	600	0.9	2.0
	LYKD-1I	800	0.5	2.6
	LYKD-1K	800	0.7	2.2
	LYKD-1L	800	0.9	2.0

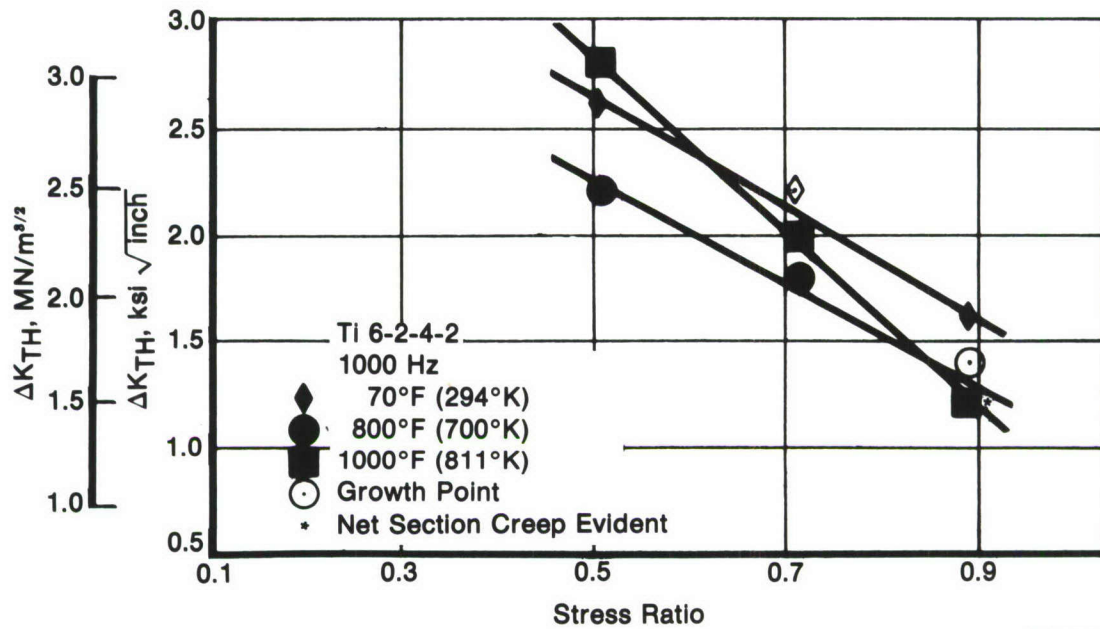*Net section creep evident.
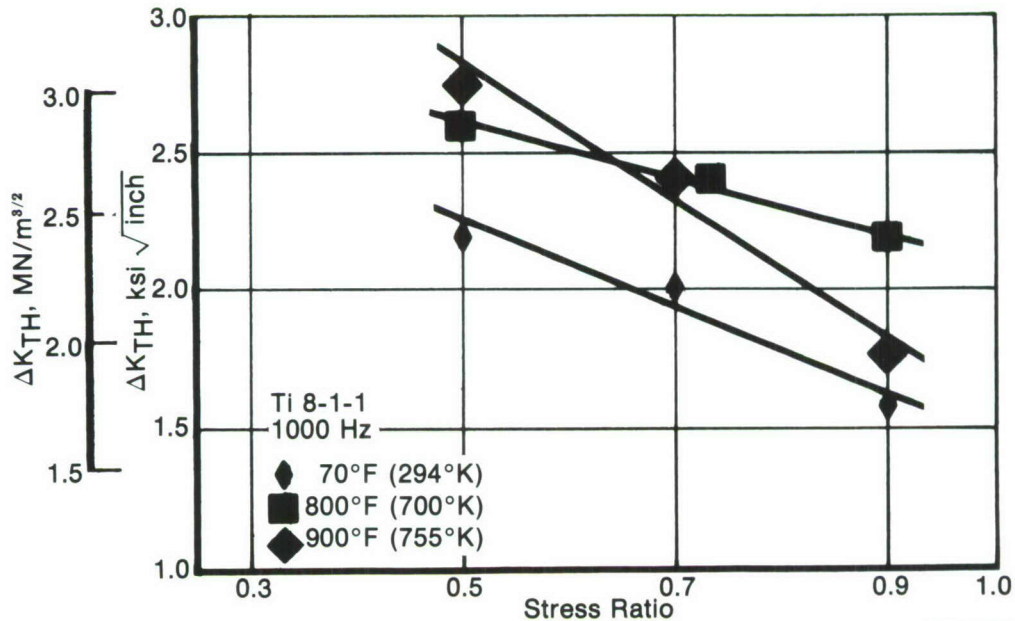
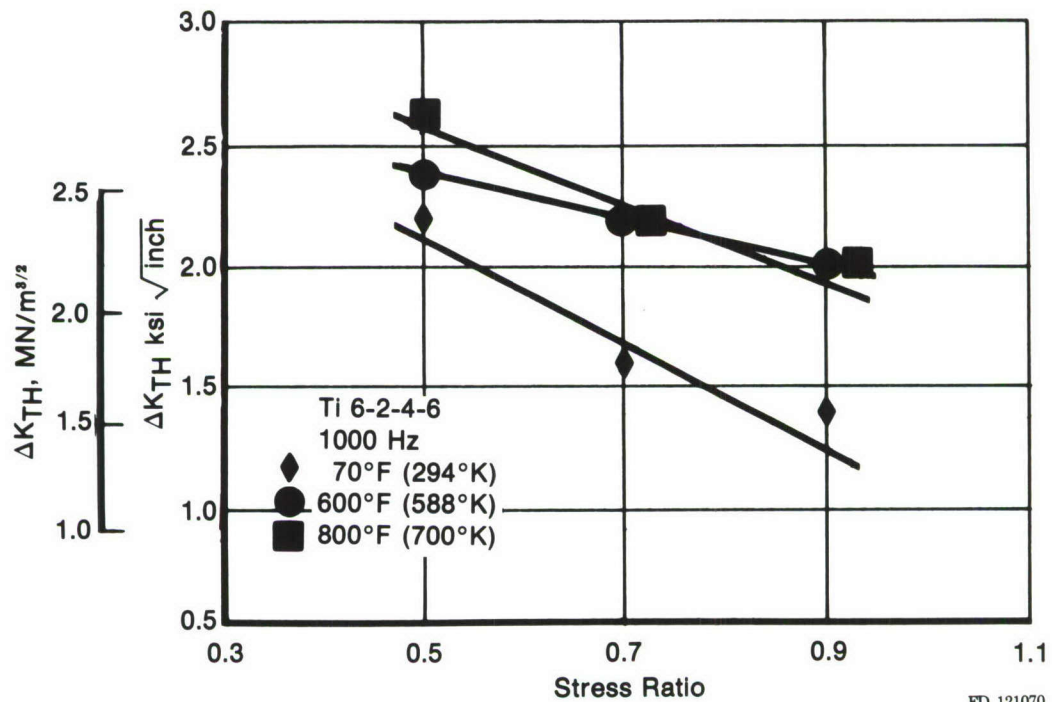
Figure 12. Effect of Stress Ratio on Stress Intensity Threshold for Ti 8-1-1

18

Figure 13. Effect of Stress Ratio on Stress Intensity Threshold for Ti 6-2-4-2

Figure 14. Effect of Stress Ratio on Stress Intensity Threshold for Ti 6-2-4-6

The results on Ti 6-2-4-2 are given in Figure 13. The ΔK_{TH} was significantly higher at room temperature than at 800°F (700°K). The 1000°F (811°K) results give the highest threshold level, 2.8 ksi $\sqrt{in.}$ (3.1 MN/m$^{3/2}$), at a stress ratio of 0.5.

Following the determination of the stress intensity thresholds, crack growth rates below 10^{-6} in. per cycle (2.5×10^{-5} mm per cycle) were obtained on the same specimens. The cyclic frequency was maintained at 1000 Hz and the stress intensity levels were increased 0.2 ksi $\sqrt{in.}$ (0.22 MN/m$^{3/2}$) above the threshold level, keeping the stress ratio constant. The direct secant method was used to reduce the a, N data because of the limited number of data points collected in the 1000 Hz testing.

The results of this testing are given in Figures 15 through 23 for Ti 8-1-1, Ti 6-2-4-2, and Ti 6-2-4-6. Each of the figures shows the crack growth rate data for stress ratios of 0.5, 0.7, and 0.9 for each temperature tested. In a few cases, the specimens failed during the threshold testing with no crack growth data being obtained.

Figures 15 through 17 show the low crack growth rate data for Ti 8-1-1 at room temperature, 800 and 900°F (700 and 755°K) respectively. The high stress ratio, low growth rate data show the crack growth rate to increase with increasing stress ratio.

The results for Ti 6-2-4-2 are given in Figures 18 through 20 for room temperature, 800 and 1000°F (700 and 811°K) respectively. Testing on this alloy resulted in several specimens failing during the threshold runs with no crack growth rate data being obtained. The 1000°F testing resulted in excessive creep in the net section of the center flaw specimen at R = 0.9, even though the maximum net stress was well below the yield stress of the material. This prevented the determination of the threshold and crack growth rate at this condition.

The results for Ti 6-2-4-6 are given in Figures 21 through 23 for room temperature, 600 and 800°F (588 and 700°K) respectively. The growth rate again is shown to increase with increasing stress ratio.

In general, the Region I crack growth rates obtained at room temperature were less than those obtained at elevated temperature for each alloy. For example the lowest growth rate obtained at 800°F (700°K) was near 10^{-7} in. per cycle (2.5×10^{-6} mm per cycle), while at room temperature growth rates near 10^{-9} in. per cycle (3×10^{-7} mm per cycle) were consistently measured.

Figure 15. Effect of Stress Ratio on Crack Growth Rate of Ti 8-1-1 at Room Temperature, 1000 Hz

21

Figure 16. Effect of Stress Ratio on Crack Growth Rate of Ti 8-1-1 at 800°F, 1000 Hz

Figure 17. Effect of Stress Ratio on Crack Growth Rate of Ti 8-1-1 at 900°F, 1000 Hz

Figure 18. Effect of Stress Ratio on Crack Growth Rate of Ti 6-2-4-2 at Room Temperature, 1000 Hz

Figure 19. Effect of Stress Ratio on Crack Growth Rate of Ti 6-2-4-2 at 800°F, 1000 Hz

Figure 20. Crack Propagation Data for Ti 6-2-4-2 at 1000°F, 1000 Hz, Stress Ratio = 0.5
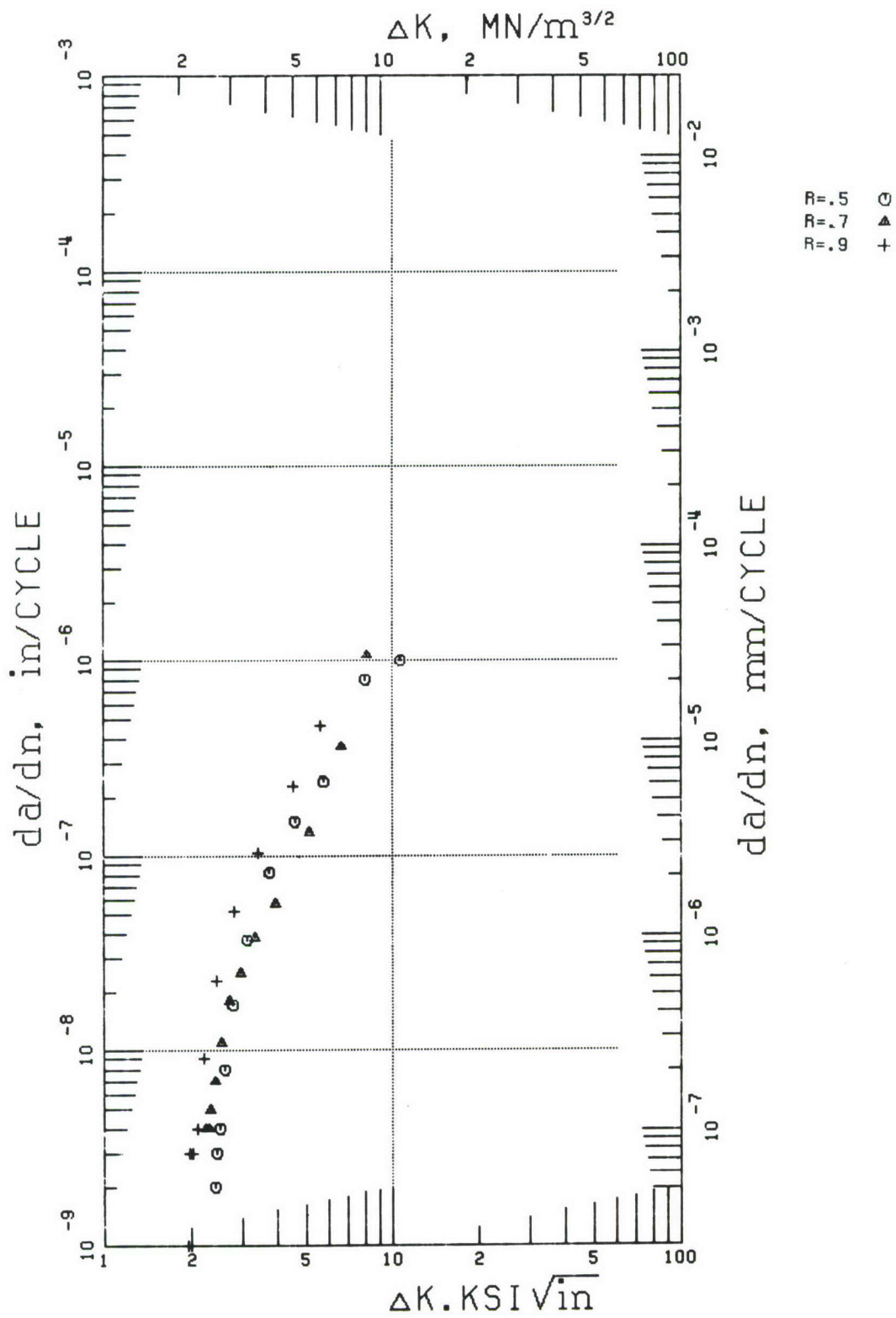
Figure 21. Effect of Stress Ratio on Crack Growth Rate of Ti 6-2-4-6 at Room Temperature, 1000 Hz
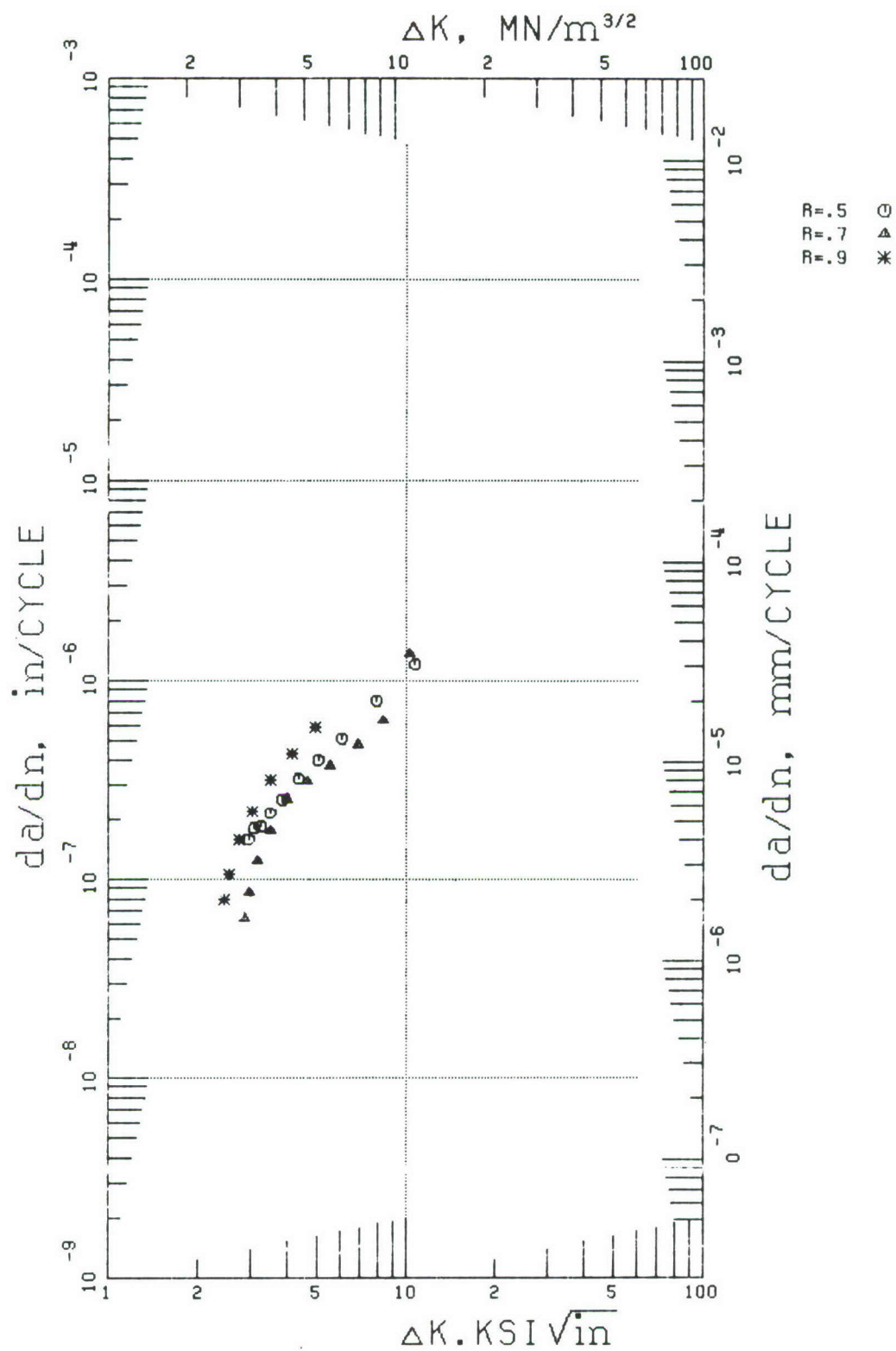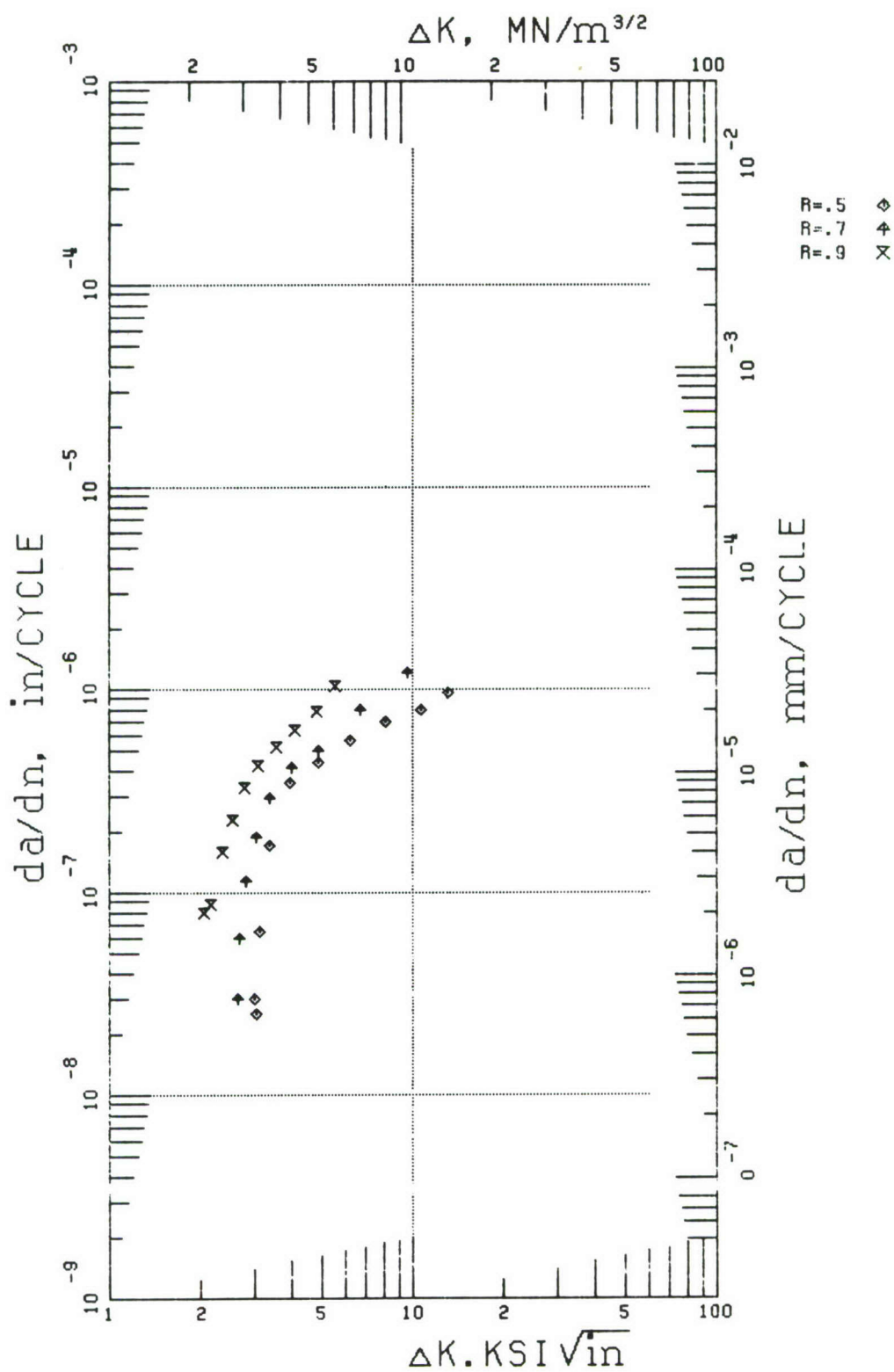
Figure 22. Effect of Stress Ratio on Crack Growth Rate of Ti 6-2-4-6 at 600°F, 1000 Hz

Figure 23. *Effect of Stress Ratio on Crack Growth Rate of Ti 6-2-4-6 at 800°F 1000 Hz*
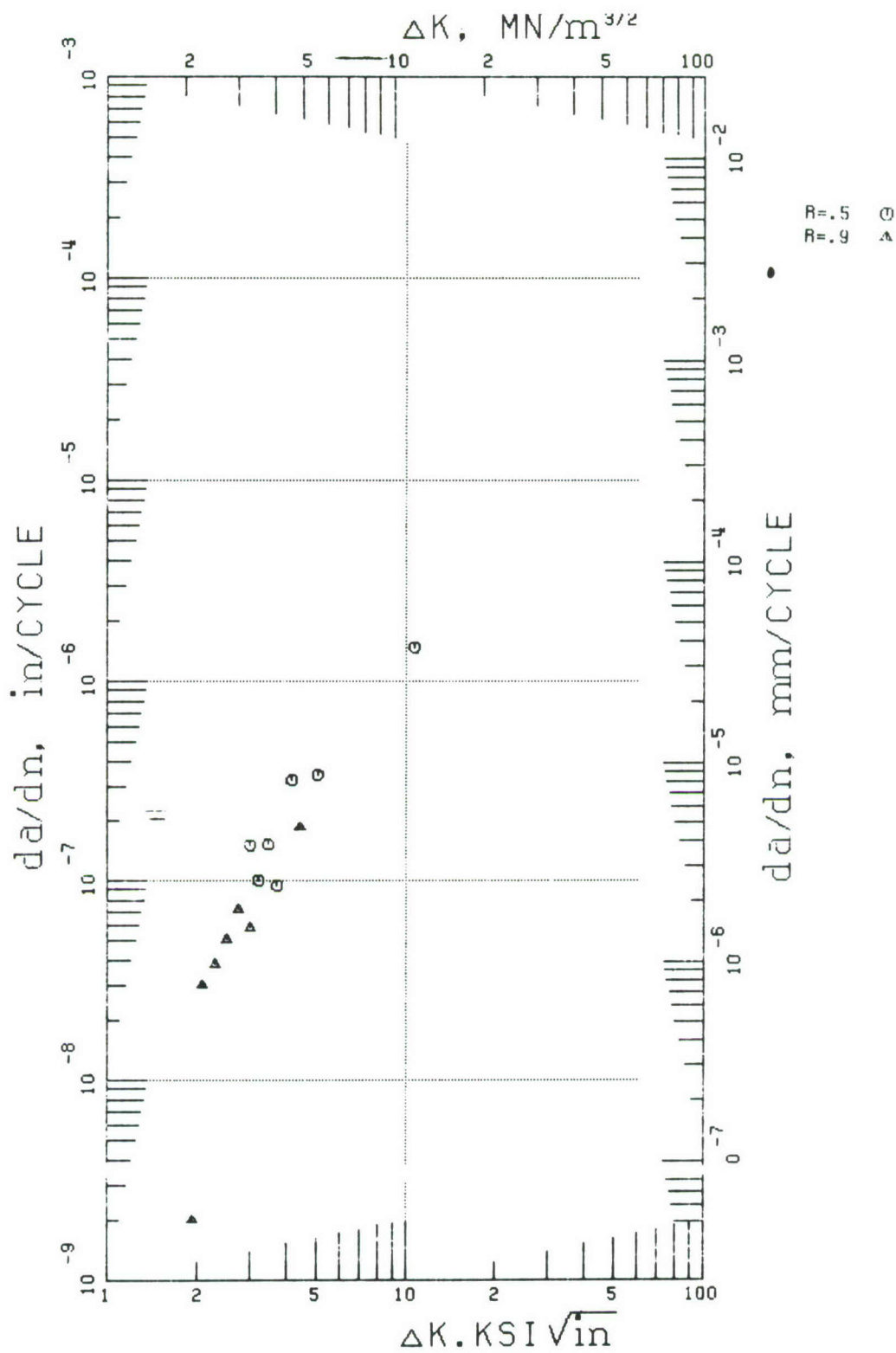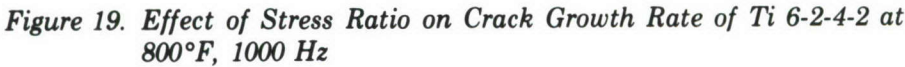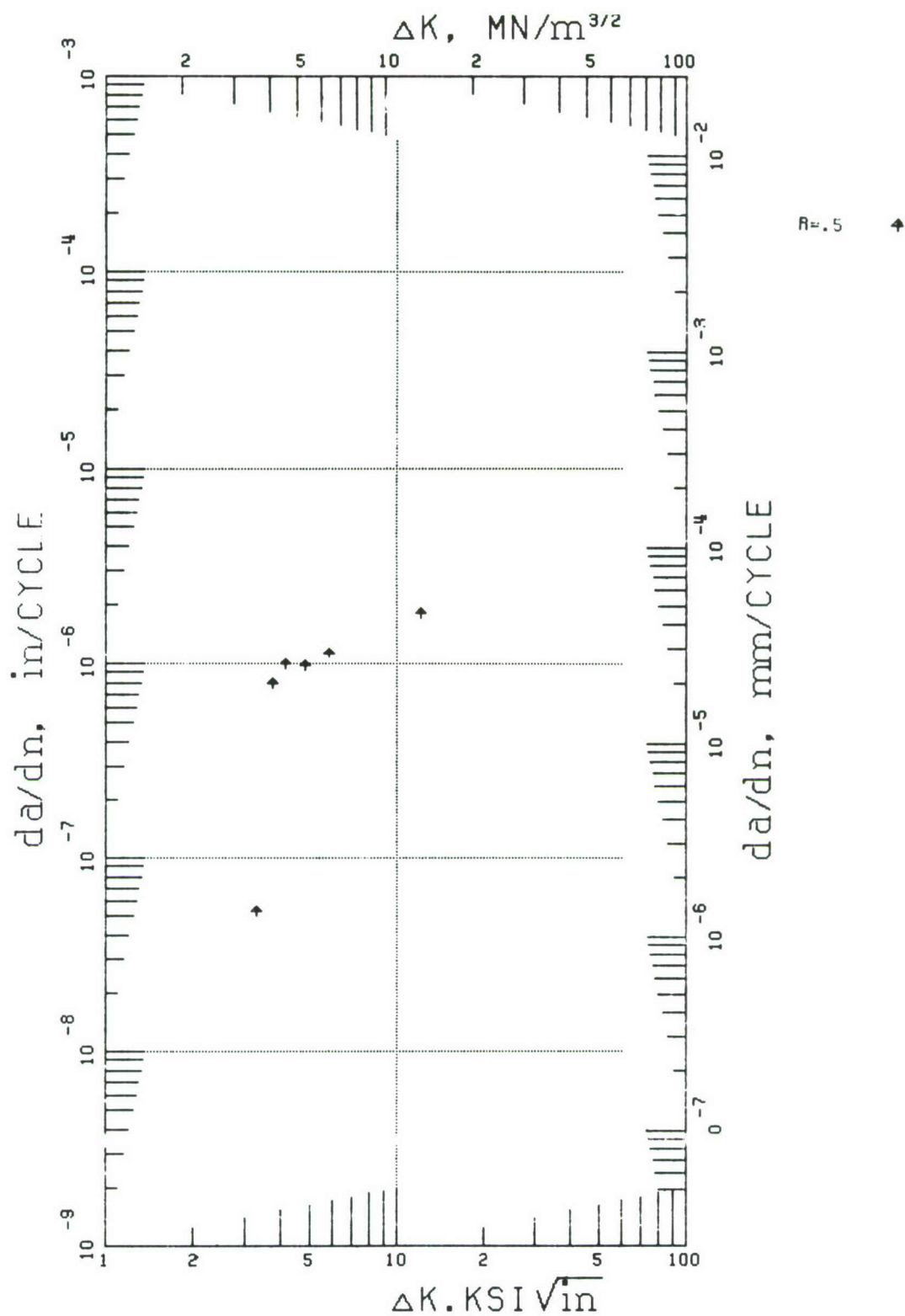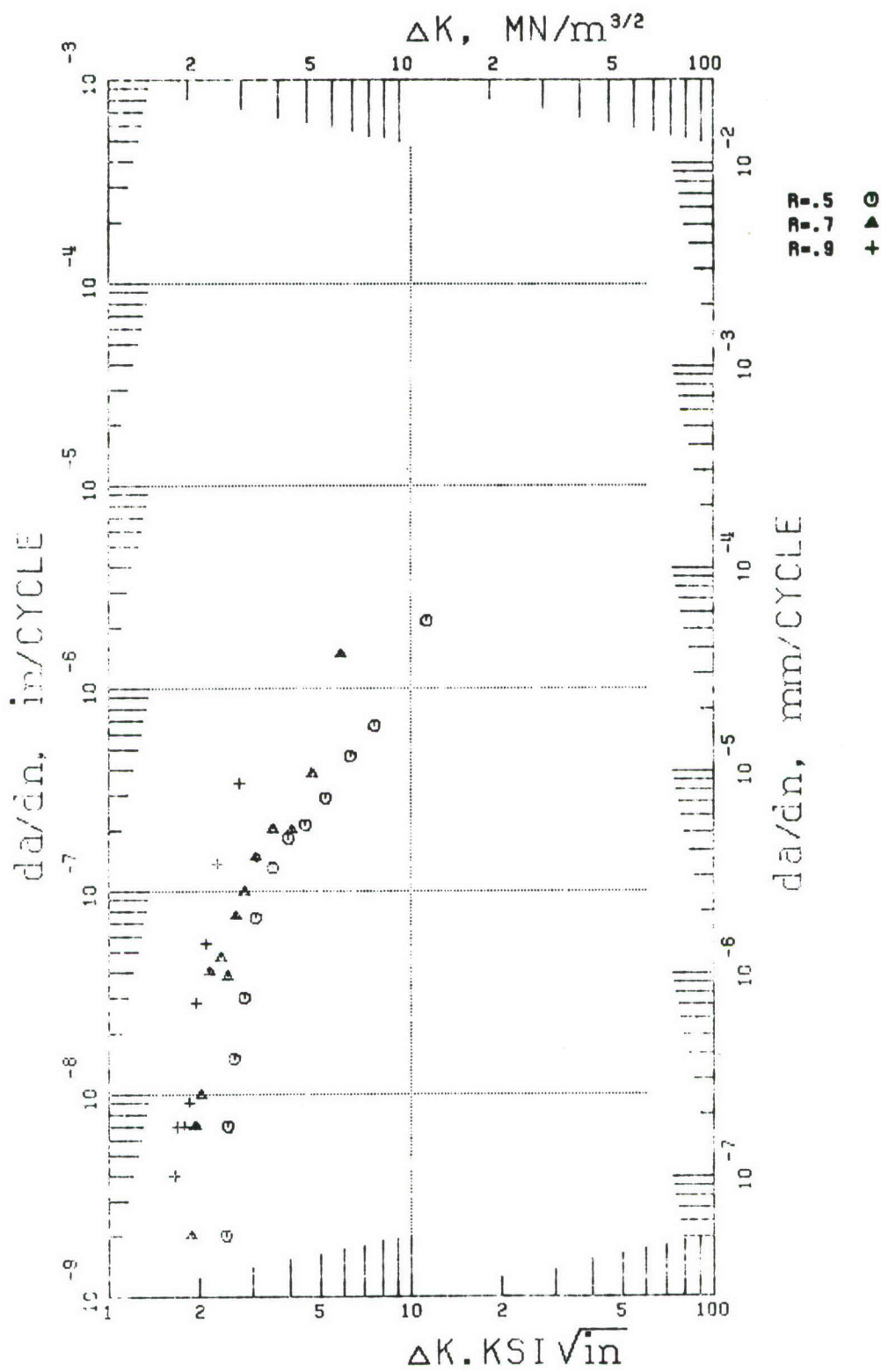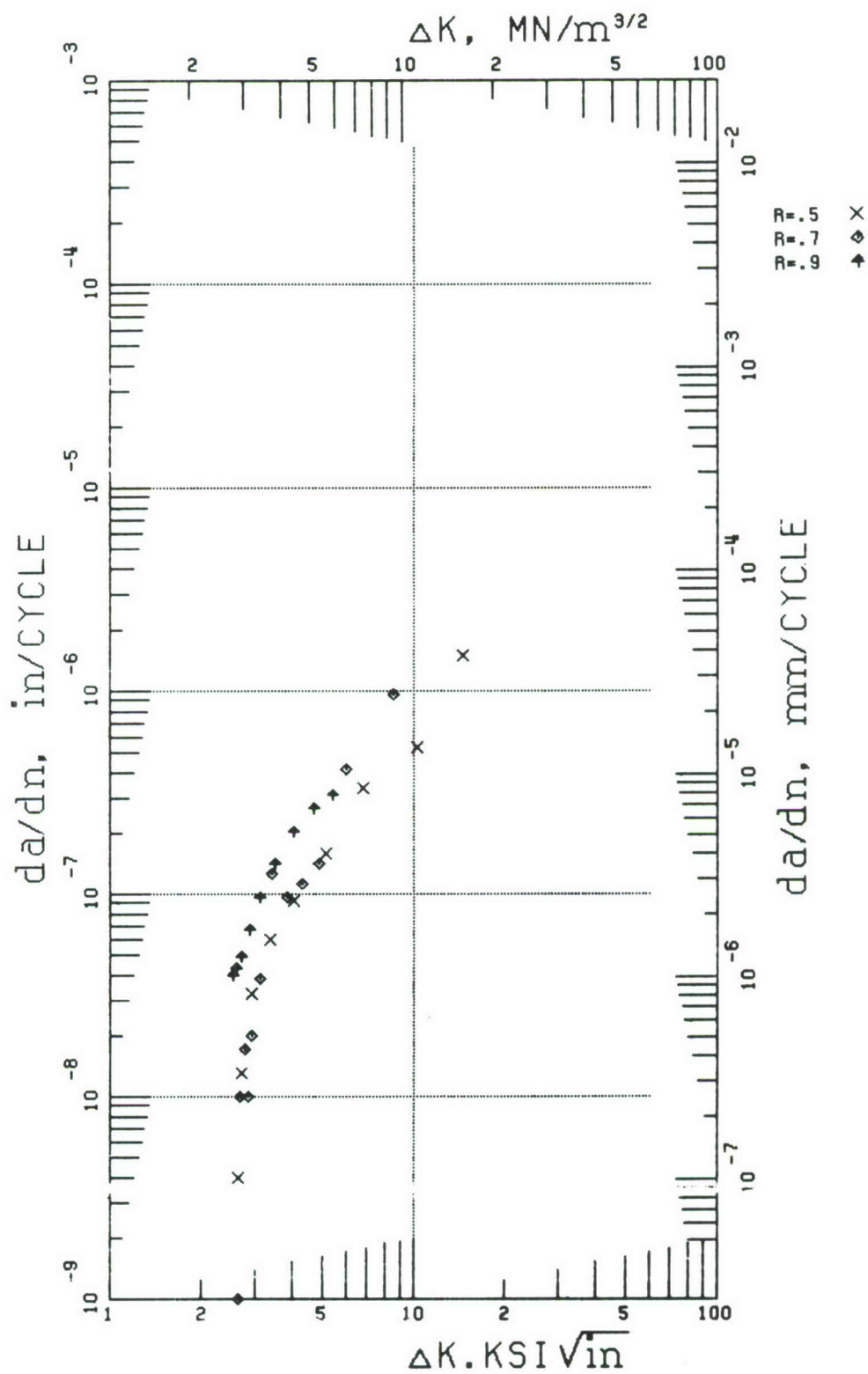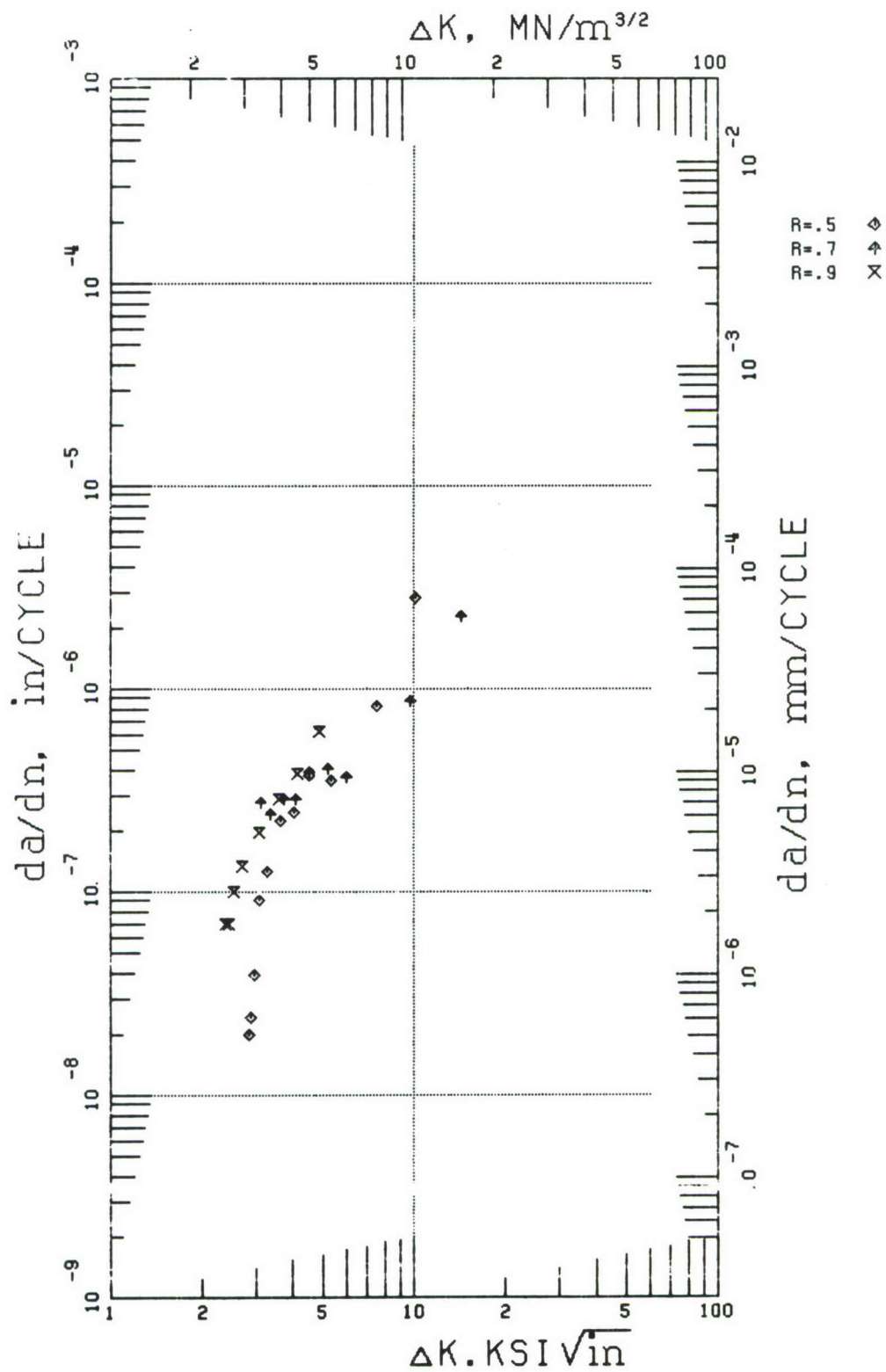
FATIGUE CRACK PROPAGATION

Extensive fatigue crack growth data were obtained in Region II, da/dn > 10⁻⁶ in. per cycle $(2.5 \times 10^{-5}$ mm per cycle), for various frequencies, stress ratios, and temperatures as shown in Tables 7 and 8. The same test conditions, with the exception of temperature, were run on the Ti 8-1-1, Ti 6-2-4-2, and Ti 6-2-4-6 alloys.

TABLE 7. TEST MATRIX IS THE SAME FOR EACH ALLOY; TEMPERATURES ARE SHOWN IN TABLE 8

		Region I	Region II				Region III		
		ΔK_{TH}	Crack Growth Data				Fracture Toughness		
			Test Frequency						
Temperature	R-Ratio	1000 CPS	1000 CPS	30 CPS	10 CPM	2 Min Dwell	Temperature	Thickness	K_c
70°	−5.0				X		70°	0.05	X
70°	−1.0				X		70°	0.10	X
70°	0.1			X	X		70°	0.50	X
70°	0.5	X	X		X		T_1	0.05	X
70°	0.7	X	X		X		T_1	0.10	X
70°	0.9	X	X				T_1	0.50	X
800°	−5.0				X		T_2	0.05	X
800°	−1.0				X		T_2	0.10	X
T_1	0.1			XX	X	X	T_2	0.50	X
T_1	0.5	X	X		X	X			
T_1	0.7	X	X		X				
T_1	0.9	X	X						
T_2	0.1			XX	X	X			
T_2	0.5	X	X		X	X			
T_2	0.7	X	X		X				
T_2	0.9	X	X						

TABLE 8. FRACTURE MECHANICS TEST TEMPERATURE MATRIX FOR T_1 AND T_2

	Ti-8Al-1Mo-1V (°F)	Ti-6Al-2Sn-4Zr-2Mo (°F)	Ti-6Al-2Sn-4Zr-6Mo (°F)
T_1	800	800	600
T_2	900	1000	800

The test techniques used in this program conform to methods presented in Reference 1. The majority of the data was reduced to da/dn vs ΔK by the Seven Point Incremental Polynomial Technique (Reference 1). There are two exceptions; the Region I data were reduced using the direct secant method, and data from tubular specimens (Figure 11) utilized in the negative stress ratio tests were reduced by smoothing the a, N data. These smoothed a, N data were reduced to da/dn in a computer program using a 5th-order curve. This curve is differentiated obtaining da/dn at each of the input points while ΔK is calculated for the same crack length.

The Region II crack growth data are plotted on log-log coordinates with da/dn on the ordinate and ΔK on the abscissa. The stress intensity range (ΔK) was calculated in the following manner: $\Delta K = K_{max} - K_{min}$ for R > 0, $\Delta K = K_{max}$ for R < 0, in accordance with Reference 1.

Alloy TI 8-1-1

The crack propagation data for Ti 8-1-1 are illustrated in Figures 24 through 33. The effects of stress ratio, temperature, and frequency are shown.

The room temperature data are given in Figure 24 for stress ratios ($\sigma_{min}/\sigma_{max}$) of 0.1, 0.5, 0.7, 0.9, −1, and −5, and cyclic frequencies of 1000, 30, and 0.17 Hz (10 cpm). The 1000 Hz data agree well with the lower frequency tests at R = 0.5 and R = 0.7. The 30 Hz test shows slightly faster crack growth rates than the 0.17 Hz test at a stress ratio of 0.1.

Figure 25 presents all of the Region II crack growth data at 800°F (700°K), showing the effect of stress ratio on Ti 8-1-1. The crack growth rate generally increases with increasing stress ratio, R > 0, for equivalent applied stress intensities. The effects of negative R on crack growth rates, as plotted, were to increase them over the R = 0.1. Figure 26 illustrates the effect of frequency on the crack propagation rate at 800°F (700°K), stress ratio = 0.1. The 2-minute dwell crack growth rate is slower than the 0.17 Hz rate, possibly due to crack tip creep relaxation effects. Figures 27 and 28 show the effects of frequency at 800°F (700°K) at stress ratios of 0.5 and 0.7 respectively. There is a significant reduction in crack growth rate at 1000 Hz.

Figure 29 shows the Region II crack growth data at 900°F (755°K) showing the effect of stress ratio on Ti 8-1-1 at several frequencies. Figures 30 through 32 show the effect of frequency at stress ratios of 0.1, 0.5, and 0.7 respectively. The 1000 Hz data are also compared to the 0.17 Hz and 2-minute dwell data. With exception to the R = 0.1 data, crack growth rates tend to decrease with increasing frequency.

Figure 33 illustrates the effects of temperature on the fatigue crack growth rate of Ti 8-1-1 at 0.17 Hz and a stress ratio of 0.1.

Alloy TI 6-2-4-2

The results for the Ti 6-2-4-2 alloy are presented in Figures 34 through 42. The effects of stress ratio, frequency, and temperature on fatigue crack growth rate are shown.

Figure 34 shows the effect of stress ratio on crack growth rate at room temperature. The 0.17 Hz (10 cpm) data show an increase in crack growth rate with increasing stress ratio, R > O, at equivalent stress intensities. The 30 Hz test at a stress ratio of 0.1 shows no difference in crack growth rate when compared to R = 0.1, 0.17 Hz data. The 1000 Hz data are also given for stress ratios of 0.5 and 0.9 with no appreciable difference in the crack propagation rates due to stress ratio effects.

Figure 35 gives all of the Region II crack growth data at 800°F (700°K) showing the effect of stress ratio on the Ti 6-2-4-2 alloy. These data are for cyclic frequencies of 30, 0.17, and 0.008 Hz (2-minute dwell cycle).

Figures 36 through 38 show the effect of cyclic frequency on crack growth rate for stress ratios of 0.1, 0.5, and 0.7 respectively at 800°F (700°K). Figure 36 shows no significant frequency effect at a stress ratio of 0.1 for frequencies from 30 Hz down to 0.008 Hz (2-minute dwell). Figure 37 shows no significant difference between 0.17 Hz and 0.008 Hz for a stress ratio of 0.5. The 1000 Hz data were added to Figure 38 for comparison.
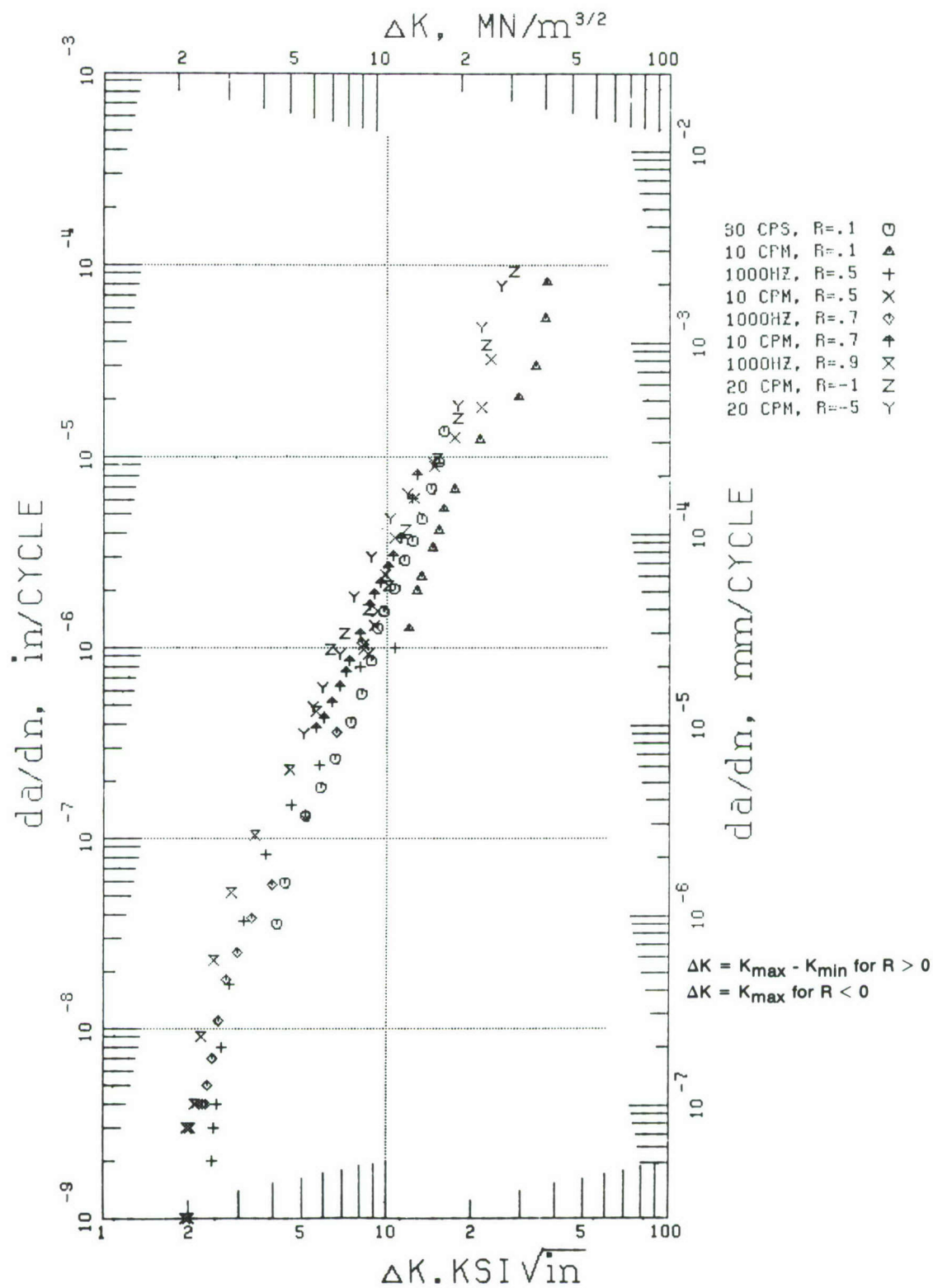
Figure 24. Crack Propagation Data for Ti 8-1-1 at Room Temperature
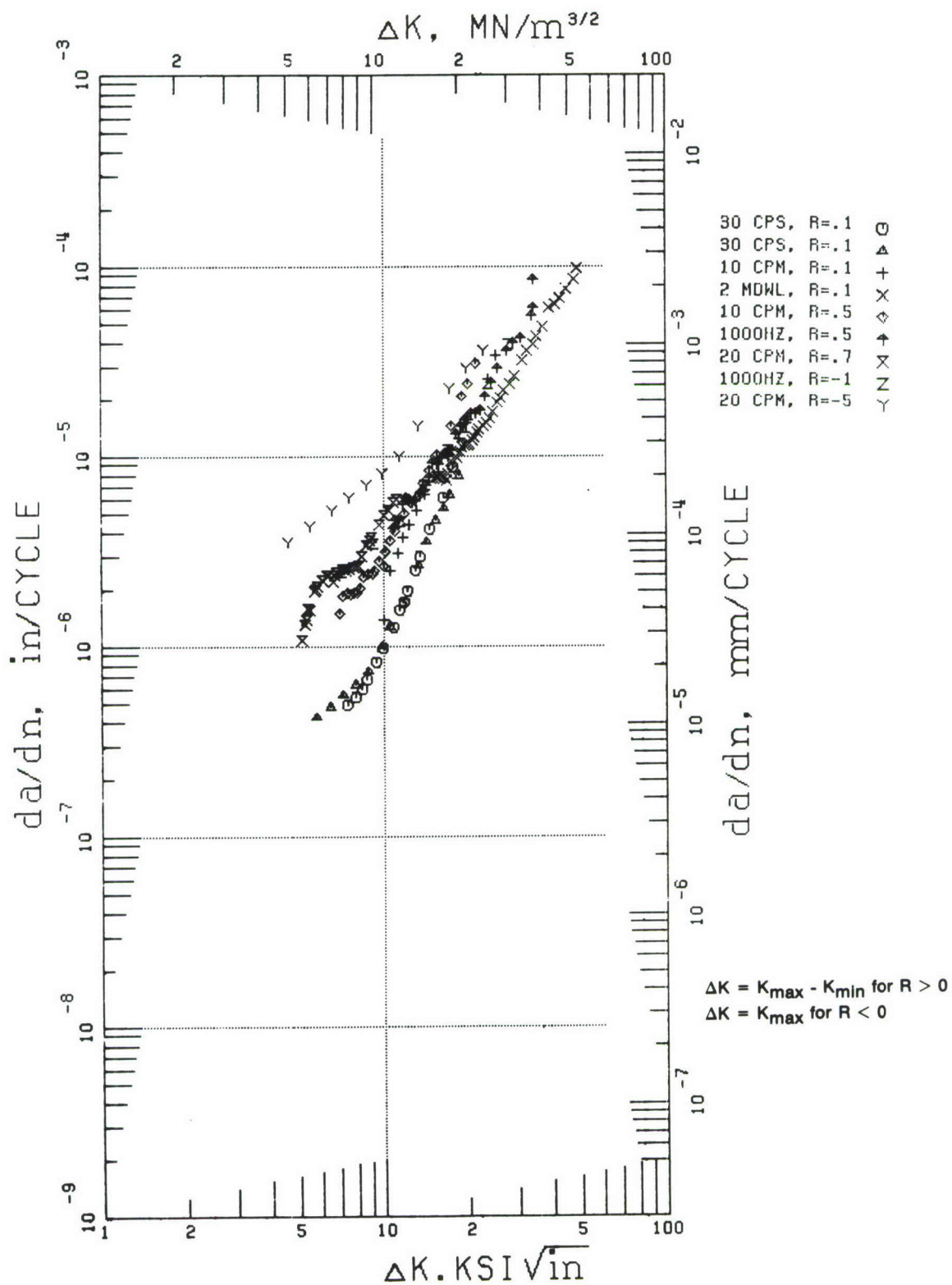
32

Figure 25. Crack Growth Data for Ti 8-1-1 at 800°F

33

Figure 26. Effect of Frequency on Crack Growth Rate of Ti 8-1-1 at 800°F,
R = 0.1

Figure 27. Effect of Frequency on Crack Growth Rate of Ti 8-1-1 at 800°F,
R = 0.5

35

Figure 28. *Effect of Frequency on Crack Growth Rate of Ti 8-1-1 at 800°F,*
R = 0.7

Figure 29. Crack Growth Data for Ti 8-1-1 at 900°F

37

Figure 30. *Effect of Frequency on Crack Growth Rate of Ti 8-1-1 at 900°F,
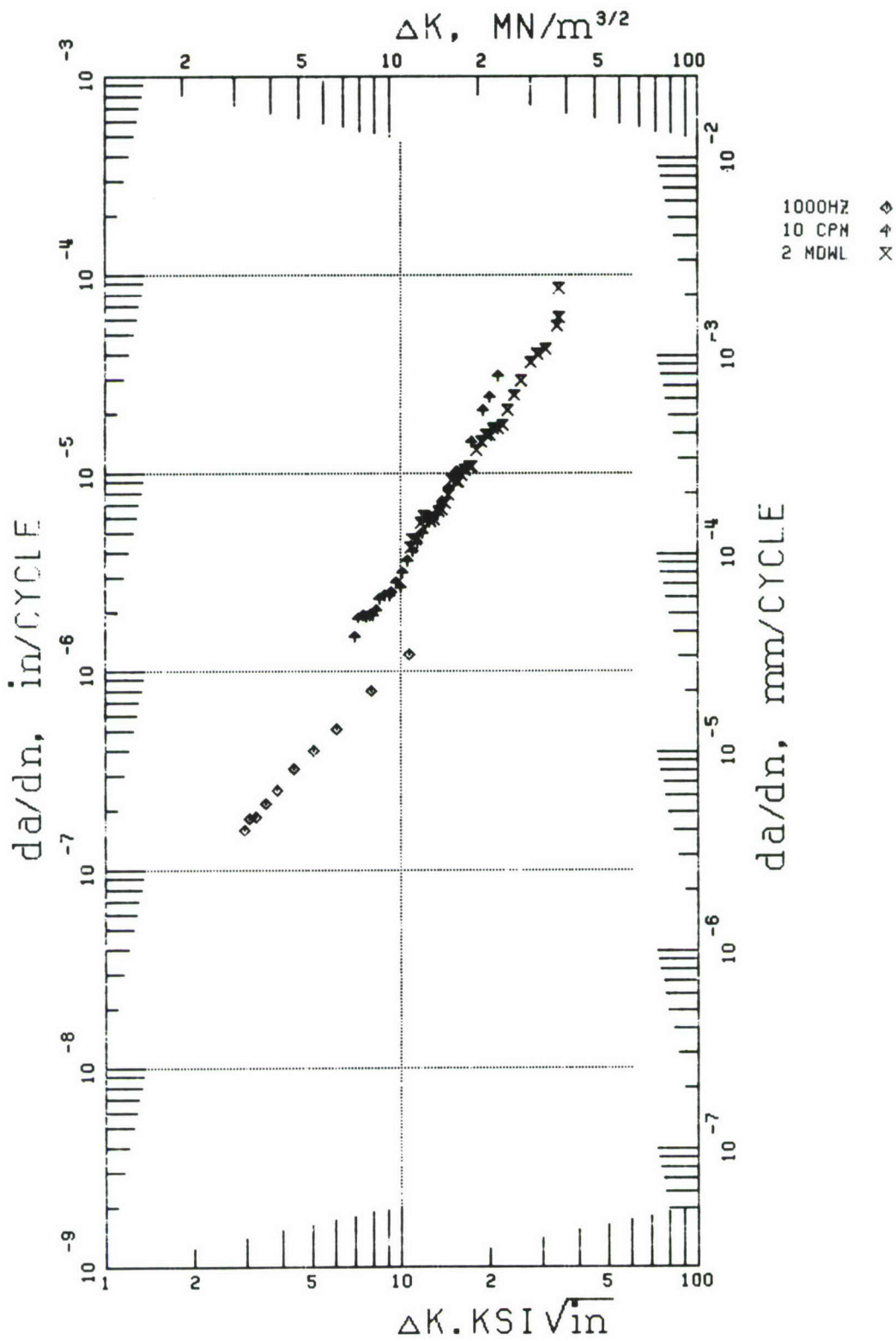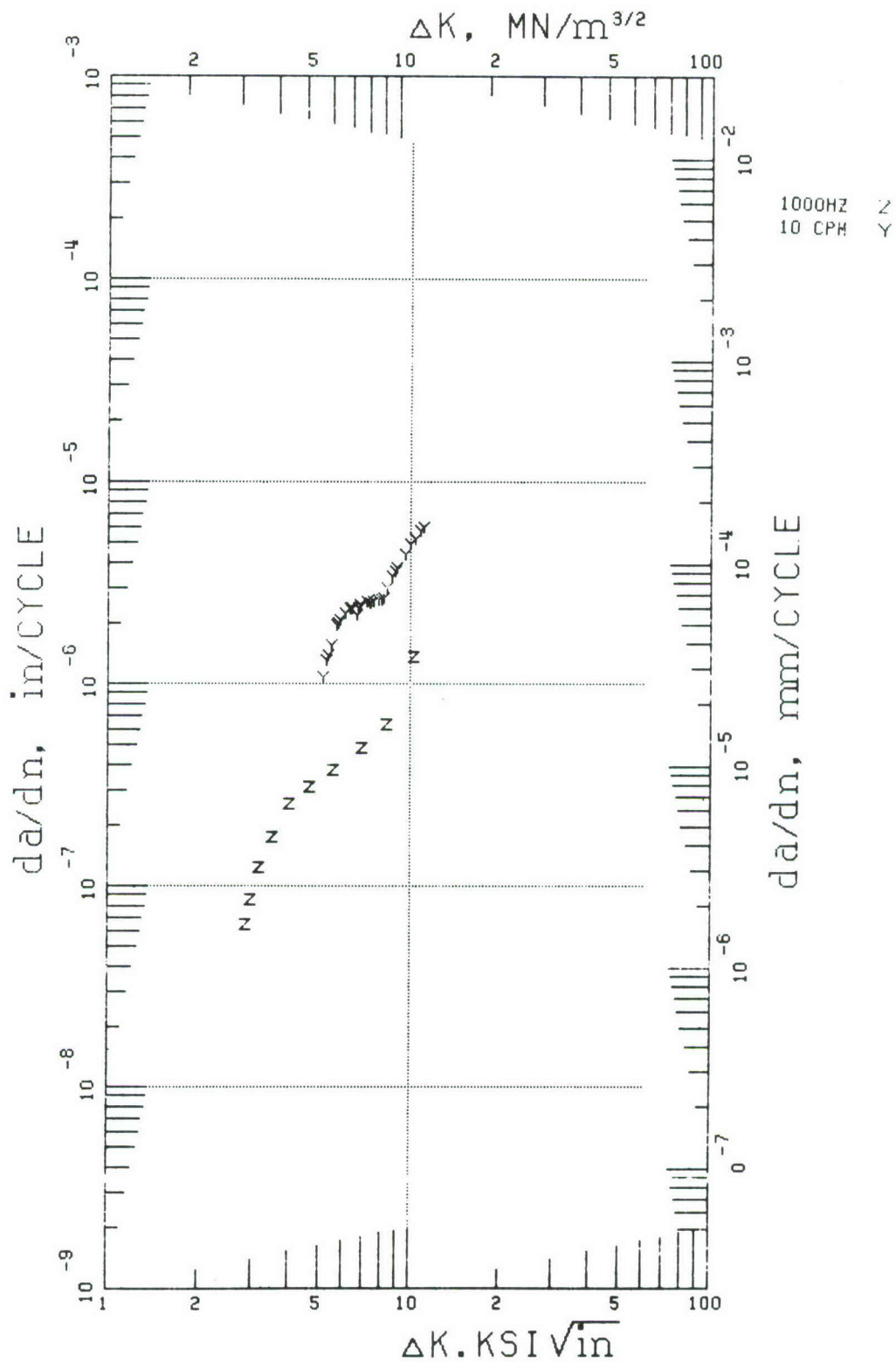R = 0.1*

38

Figure 31. *Effect of Frequency on Crack Growth Rate of Ti 8-1-1 at 900°F,*
R = 0.5

*Figure 32. Effect of Frequency on Crack Growth Rate of Ti 8-1-1 at 900°F,
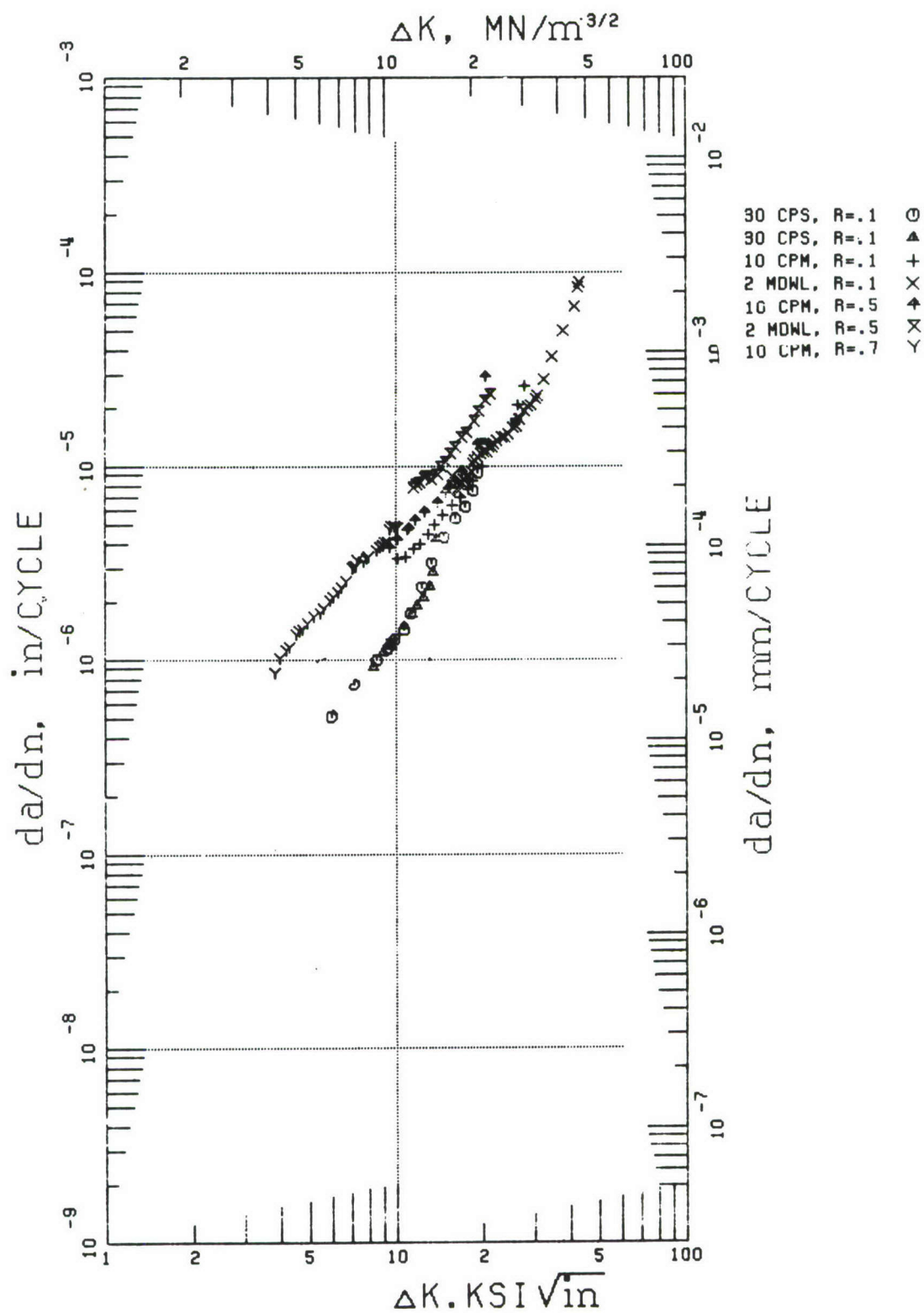R = 0.7*

Figure 33. *Effect of Temperature on Crack Growth Rate of Ti 8-1-1 at 10 cpm, R = 0.1*
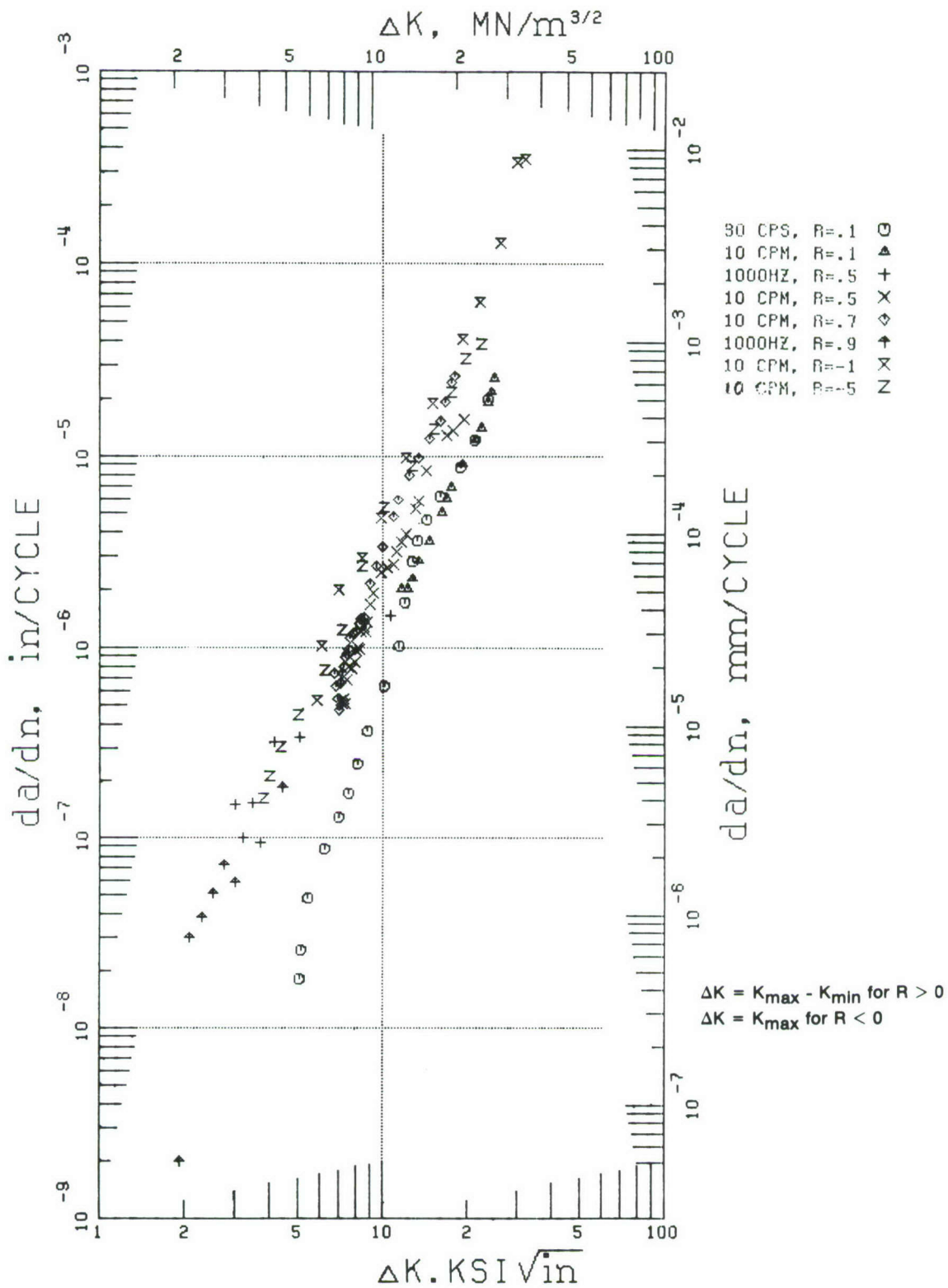
Figure 34. Crack Propagation Data for Ti 6-2-4-2 at Room Temperature

42

Figure 35. Crack Propagation Data for Ti 6-2-4-2 at 800°F

43

Figure 36. Effect of Frequency on Crack Growth Rate of Ti 6-2-4-2 at
800°F, R = 0.1

Figure 37. Effect of Frequency on Crack Growth Rate of Ti 6-2-4-2 at 800°F, R = 0.5

Figure 38. Effect of Frequency on Crack Growth Rate of Ti 6-2-4-2 at 800°F, R = 0.7

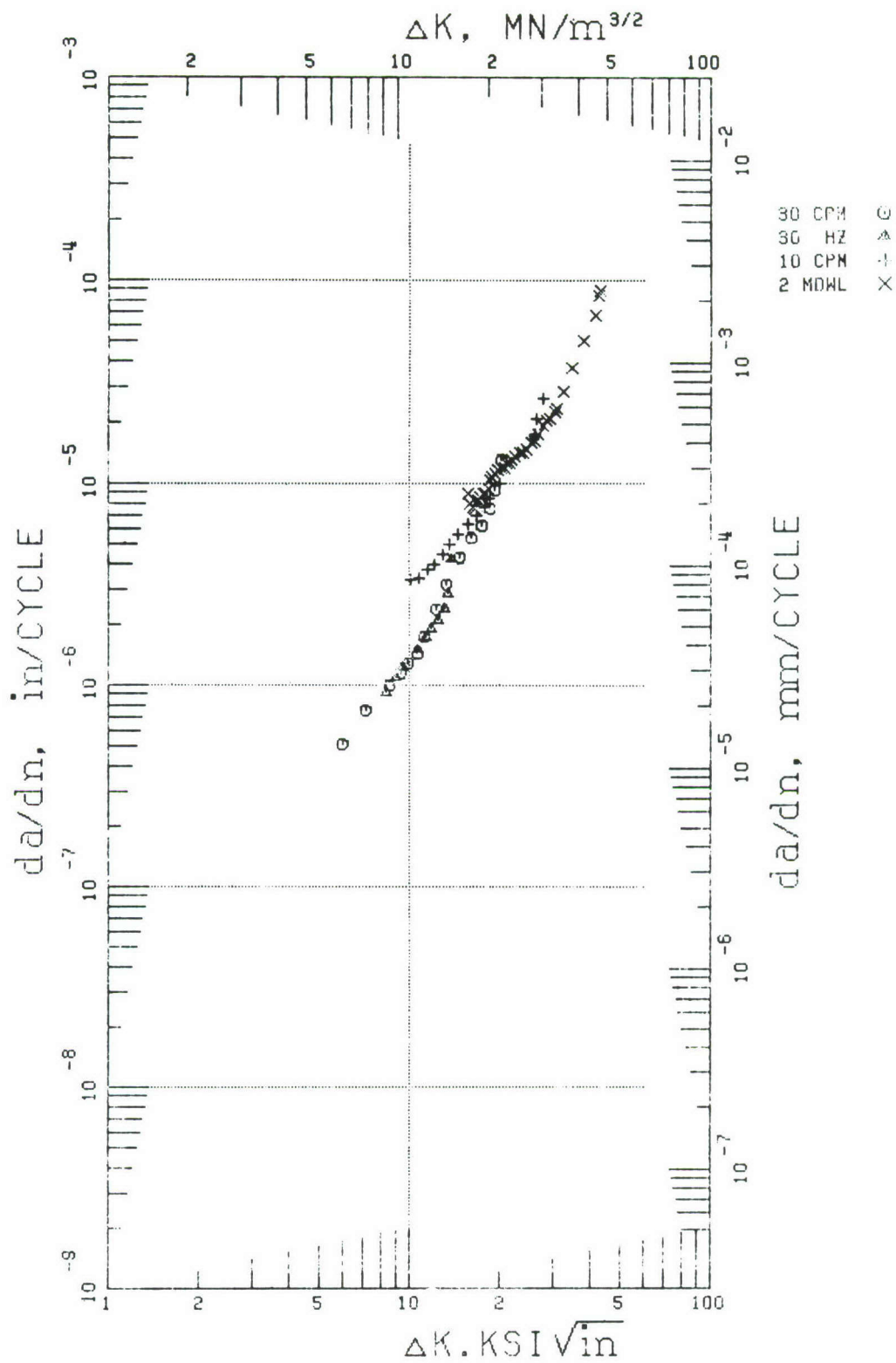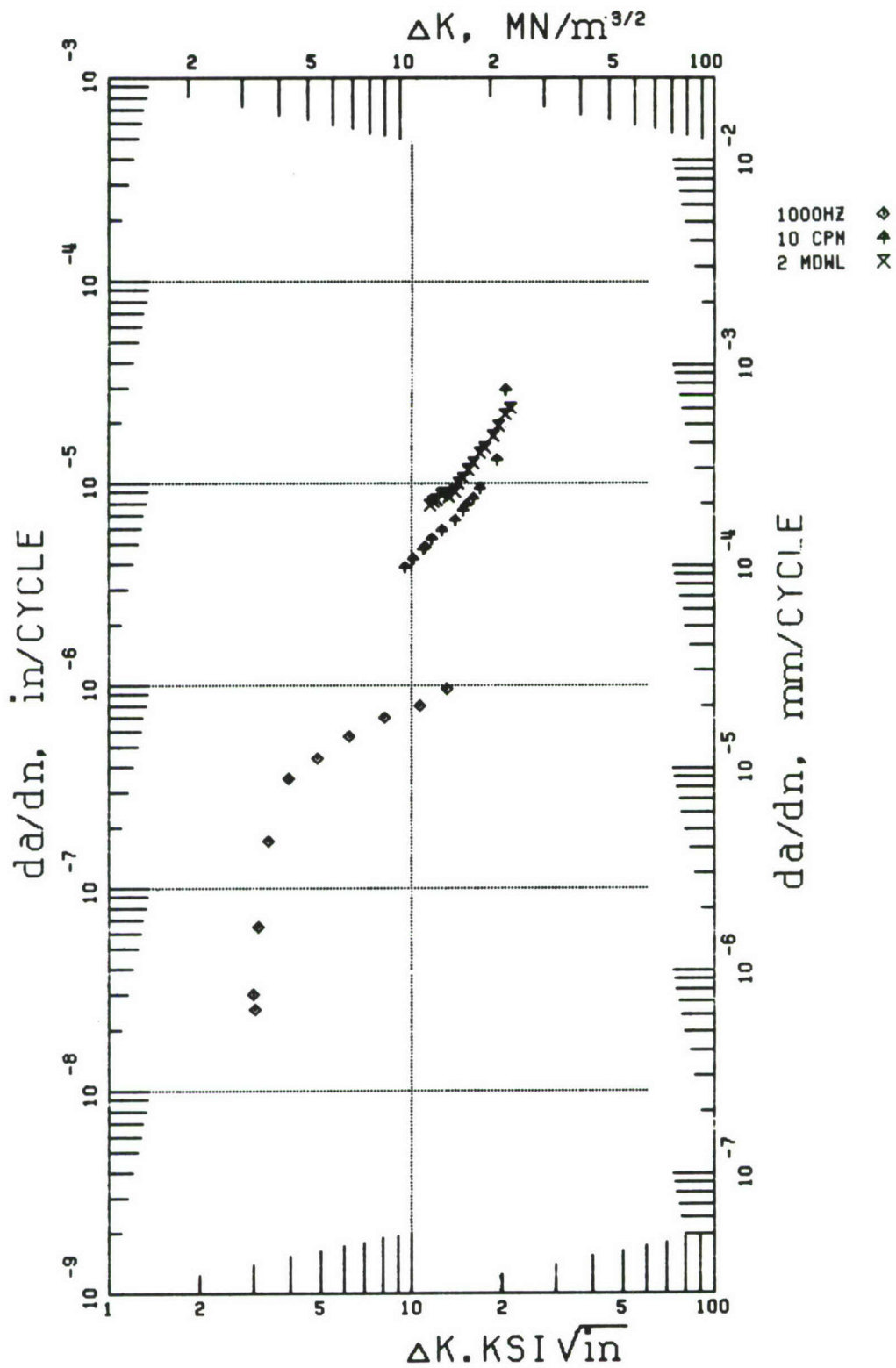Figure 39. *Crack Propagation Data for Ti 6-2-4-2 at 1000°F*

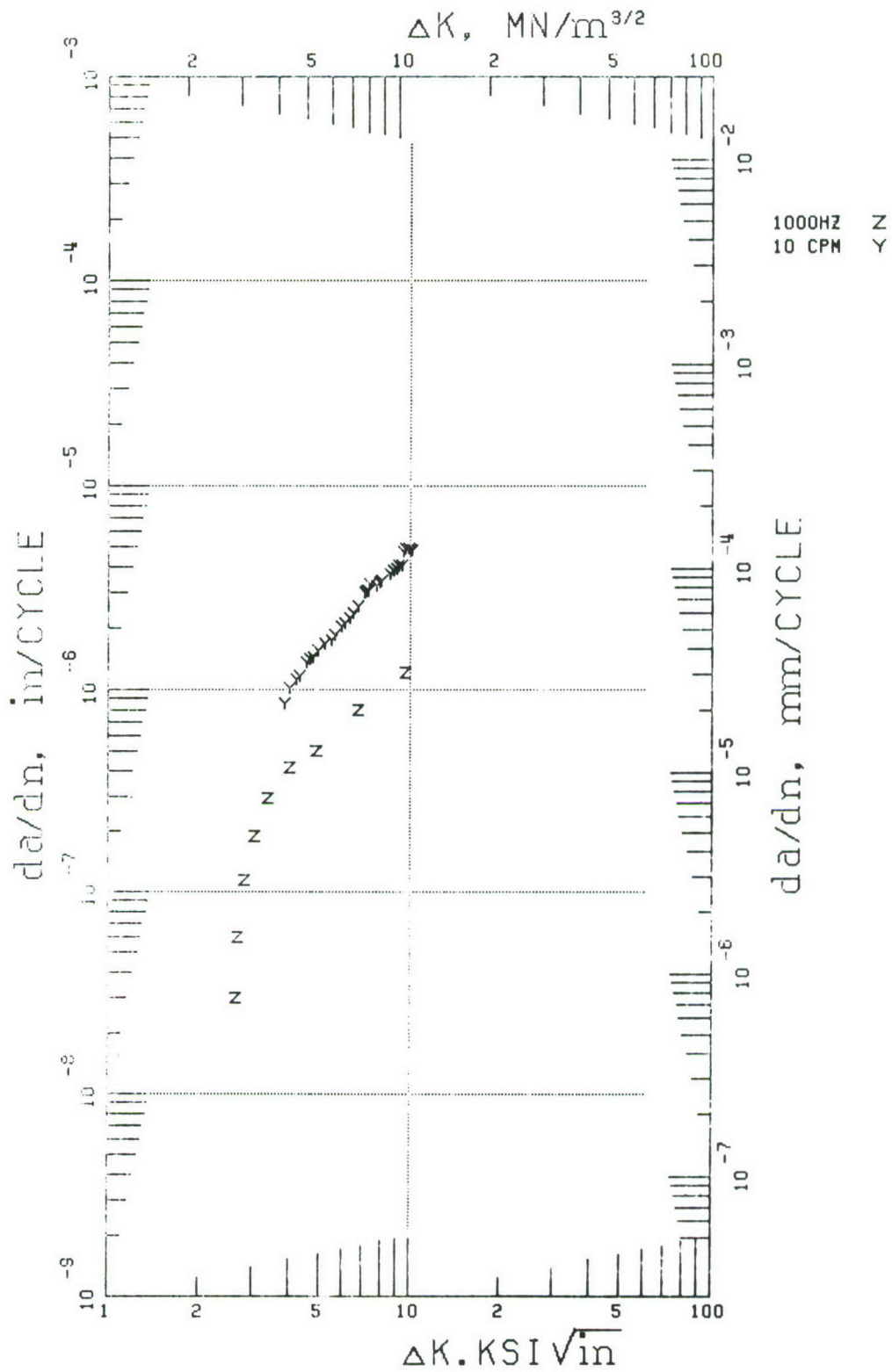Figure 40. *Effect of Frequency on Crack Growth Rate of Ti 6-2-4-2 at 1000°F, R = 0.1*

Figure 41. Effect of Frequency on Crack Growth Rate of Ti 6-2-4-2 at 1000°F, R = 0.5
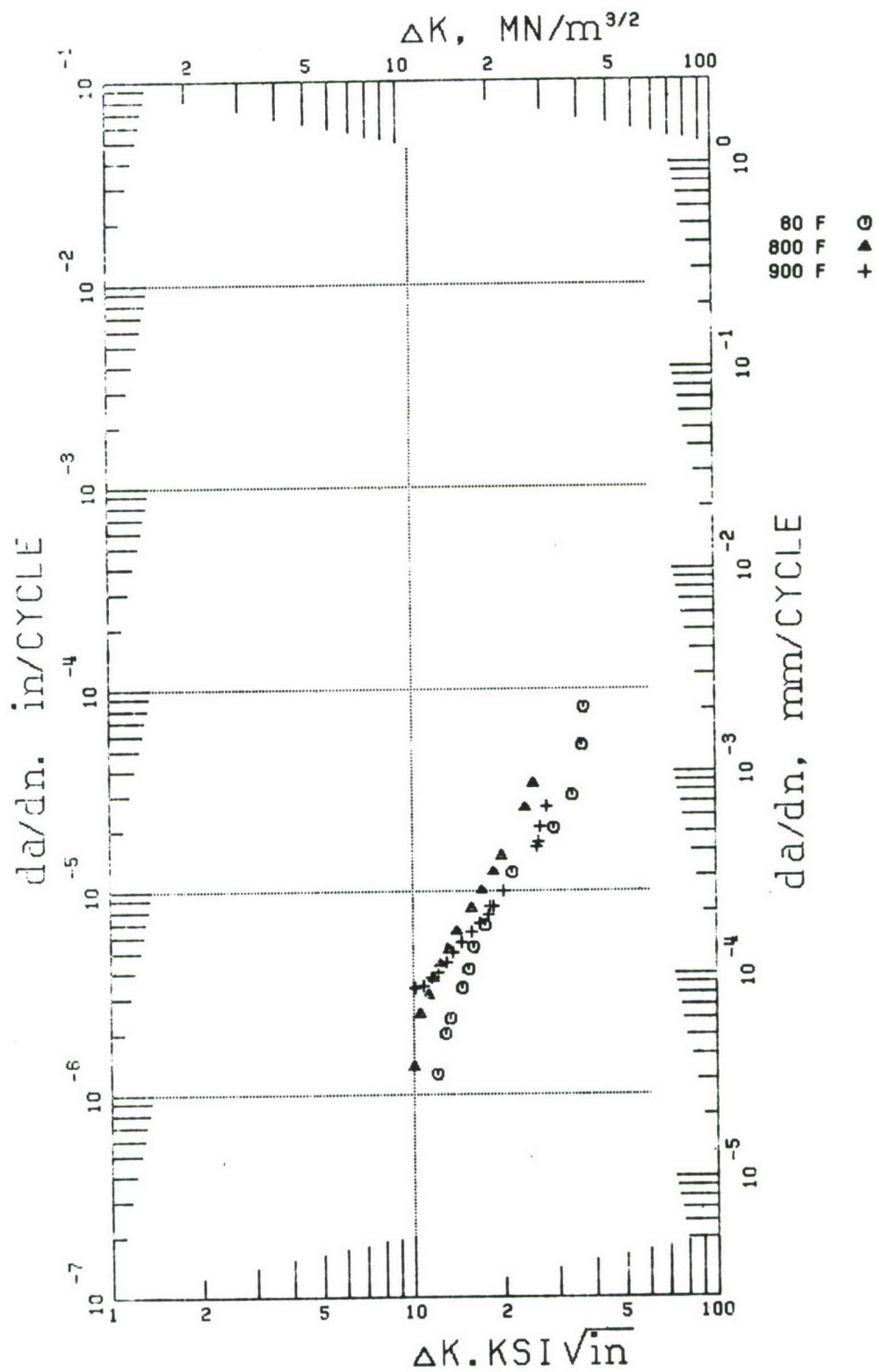
Figure 42. *Effect of Temperature on Crack Growth Rate of Ti 6-2-4-2 at 10 cpm, R = 0.1*
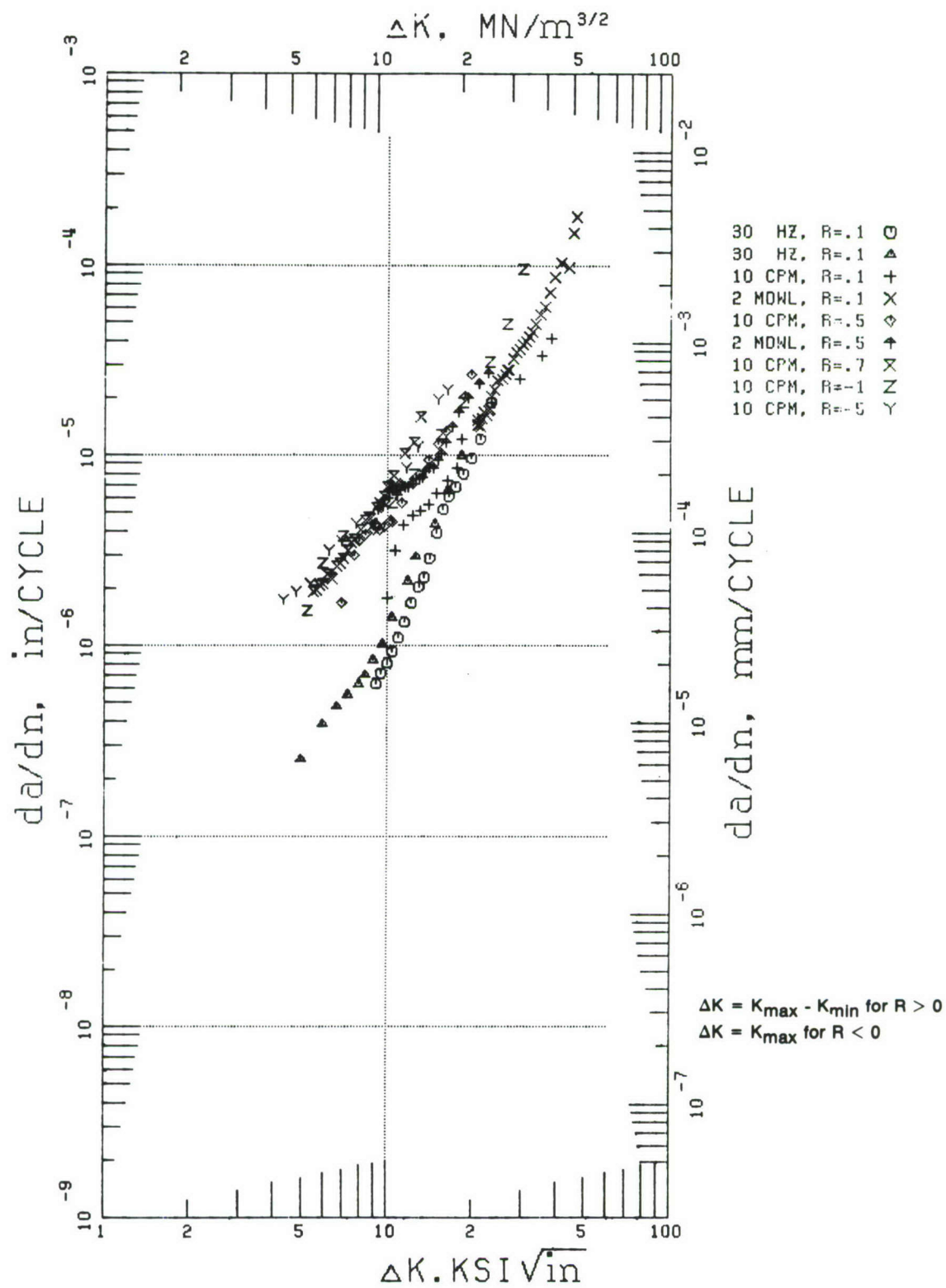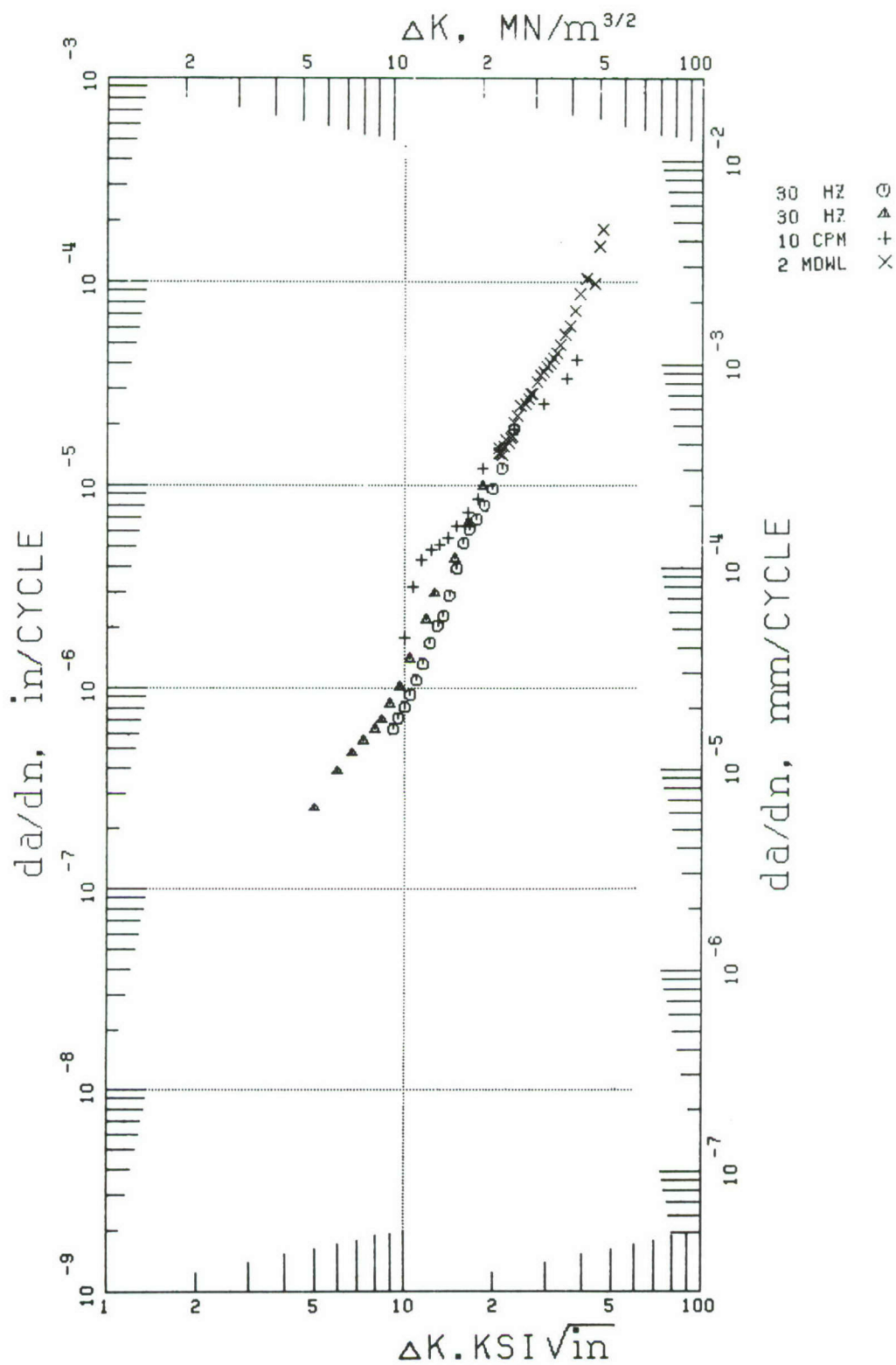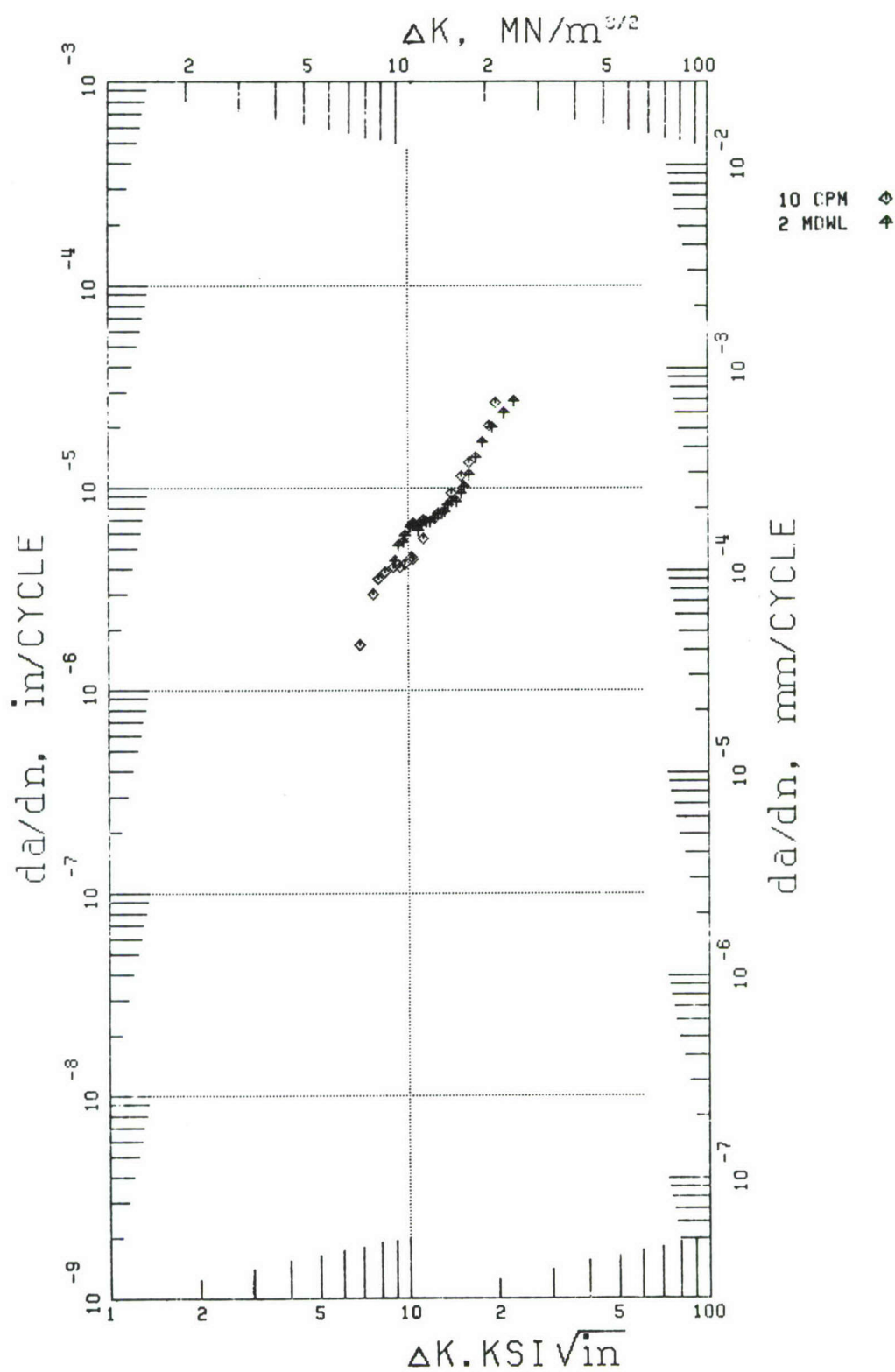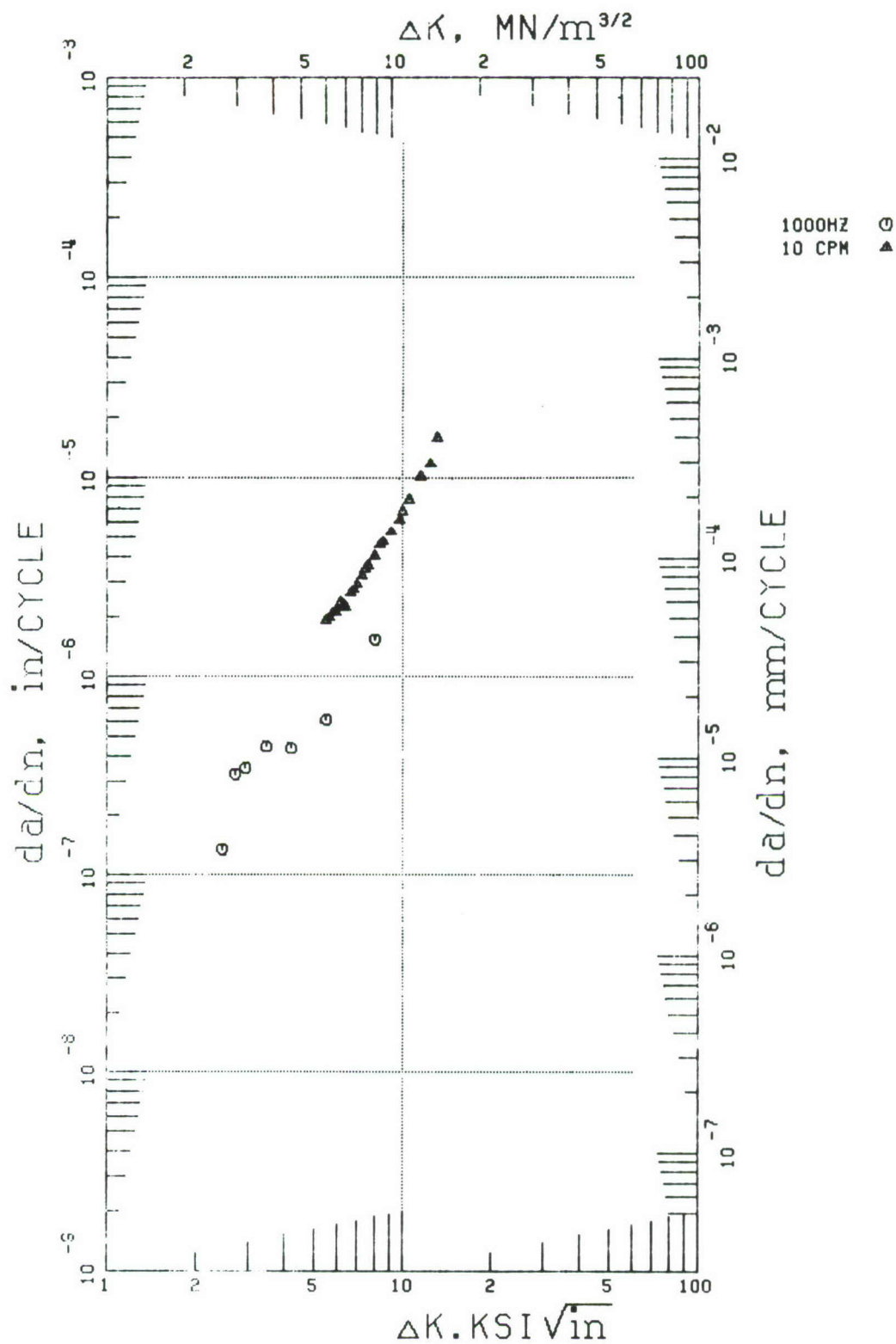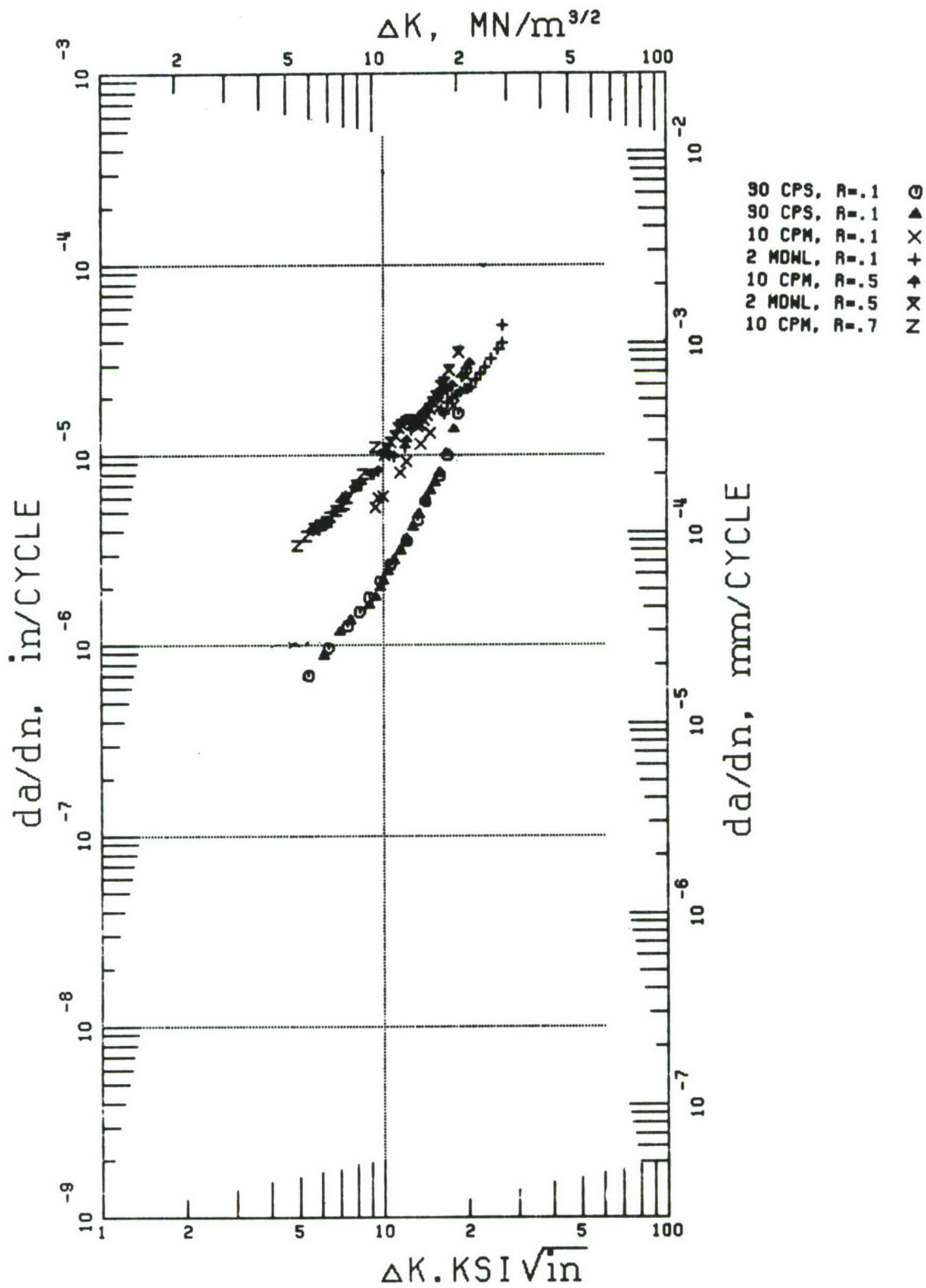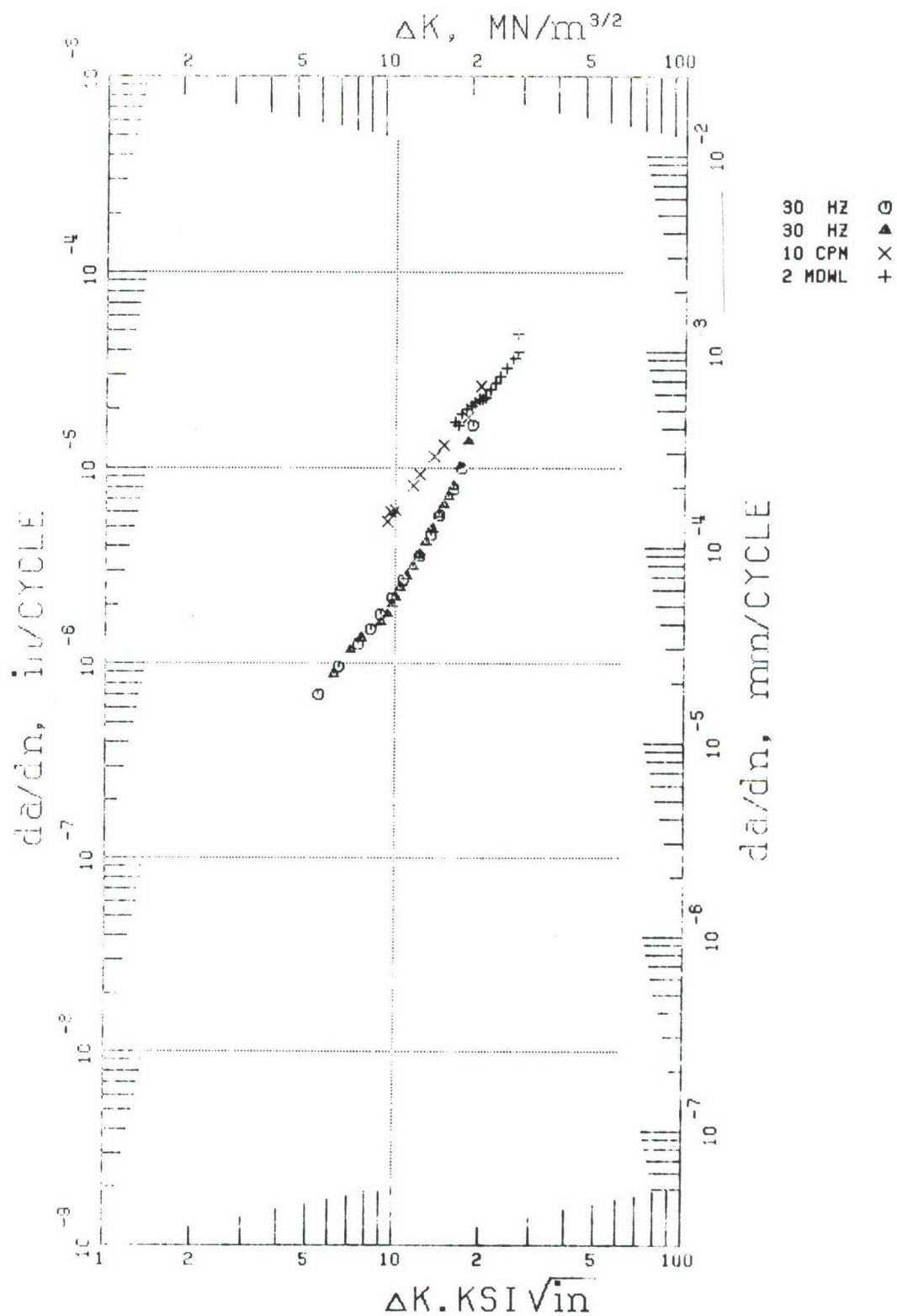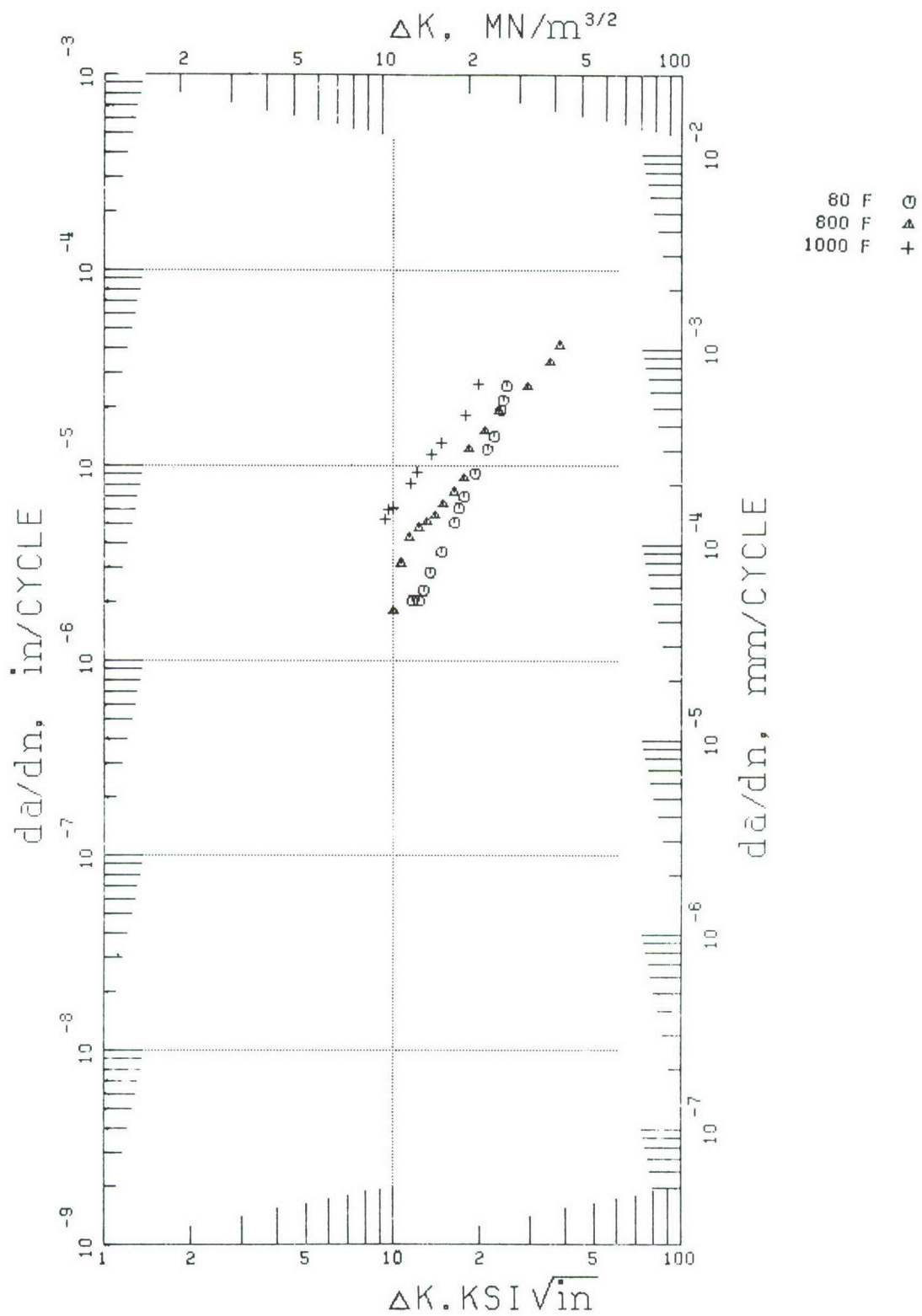
Figure 39 presents the Region II crack growth data at 1000°F (811°K), showing the effect of stress ratio on Ti 6-2-4-2 alloy at various frequencies. Figures 40 and 41 show the effect of frequency at stress ratios of 0.1 and 0.5 respectively at 1000°F (811°K). Figure 40 shows a decrease in crack growth rate for the 30 Hz data compared to the 0.17 Hz and the 0.008 Hz (2-minute dwell) data below an applied stress intensity range of 20 ksi $\sqrt{in}$. (22 MN/m$^{3/2}$). The 2-minute dwell and the 0.17 Hz tests resulted in similar crack growth rates (Figure 41). However, these tests were discontinued prior to failure due to net section creep. The final portion of these tests has not been reported because of the questionable validity of the data.

Figure 42 shows the effect of temperature on the fatigue crack growth rate of Ti 6-2-4-2 for a cyclic frequency of 0.17 Hz and 0.1 stress ratio. The room temperature data increase at a faster rate and cross the 800°F (700°K) data at $\Delta K \sim 25$ ksi $\sqrt{in}$. (22.7 MN/m$^{3/2}$). This was not expected because the K_C for this specimen thickness is highest at room temperature.

Alloy Ti 6-2-4-6

The fatigue crack propagation data for Ti 6-2-4-6 are given in Figures 43 through 52, showing the effects of stress ratio, frequency, and temperature. The effect of stress ratio at room temperature is given in Figure 43. The low fracture toughness of this alloy is evident at room temperature resulting in early failure of the positive stress ratio tests. A larger than expected decrease in growth rate was observed in the first specimen run at R = −1.0. A second test yielded similar results. These specimens were examined on the Scanning Electron Microscope (SEM) and revealed no abnormalities. R = −1.0 and 0.1 tests were examined on the SEM with cleavage dominating both fracture surfaces (Figures 44 and 45). The remaining data showed the crack growth rate to increase with increasing stress ratio as observed in Ti 8-1-1 and Ti 6-2-4-2.

Figure 46 shows the fatigue crack propagation data for Ti 6-2-4-6 at 600°F (588°K). The effect of increasing stress ratio is to increase the crack growth rate.

Figures 47 through 49 show the effect of frequency on crack growth rate at 600°F (588°K) for stress ratios of 0.1, 0.5, and 0.7 respectively. The effect of frequency is minimal at 600°F between 30 and 0.008 Hz; however, the 1000 Hz testing shows a substantial reduction in crack growth rate at the high stress ratios.

Figure 50 shows the fatigue crack propagation data at 800°F (700°K). The effect of increasing stress ratio is again to increase the crack growth rate for a given applied stress intensity (ΔK). The R = −1 tests resulted in an increase in crack growth rate, while the R = −5 showed a decrease when compared to the R = 0.1 data and plotted as K_{max}.

Figures 51 through 53 show the effect of frequency on crack growth rate at 800°F (700°K) for stress ratios of 0.1, 0.5, and 0.7 respectively. The effect of frequency is minimal at 800°F (700°K) for Ti 6-2-4-6 between 30 and 0.008 Hz. The 1000 Hz data show a reduction in crack growth at the high stress ratios.

Figure 54 shows the effect of temperature on the crack growth rate of Ti 6-2-4-6 at a stress ratio of 0.1 and a cyclic frequency of 0.17 Hz. The temperature influence is unusual with the 600°F (588°K) crack growth rate being slower than room temperature rate and the 800°F (700°K) crack growth rate being between the room temperature and 600°F (588°K) rates below ΔK of about 40 ksi $\sqrt{in}$. (44 MN/m$^{3/2}$).
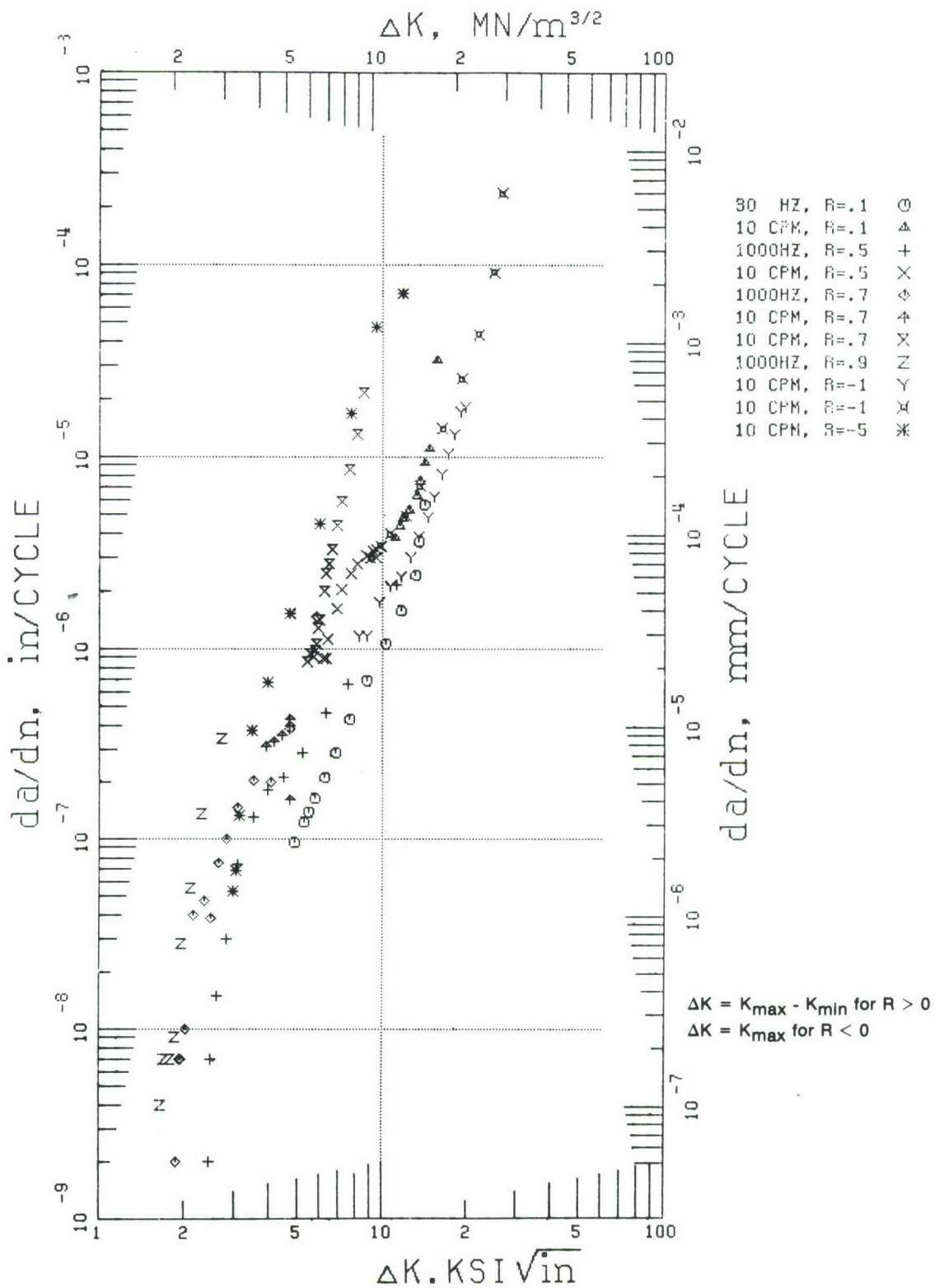
Figure 43. Crack Propagation Data for Ti 6-2-4-6 at Room Temperature
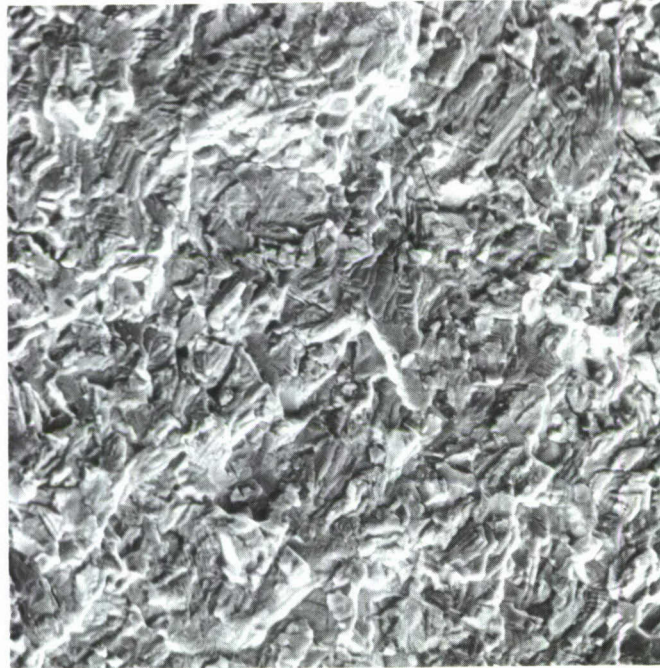
Mag: 500X

Mag: 1000X

FD 121071

*Figure 44. SEM Fractographs Showing a Cleavage
Mode of Crack Propagation in the R = −1
Test for Ti 6-2-4-6 at Room Temperature*

53
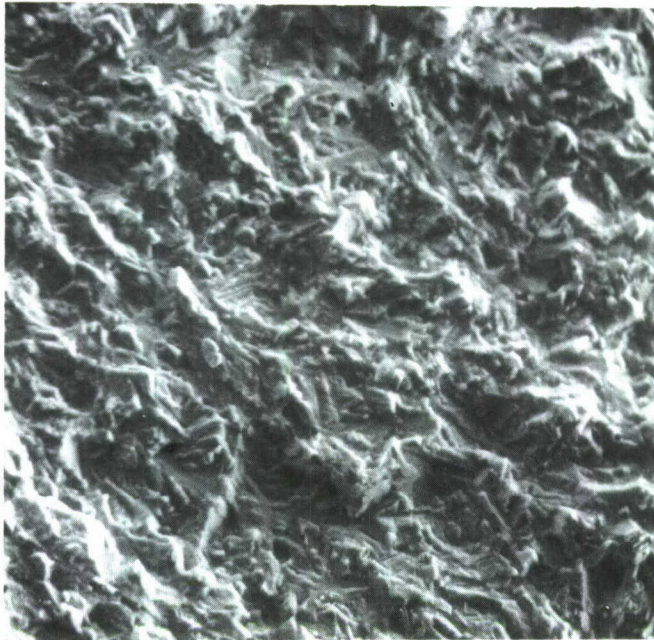
Mag: 500X

FD 121072

Figure 45. SEM Fractographs Showing a Cleavage Mode of Crack Propagation in the R = 0.1, Room Temperature Test For Ti 6-2-4-6
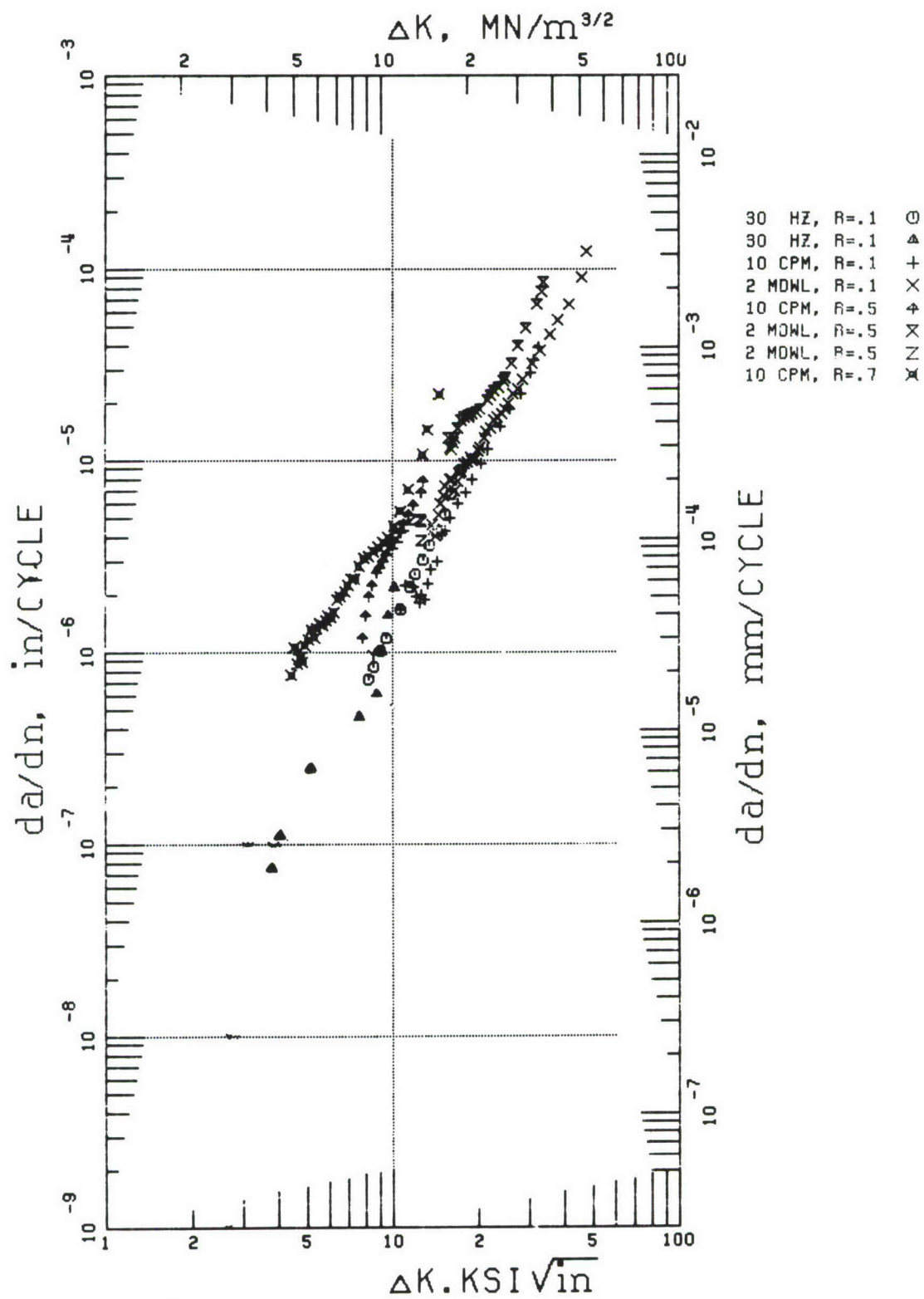
Figure 46. Crack Propagation Data for Ti 6-2-4-6 at 600°F

55
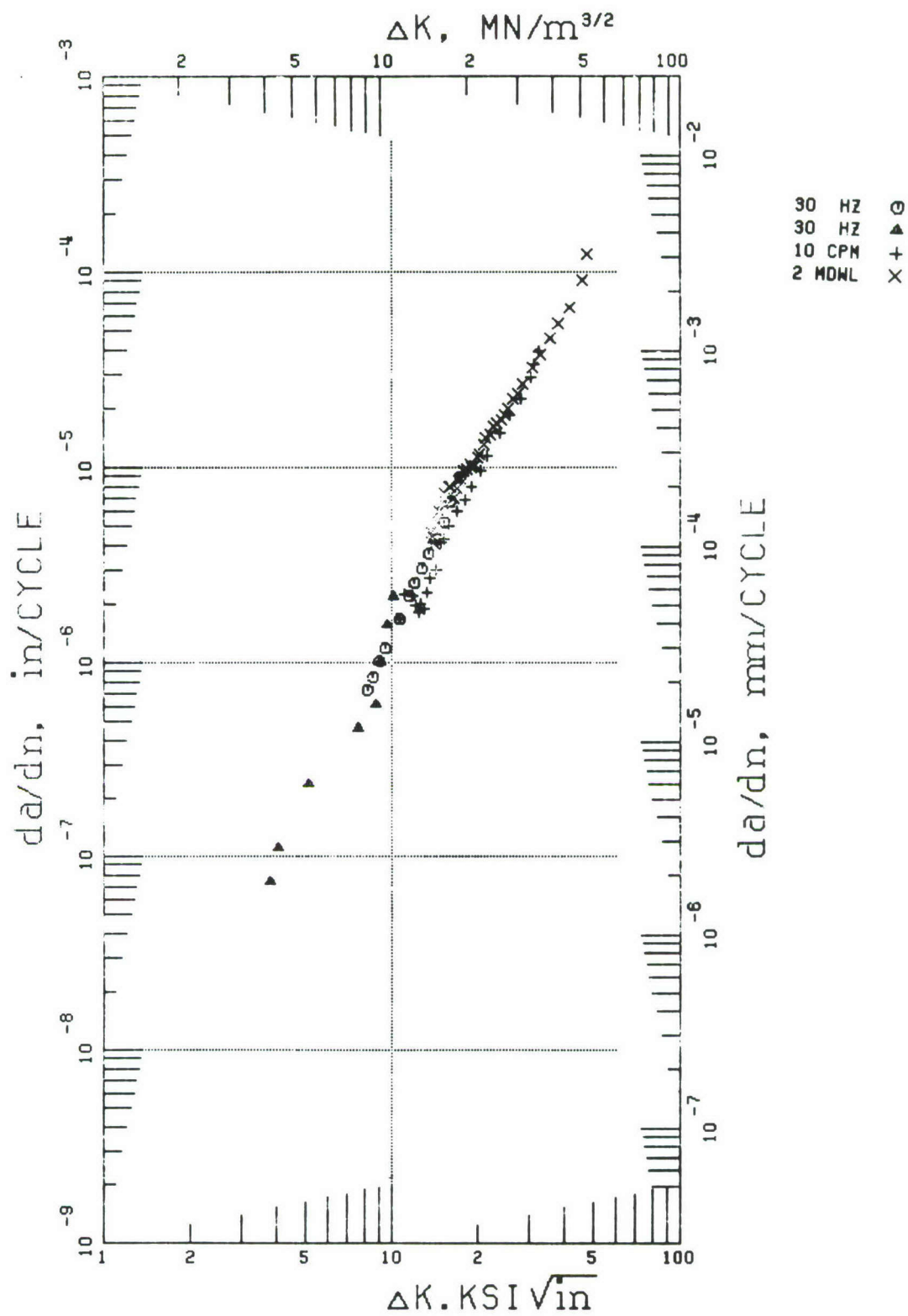
Figure 47. Effect of Frequency on Crack Growth Rate of Ti 6-2-4-6 at
600°F, R = 0.1
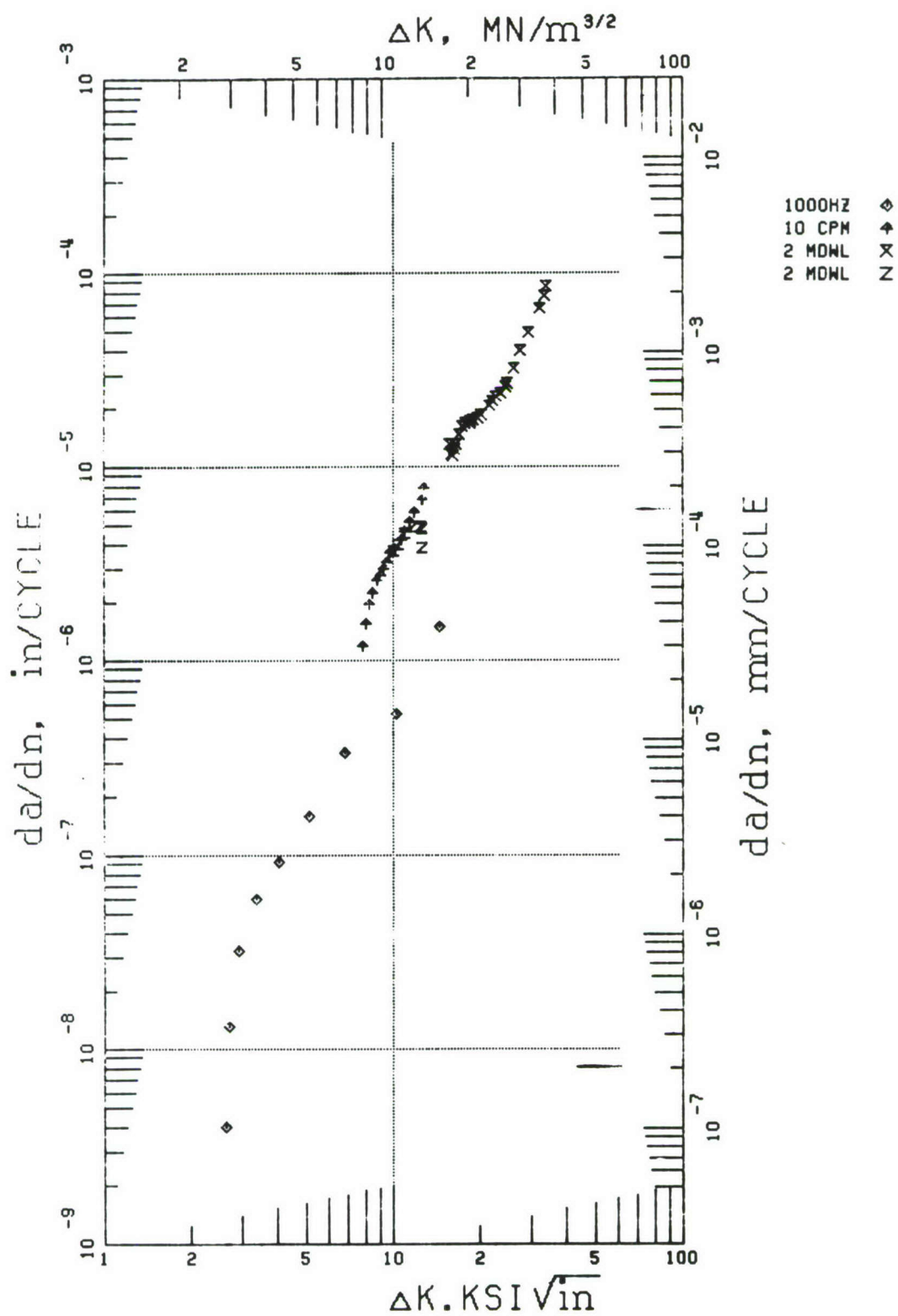
Figure 48. Effect of Frequency on Crack Growth Rate of Ti 6-2-4-6 at 600°F, R = 0.5
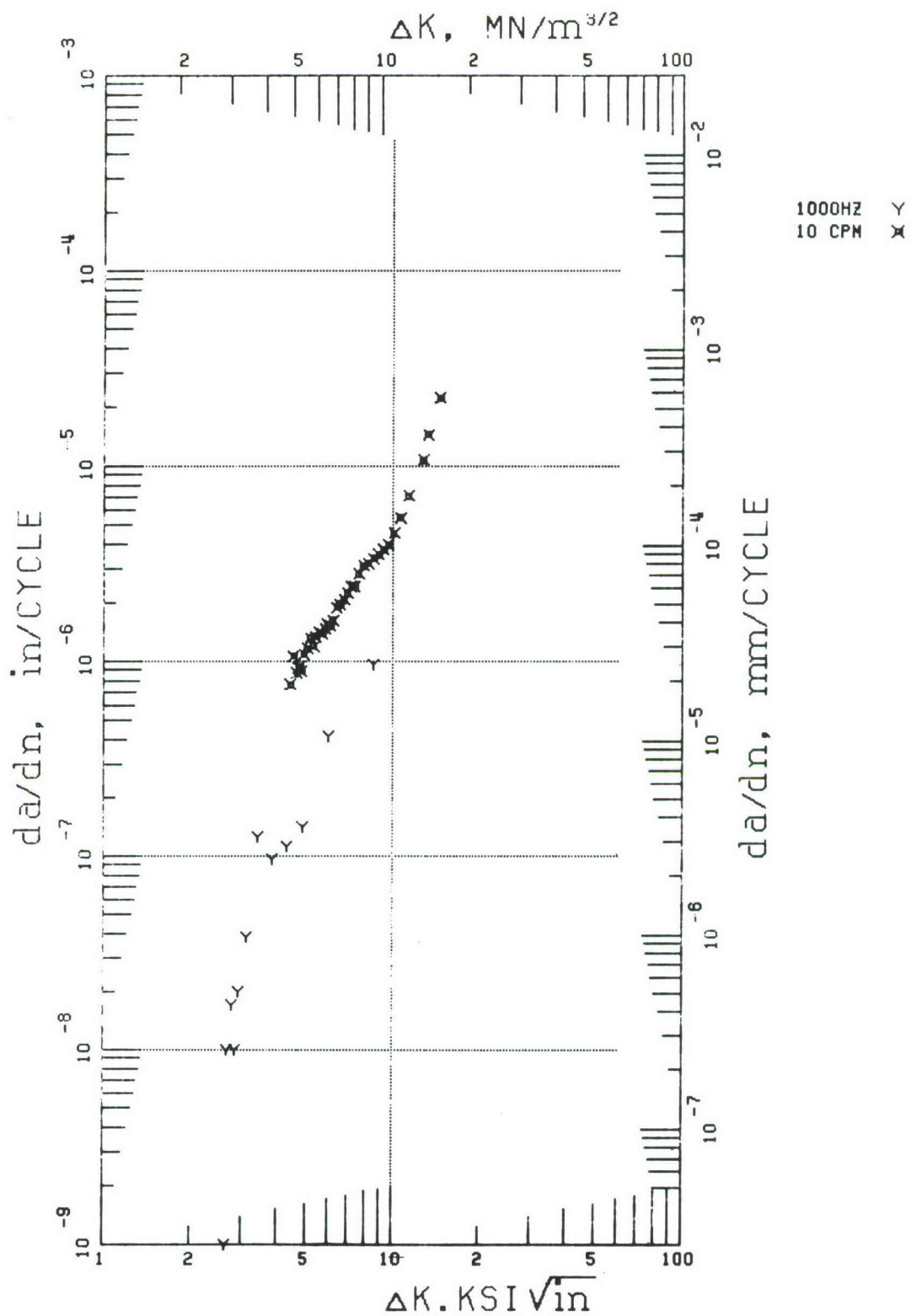
Figure 49. *Effect of Frequency on Crack Growth Rate of Ti 6-2-4-6 at 600°F, R = 0.7*
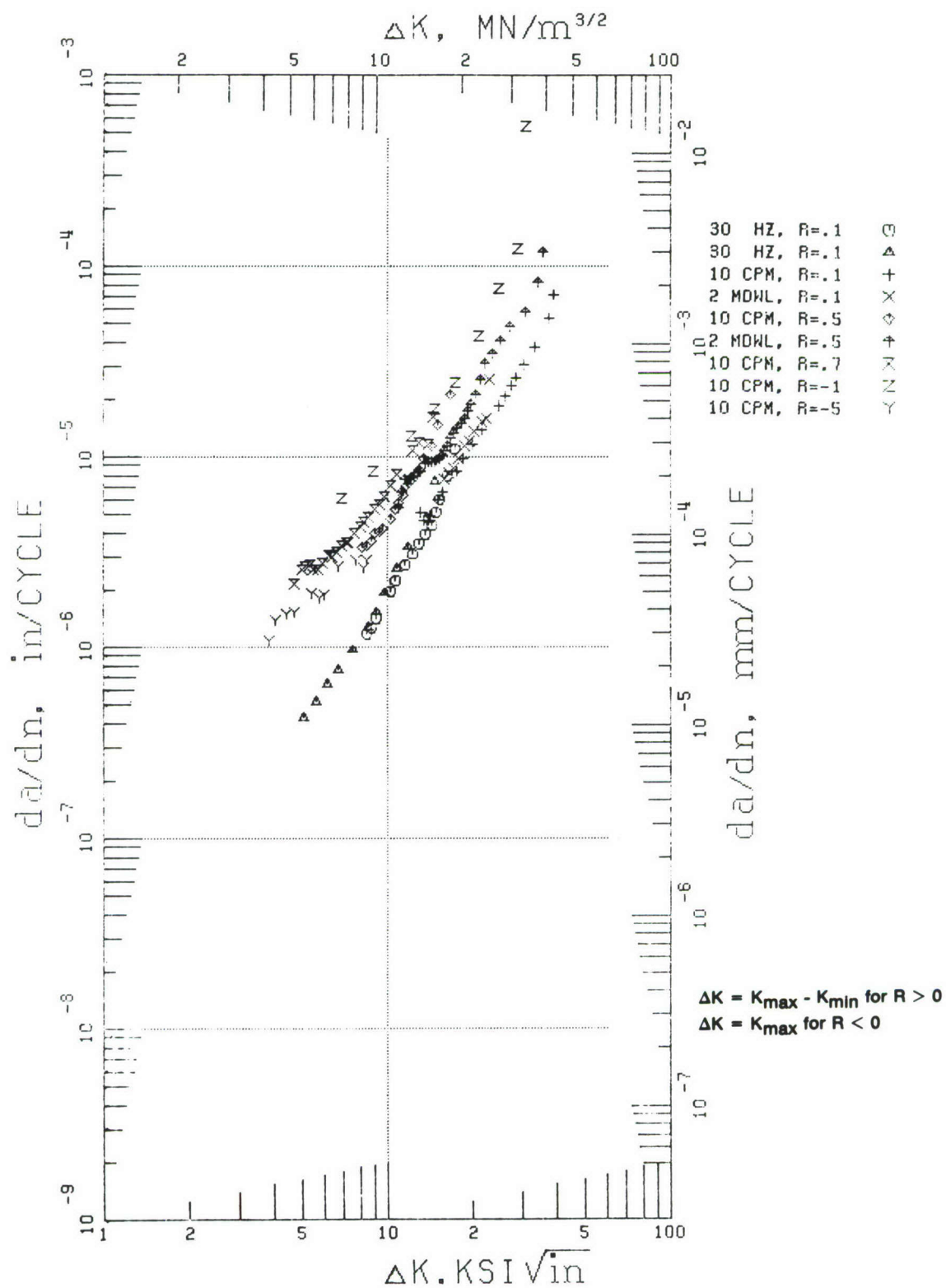
Figure 50. Crack Propagation Data for Ti 6-2-4-6 at 800°F
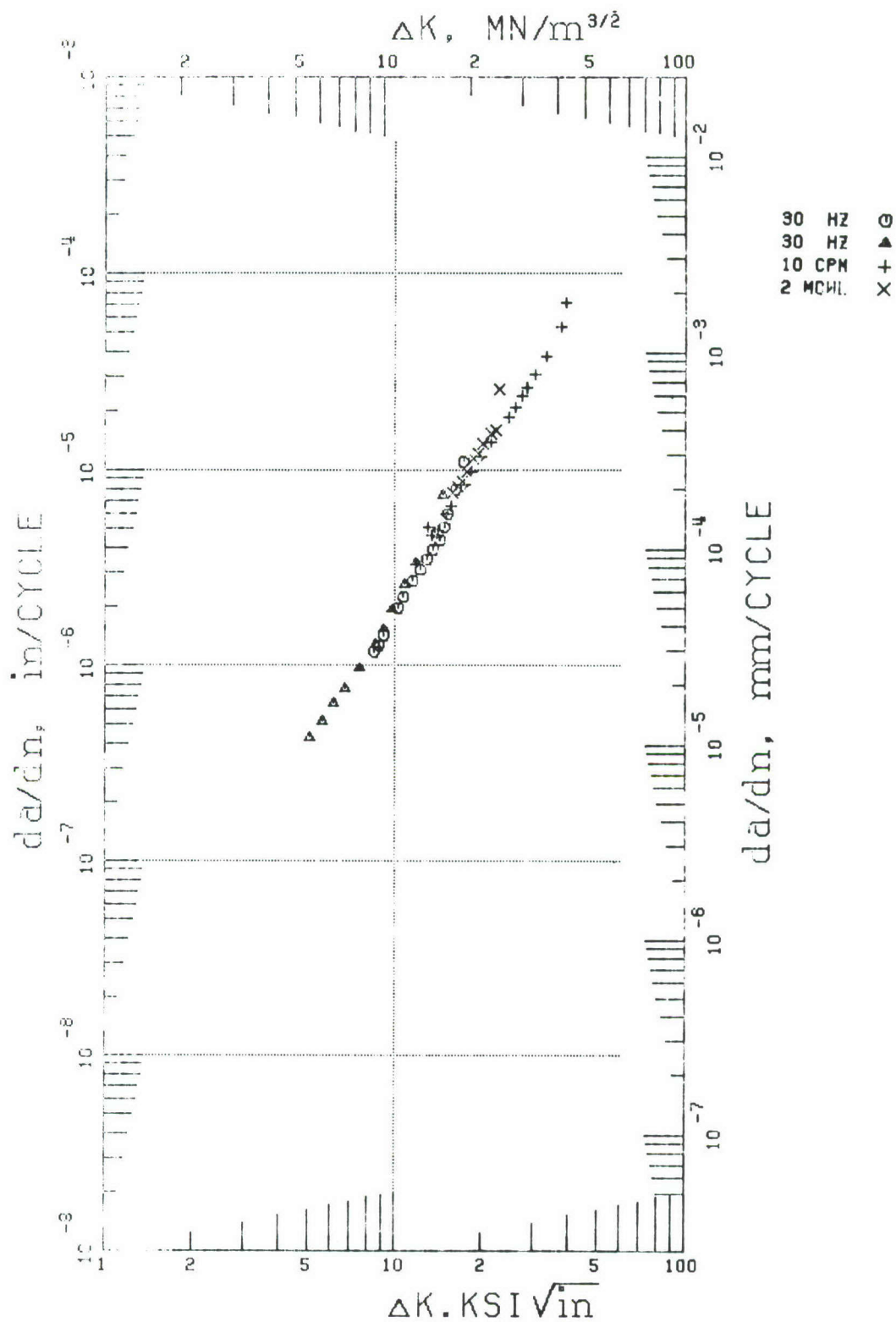
Figure 51. Effect of Frequency on Crack Growth Rate of Ti 6-2-4-6 at 800°F, R = 0.1
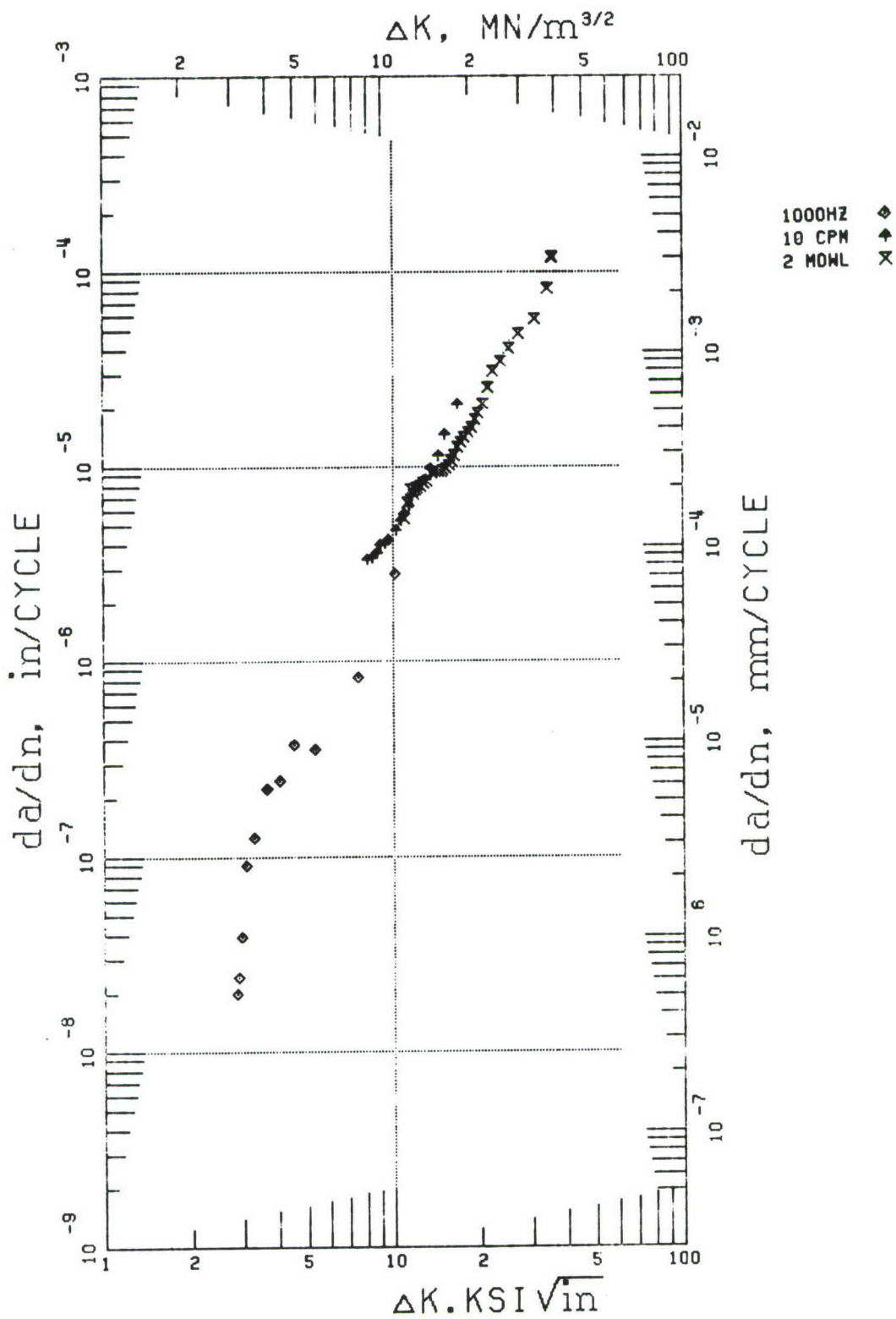
Figure 52. *Effect of Frequency on Crack Growth Rate of Ti 6-2-4-6 at 800°F, R = 0.5*

Figure 53. *Effect of Frequency on Crack Growth Rate of Ti 6-2-4-6 at 800°F, R = 0.7*

Figure 54. Effect of Temperature on Crack Growth Rate of Ti 6-2-4-6 at 10 cpm, R = 0.1

FRACTURE TOUGHNESS

Region III analysis consisted of fracture toughness (K_{I_c}) tests at various temperatures on the Ti 8-1-1, Ti 6-2-4-2, and Ti 6-2-4-6 alloys. Three specimen thicknesses were precracked in accordance with the standards given in ASTM E-399. In addition, a precracking procedure was employed at the test temperature to ensure crack propagation in the proper mode for the final test.

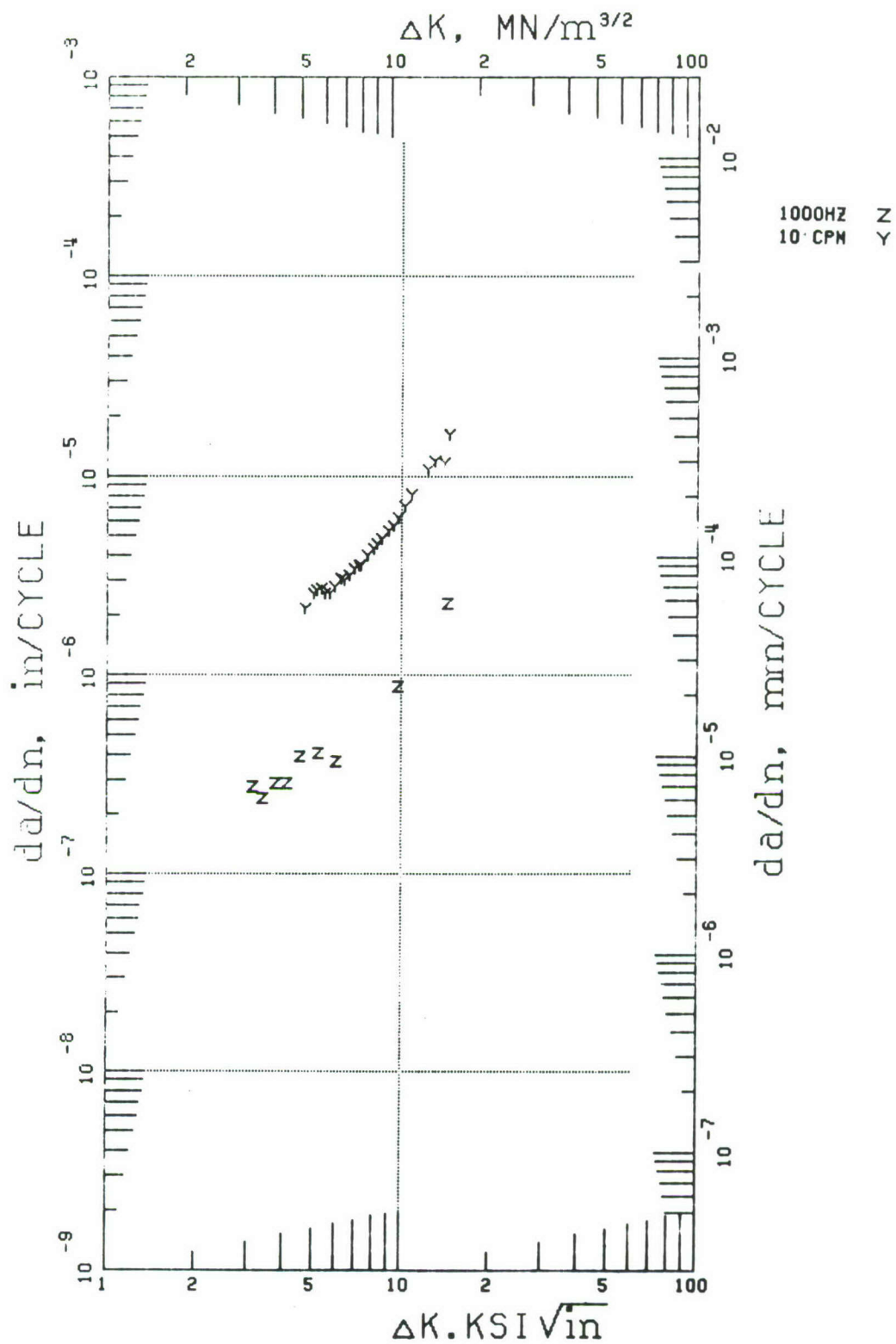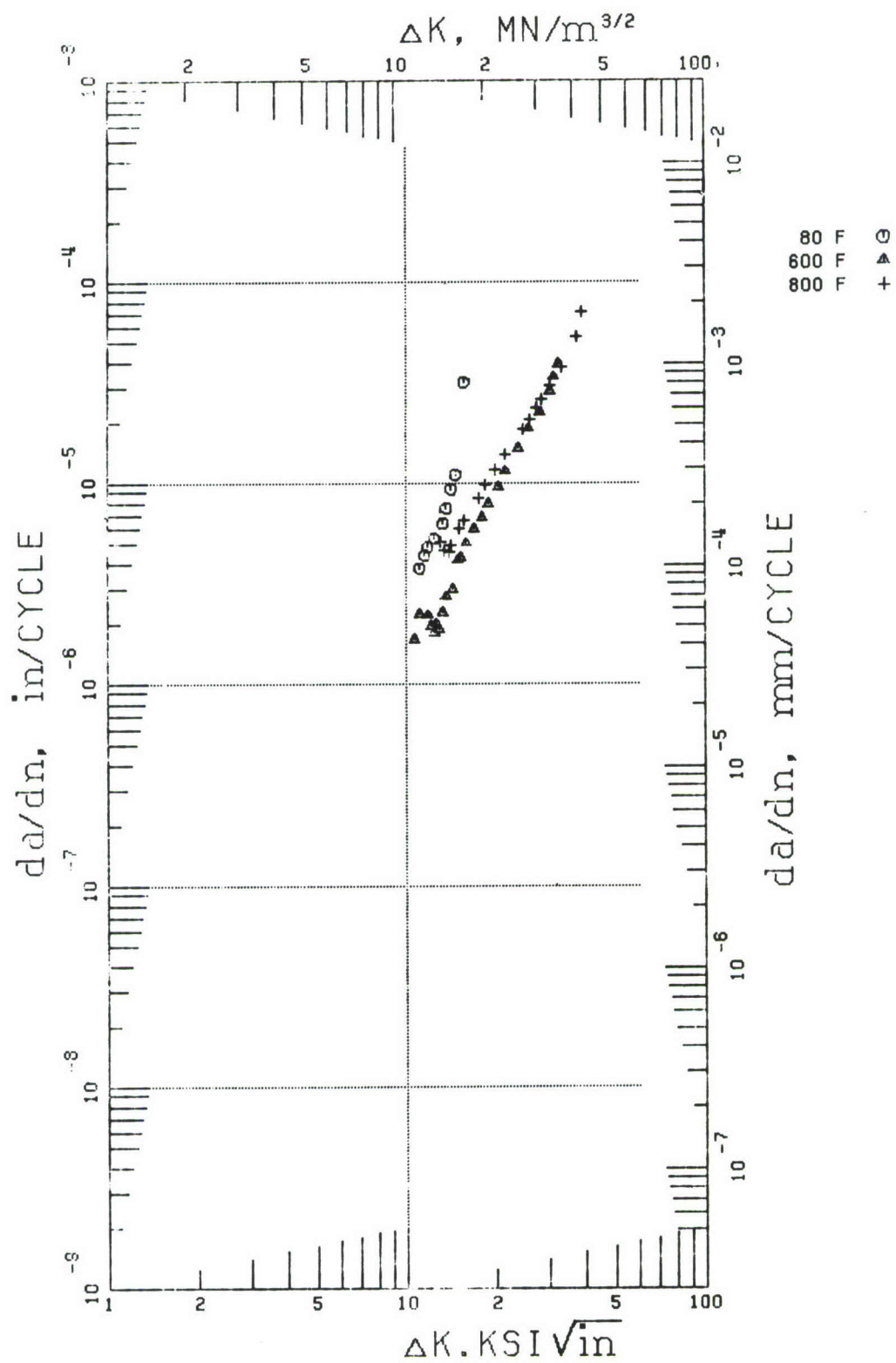The results of K_{I_c} testing are given in Table 9, and Figures 55 through 57 for Ti 8-1-1, Ti 6-2-4-2, and Ti 6-2-4-6, respectively. Three thicknesses, 0.050, 0.10, and 0.50 in. (0.127, 0.254, and 1.27 mm) were chosen to represent actual engine hardware thicknesses rather than to give theoretically valid K_{I_c} values. The room temperature 0.50 in. thick specimens gave the only valid K_{I_c} values of 38.2, 42.9 and 24.4 ksi $\sqrt{in}$. (42.0, 47.1, 26.8 MN/m^{1½}) for Ti 8-1-1, Ti 6-2-4-2, and Ti 6-2-4-6 respectively. Valid values of K_{I_c} were also obtained at a thickness of 0.10 in. (0.254 mm) on the Ti 6-2-4-6 alloy at room temperature.

Figure 55a shows the fracture toughness of Ti 8-1-1 to increase substantially with temperature for the thicker 0.50-in. (1.27-mm) specimen. Figure 55b shows that fracture toughness increases with thickness at 800 and 900°F (700 and 755°K) while at room temperature there is a decrease in the fracture toughness as it becomes a valid K_{I_c} in the 0.50-in. thick specimen.

The fracture toughness of Ti 6-2-4-2 is given in Figure 56. Figure 56a shows the K_c to decrease with temperature for the 0.05 and 0.10-in. thick specimens. The 0.50-in. thick specimen again shows an increase in K_c with increasing temperature. Figure 56b shows that K_c increases with thickness at 800 and 1000°F (700 and 811°K).

Figure 57 shows the effects of temperature and thickness on the fracture toughness of Ti 6-2-4-6. At room temperature, this alloy exhibits the lowest K_c of the three alloys tested. Figure 57a shows the K_c of Ti 6-2-4-6 to increase with temperature in all three thicknesses tested. Figure 57b shows the K_c to increase with thickness in the 0.05 to 0.10-in. range at high temperatures but to level out very quickly above 0.100 in. in thickness. The value for the 0.50-in. (1.27 mm) thick specimen at high temperature is approaching valid K_{I_c} levels. At room temperature, the K_c level shows a very slight decrease with thickness with both of the thicker specimens giving a valid K_{I_c} value.

Figure 58 shows representative fracture surfaces for the three fracture toughness specimen types and thicknesses used in this program. The room temperature and high temperature precracks show up very clearly on the 0.5-in. (1.25-mm) MCT specimen as labeled on Figure 58.

LOW-CYCLE FATIGUE CRACK INITIATION

Low-cycle fatigue tests were performed on the Ti 8-1-1 alloy to determine its strain-controlled crack initiation capabilities. Such conditions occur on the surface of fan blade airfoils and fillets where local stresses are high. When combined with the fracture mechanics data, a total cyclic life prediction, including crack initiation and propagation, is possible.

The Ti 8-1-1 alloy was chosen for characterization since it is widely used in military engines and is not subject to a wide variety of heat treatments.

TABLE 9. FRACTURE TOUGHNESS DATA FOR TITANIUM ALLOYS

Alloy	Heat Code	Temperature (°F)	Specimen Dimensions		Precrack Conditions		K_c/K_{Ic} (ksi $\sqrt{in.}$)				Remarks
			Thickness	Width	Load	Crack Length	P_s	P_c	P_{max}	K_c	K_{max}
Ti 8-1-1	LULS-21B	70	0.050	0.746	708	0.284	2400	2400	2990	46.9	54.6
	LZBF-11A	70	0.099	1.746	1900	0.852			9200		71.8
	LYSJ-15	70	0.5	2.5	1388	1.483	2275	2275	2275	38.22[1]	38.22[a]
	LULS-18C	800	0.050	0.714	536	0.376	1200	1200	1595	30.9	41.1[a]
	LZBF-11B	800	0.101	1.746	1950	0.887	5200	5200	8000	41.0	63.1
	LYSJ-17	800	0.5	2.5	1388	1.449	5900	5900	6100	94.4	100.8
	LULS-21A	900	0.051	0.746	571	0.423	1370	1370	1730	37.3[a]	47.1
	LZBF-12A	900	0.102	1.746	1958	0.860	5600	5600	9080	42.8	69.4
	LYSJ-16	900	0.5	2.5	1388	1.422	6000	6000	6400	92.4	98.6
	LULS-19A	70	0.050	0.750	562	0.396			2165		59.75
Ti 6-2-4-2	LWDD-6B	70	0.051	0.744	682	0.305	2280	2280	2990	47.0	61.7
	LWDD-1F	70	0.101	1.746	1939	0.889	7500	7500		59.5	77.8
	LWCC-9A	70	0.502	2.5	1700	1.289	3300	3300	3300	42.9[1]	42.9
	LWDD-6G	800	0.051	0.743	800	0.572	840	840	840	35.2[a]	35.2
	LWDD-1E	800	0.101	0.746	1947	0.948	5280	5280	7220	44.5	60.8
	LWCC-9B	800	0.501	2.5	1800	1.327	6720	6720	6980	91.4	94.9
	LWDD-6F	1000	0.050	0.745	595	0.260	1290	1290	1770	30.4	41.8
	LWDD-1G	1000	0.089	1.746	1717	0.838	5340	5340	7280	34.4	46.8
	LWCC-9C	1000	0.502	2.5	1700	1.346	5760	5760	7350	80.6	102.9
Ti 6-2-4-6	LYKD-1H	70	0.053	0.749	515	0.353	1200	1200	1250	27.9	29.1
	LYKD-9A	70	0.102	1.752	1969	0.844	3480	3480	3700	26.1[1]	27.7
	LYKD-10A	70	0.501	2.5	1500	1.279	1895	1895	1895	24.4[1]	24.4
	LYKD-1F	600	0.040	0.748	478	0.385	1470	1470	1880	46.1	59.0
	LYKD-9C	600	0.103	1.752	2003	0.738	8400	8400	11380	55.6	75.2
	LYKD-10B	600	0.5025	2.5	1500	1.307	4770	4770	4770	63.4	63.4
	LYKD-1J	800	0.041	0.752	585	0.446	1320	1320	1555	46.9[a]	55.3
	LUNC-2C	800	0.100	1.742	1925	0.777	8460	8460	10700	60.2	26.1
	LYKD-10C	800	0.502	2.5	1500	1.340	4620	4620	4660	64.2	64.7

[1] Valid K_{Ic}
[a] Nonsymmetric Cracking >25%
[3] $\sigma_{net} > \sigma_y$

65
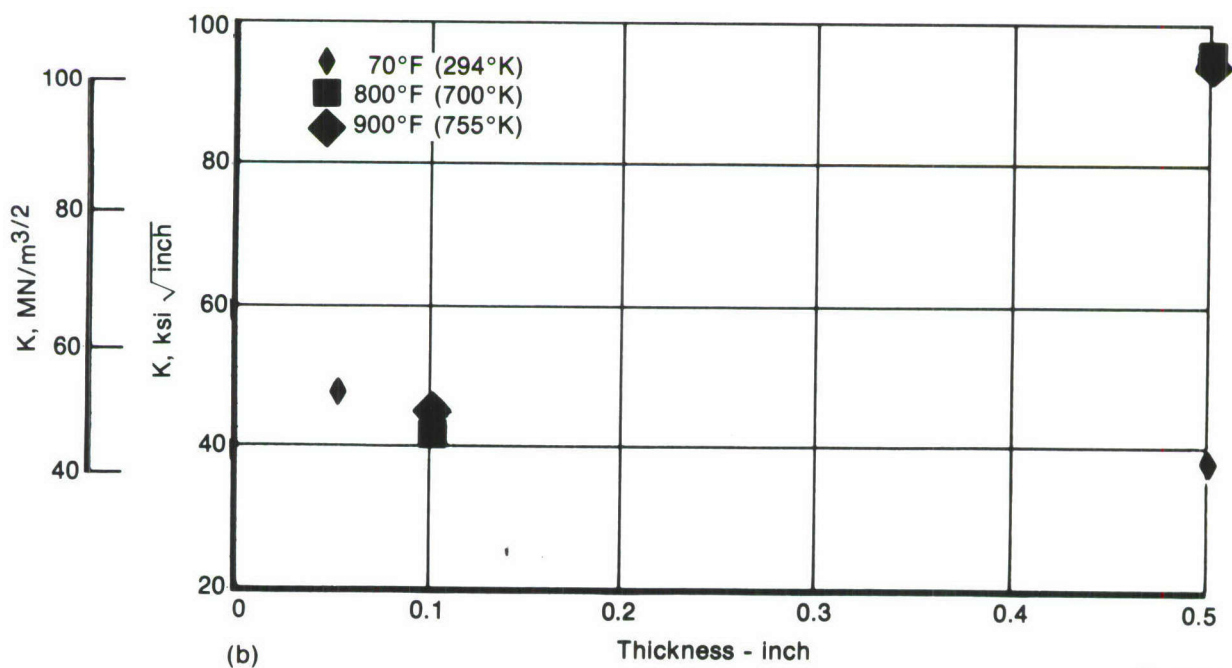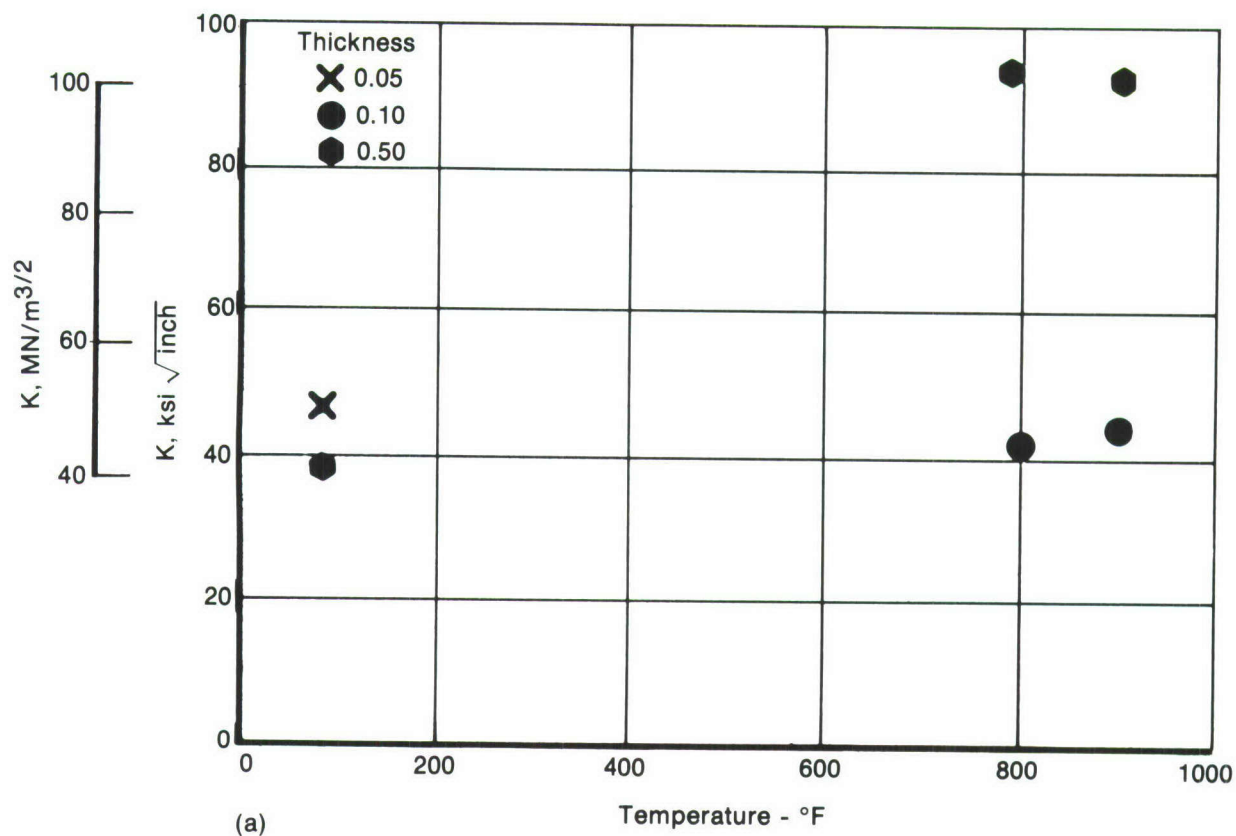
Figure 55. *Fracture Toughness of Ti 8-1-1 Showing the Effect of Temperature and Thickness*

FD 121073

66
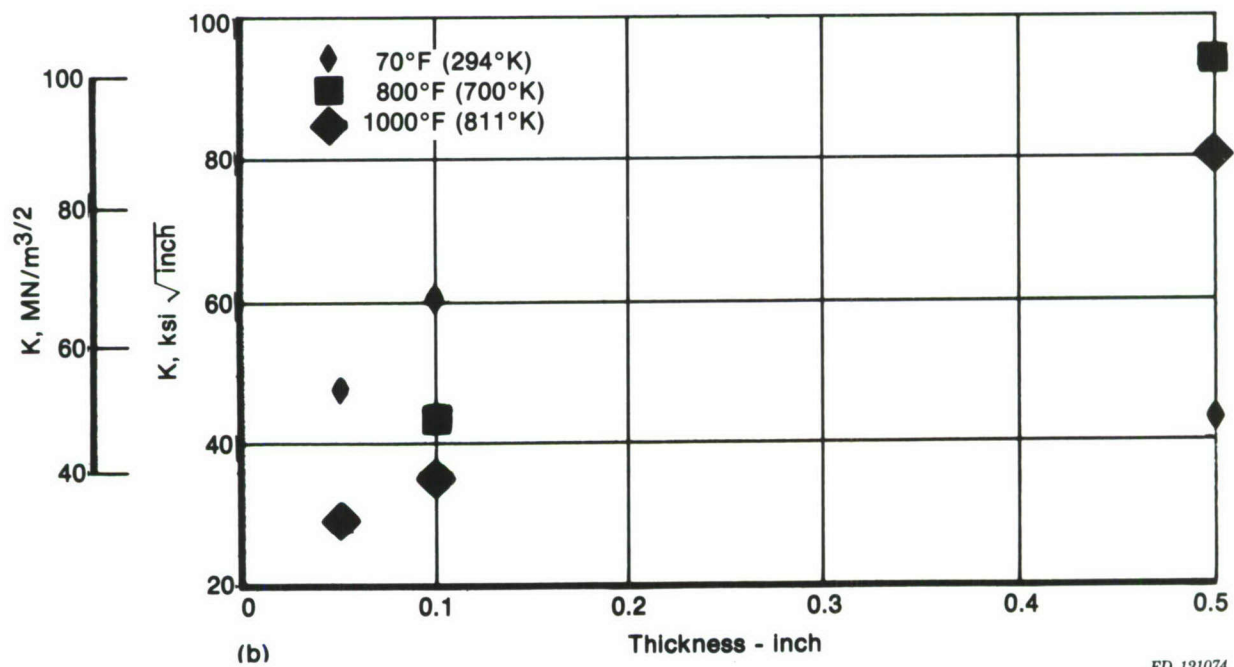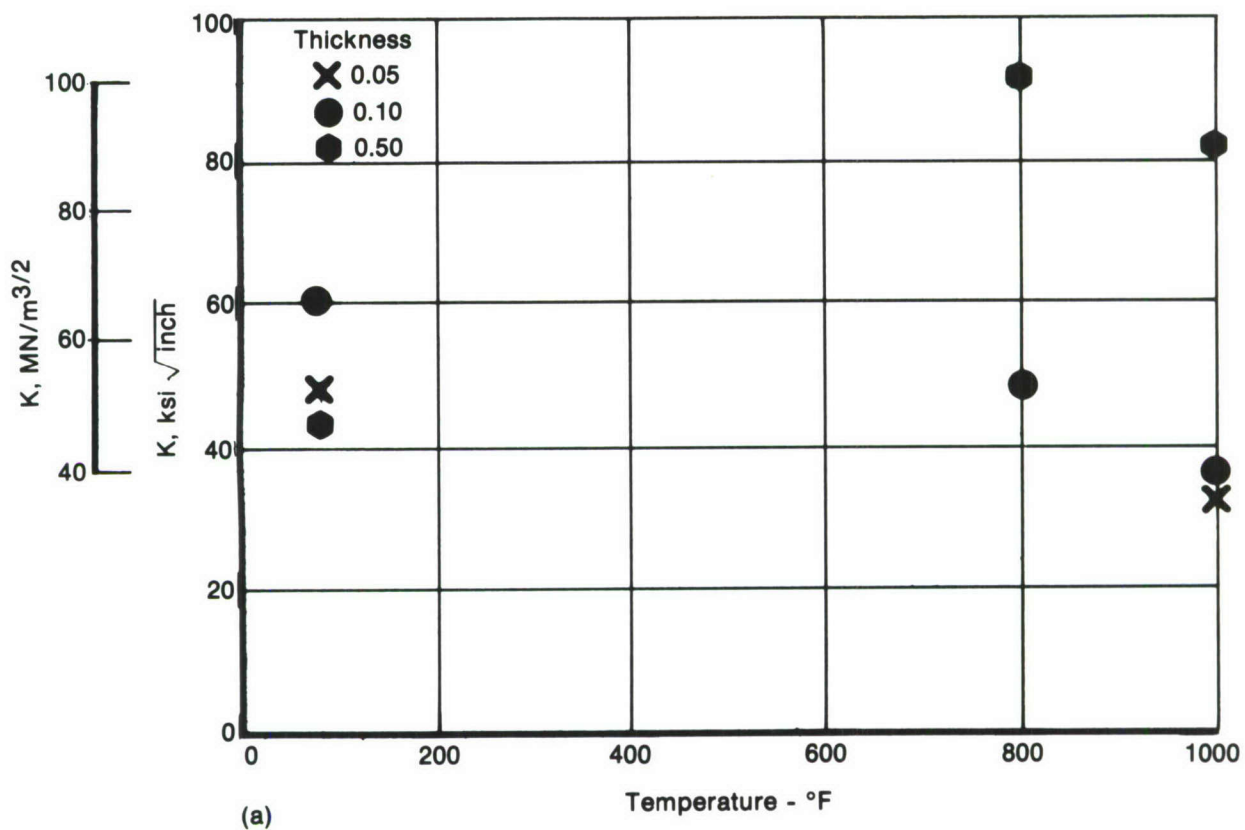
Figure 56. Fracture Toughness of Ti 6-2-4-2 Showing the Effect of Temperature and Thickness
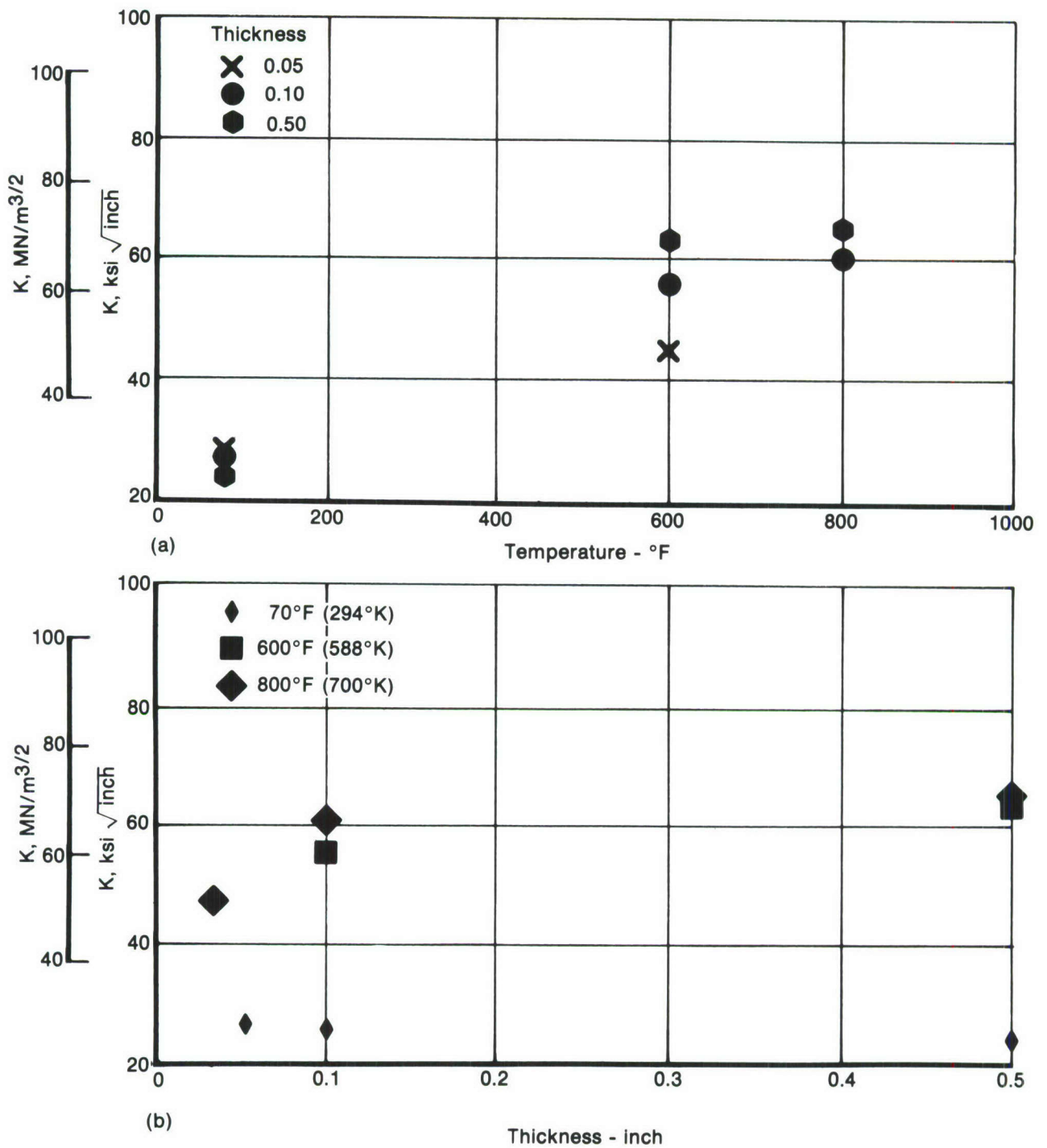
FD 121074

Figure 57. *Fracture Toughness of Ti 6-2-4-6 Showing the Effect of Temperature and Thickness*

FD 121075

Room Temperature Precrack

Temperature Precrack

FD 121076

Figure 58. Comparison of Fracture Surfaces from Specimens Used for K_c Testing: 0.05 inch Thick Center Flaw, 0.10 inch Thick Center Flaw, and 0.50 inch Thick Modified Compact Tension

The techniques used in the LCF testing were previously described in the literature (Reference 4), and in the recommended practice for constant amplitude, low-cycle fatigue testing now being drafted by the E-9.08 committee of ASTM. A smooth strain-controlled cylindrical specimen (Figure 59) was used because it produces a nearly uniform strain field and evaluates both a relativ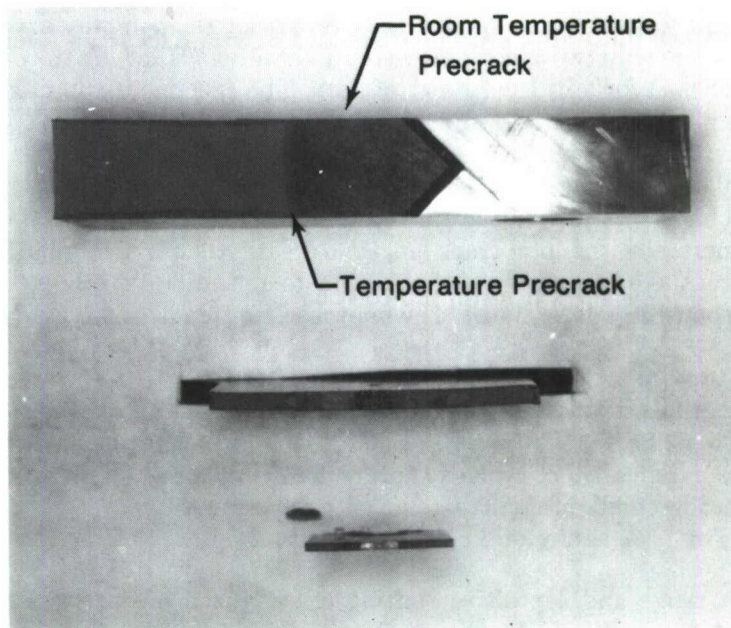ely large surface area and volume. The specimens were tested on a closed-loop servo-hydraulic test rig using a sine wave function. The dwell tests utilized the same loading rate as the 10 cycles per minute tests with a 2-minute hold at maximum tensile strain. The axial strains were controlled through the use of an averaging type extensometer measuring displacements between ridges defining a 1-in. gage length. The gage section of the specimen was electropolished before testing to remove any residual surface stresses resulting from the machining process.

The LCF tests were run at three strain ranges and three strain ratios to produce failures between 10^3 and 3.0×10^4 cycles. A list of the test conditions and resulting stresses, plastic strain, and cycles to failure are given in Table 10. Tests were also run at two cyclic frequencis used in the crack growth testing, 10 cycles per minute and 2-minute dwell cycle. The 2-minute dwell tests at 800 and 900°F (700 and 755°K) showed a small amount of stress relaxation, and the resulting inelastic strain observed at maximum tensile load is also given in Table 10. The 10 cycles per minute testing indicated no stress relaxation.

Figure 60 shows a typical hysteresis loop obtained from the 10 cycle per minute and 2-minute dwell testing with a schematic representation of stress range, mean stress, elastic and plastic strains, and strain range.

Four specimens were tested at several of the strain ranges to increase the statistical significance of the data while only two specimens were run at others, allowing the effect of strain range on life to be established for a broader range of data. The specimens run in groups of four were inspected for crack initiation, designated to be a surface macrocrack equal to 1/32 in. (0.0128 mm). The results of these inspections are given in Table 10. Difficulties were encountered in determining a 1/32-in. (0.0128-mm) crack because of multiple crack initiation sites in most of the testing. Cracks approaching 1/32 in. (0.0128 mm) in surface length generally linked up with adjacent small cracks, increasing the total crack length to greater than 1/32 in. (0.0128 mm). This made it very difficult to make comparisons of the data to initiation of 1/32-in. (0.0128-mm) cracks. These data are shown in a later figure showing the same trends as failure data discussed below.

The effect of alternating strain on fatigue life to failure of Ti 8-1-1 is shown in Figure 61 for 800°F (700°K) and Figure 62 for 900°F (755°K). At both temperatures little effect of mean strain or strain ratio ($\epsilon_{min}/\epsilon_{max}$) is indicated for cycles to failure. The tests run at strain ratios of zero and $-\infty$, given in Figure 61, show small differences in life with the strain ratio of $-\infty$ having a shorter life above a strain range of 1.5% and a longer life below that level.

Increases in strain range and a positive shifting of stabilized mean stress are shown to decrease fatigue life of Ti 8-1-1 alloy in Figure 63. Constant life lines are given on Figure 63 for 1, 10, and 30K lives showing a strong dependence on alternating strain range and a limited effect caused by stabilized mean stress. These curves were developed by interpolation of the data given on Figures 61 and 62 for 800 and 900°F (700 and 755°K) respectively to the 1, 10, and 30K levels for a specific point. Similar plots were made for stabilized mean stress, which were also interpolated for the 1, 10, and 30K life levels.
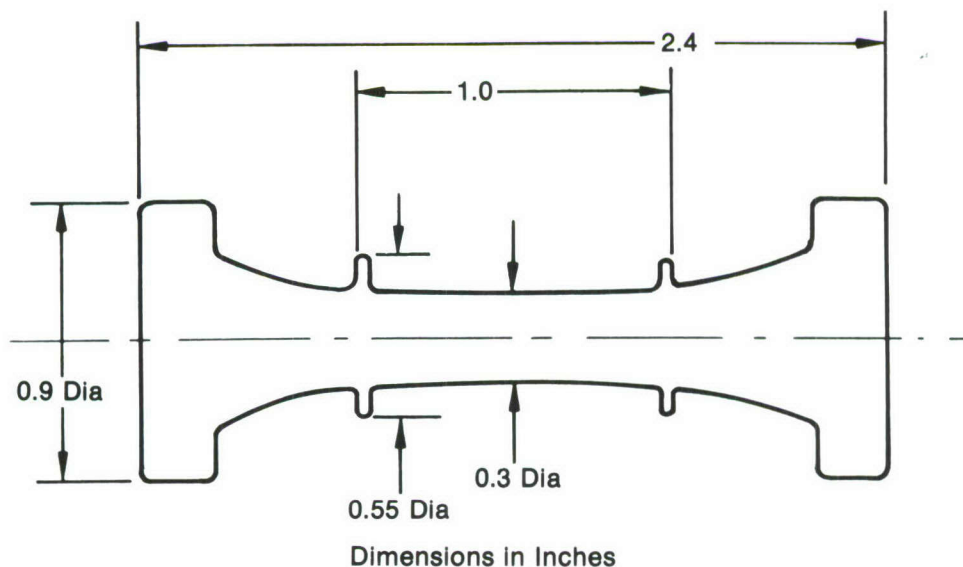
FD 121077

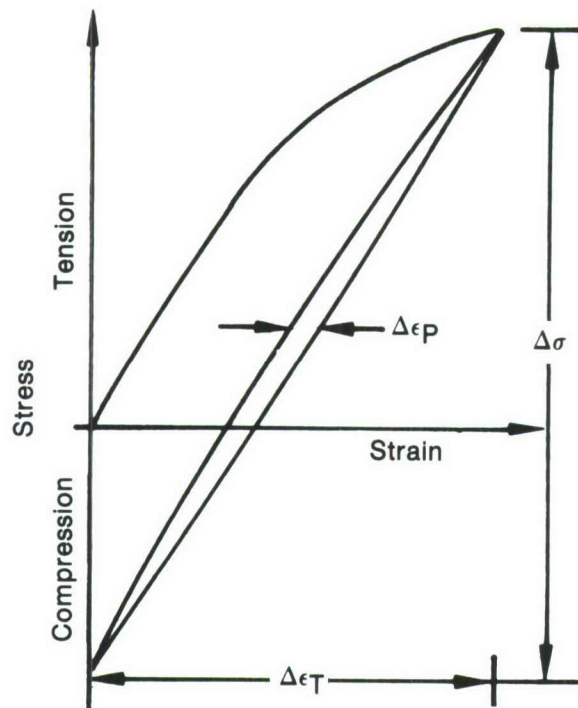*Figure 59. Strain Controlled LCF Specimen*

70

TABLE 10. LOW-CYCLE FATIGUE DATA FOR Ti 8-1-1 STRAIN CONTROL TESTING

| Heat Code	Strain Range (%)	Strain Ratio	Temperature (°F)	Frequency (cpm)	Initiation Crack (length/cycles)	Cycles To Failure	Conditions - 50% LIFE			
							Plastic Strain (%)	Mean Stress	Total Stress Range	Comments
LYSJ-9A	2.3	−∞	800	10		386	1.12	− 0.75	189.4	
LZDH-8C	2.3	−∞	800	10		630	1.02	− 1.47	178.3	
LYSJ-8A	1.0	−∞	800	10		20,100	0.08	−14.8	134.2	
LYBF-9B	1.0	−∞	800	10		15,500	0.08	−14.0	138.3	
LZBF-8B	1.4	−∞	800	10		3,920	0.33	− 8.1	165.2	
LZDH-7C	1.4	−∞	800	10		3,550	0.34	− 7.58	166.6	
LULS-8	1.2	−1.0	800	10	0.058/4,000	5,985	0.14	− 1.85	157.3	
WFTS-1	1.2	−1.0	800	10	0.052/3,000	4,540	0.23	− 1.55	149.9	
LZDH-1C	1.2	−1.0	800	10	0.023/4,000	6,370	0.18	− 2.14	154.2	
LYSJ-1A	1.2	−1.0	800	10	0.028/4,000	7,150	0.15	− 1.43	153.5	
LULS-6	2.0	0	800	10	0.042/750	1,330	0.7	+ 1.4	170.6	
LYSJ-2A	2.0	0	800	10	0.035/750	1,400	0.77	+ 0.7	175.4	
LZBF-2B	2.0	0	800	10	0.027/750	1,355	0.78	+ 1.1	172.3	
LZDH-2C	2.0	0	800	10	0.056/750	1,235	0.8	+ 1.4	167.6	
LYSJ-3A	0.7	0	800	10	0.023/18,000	26,975	0.03	+22.6	104.2	
LULS-5	0.7	0	800	10	0.013/10,100	12,640	0.02	+35.1	105.4	
LZBF-3B	0.7	0	800	10	No Cracks	15,745	0.02	+24.4	107.0	Failed Outside Ridges
LZDH-3C	0.7	0	800	10	No Cracks	59,901	0.0	+20.6	105.8	Discontinued
LYSJ-7A	0.75	0	800	10		31,340	0.02	+25.43	109.0	Discontinued
LULS-7	0.9	0	800	10	0.027/8,500	13,300	0.01	+17.75	126.0	
LYSJ-10A	0.9	0	800	10		10,300	0.055	+13.86	127.1	
LZBF-10B	1.15	−∞	900	10		10,500	0.18	−10.0	143.4	
LZDH-10C	1.15	−∞	900	10		9,376	0.18	− 9.24	141.4	
LYSJ-4A	2.0	0	900	10	0.029/500	1,318	0.8	+ 0.74	159.5	
LZBF-4B	2.0	0	900	10	0.024/550	1,210	0.8	+ 0.73	164.2	
WFTS-3	2.0	0	900	10	0.035/500	850	0.86	+ 0.72	160.7	
WFTS-2	2.0	0	900	10	0.042/500	1,055	0.84	− 0.28	159.0	
LZBF-7B	1.0	0	900	10		10,700	0.10	+13.4	132.4	
LZDH-9C	1.0	0	900	10		7,153	0.11	+13.5	127.5	
LULS-9	2.0	0	800	0.5[1]	0.032/700	1,483	0.8	− 5.0	179.6	0.02[2]
LYSJ-5A	2.0	0	800	0.5[1]	0.035/600	1,308	0.86	− 4.1	171.6	0.02[2]
LZBF-5B	2.0	0	800	0.5[1]	0.032/500	1,305	0.84	− 4.4	172.1	0.02[2]
LZDH-5C	2.0	0	800	0.5[1]	0.032/500	1,316	0.88	− 4.5	171.9	<0.02[2]
LYSJ-6A	2.0	0	900	0.5[1]	0.035/400	878	0.85	− 6.34	166.1	0.035[2]
LYSJ-11A	2.0	0	900	0.5[1]	0.045/450	722	0.92	− 7.42	166.6	0.06[2]
LSBF-6B	2.0	0	900	0.5[1]	0.040/350	620	0.84	− 6.71	177.1	0.06[2]
LZDH-6C	2.0	0	900	0.5[1]	0.035/500	784	0.88	− 6.76	167.8	0.08[2]

[1] Dwell cycle 2-minute

[2] $\Delta\epsilon_{IR}$ = Inelastic strain due to relaxation
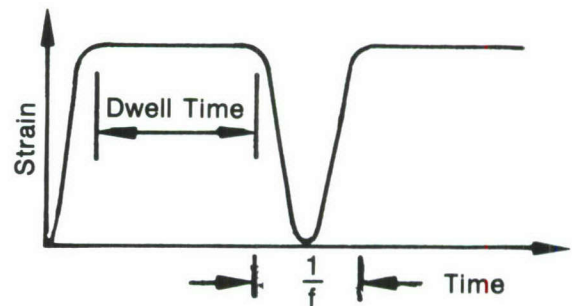
$\Delta\sigma$ = Total Stress Range
$\Delta\sigma_R$ = Relaxation Stress
$\Delta\epsilon_T$ = Total Strain Range
$\Delta\epsilon_P$ = Plastic Strain Range
$\Delta\epsilon_R$ = Inelastic Strain Due To Relaxation
f = Cyclic Frequency

Typical Nondwell Cycle
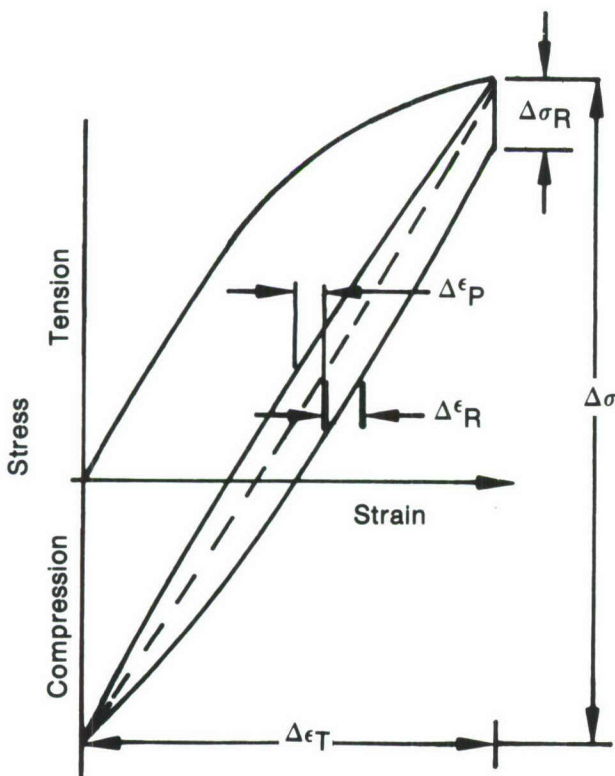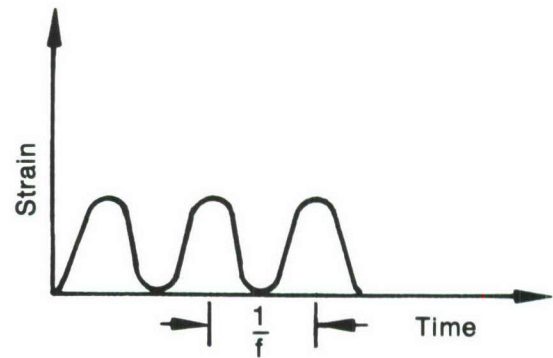
Typical Strain Dwell Cycle

FD 121078

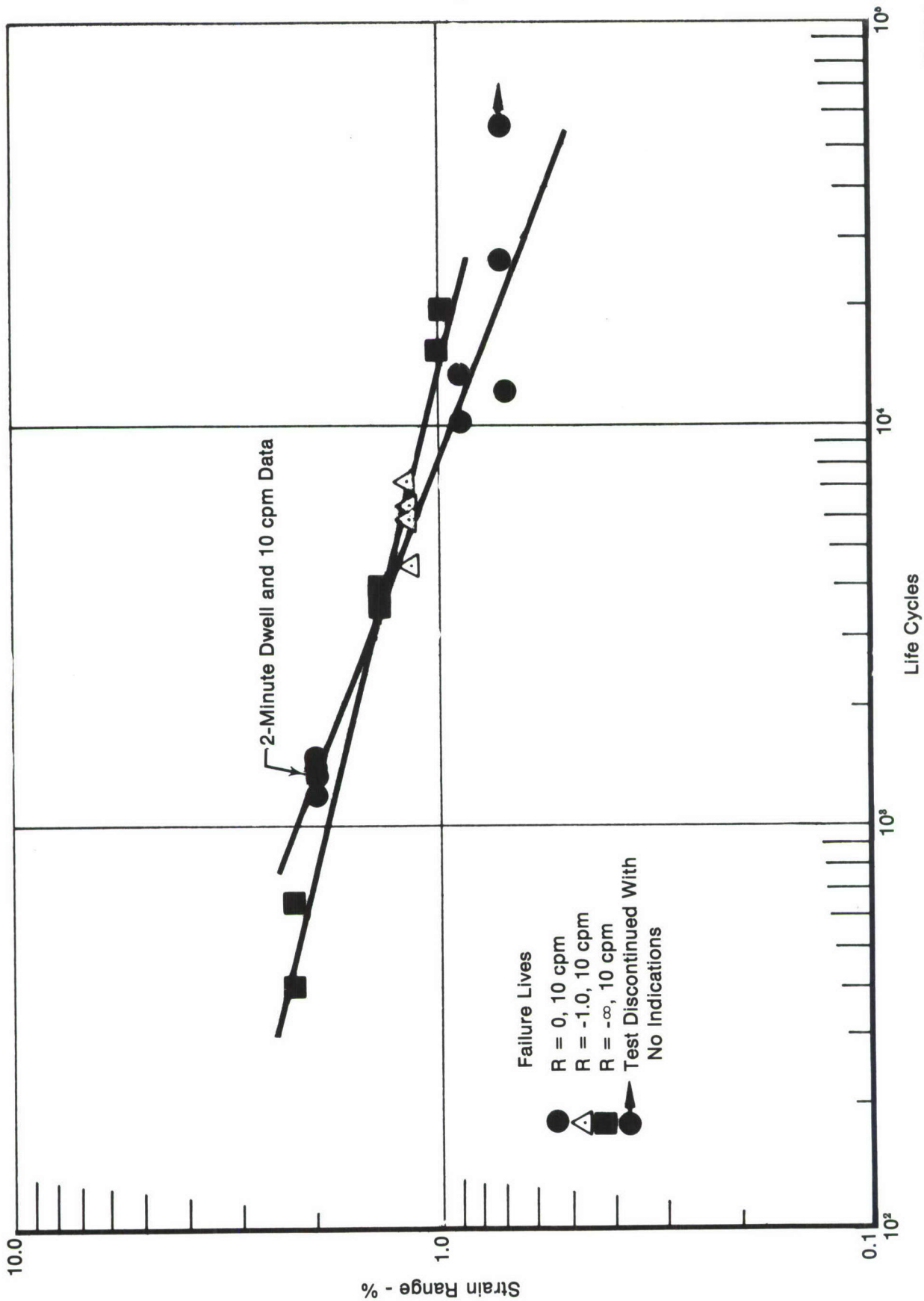*Figure 60. Waveforms and Resulting Hysteresis Plots for LCF Test with Mean Strain on One-Half Maximum Strain*

72

Figure 61. Low-Cycle Fatigue Life for Ti 8-1-1 Showing Effect of Mean Strain and Alternating Strain at 800°F (700°K)
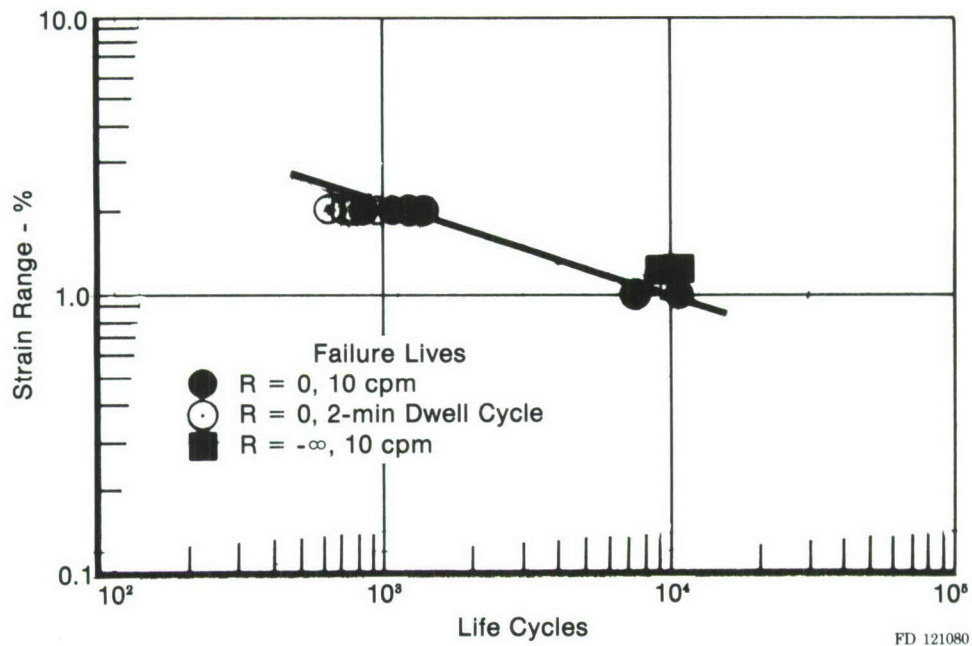
73

FD 121079

Figure 62. *Low-Cycle Fatigue Life for Ti 8-1-1 Showing the Effect of Mean Strain, Dwell, and Alternating Strain at 900°F (755°K)*
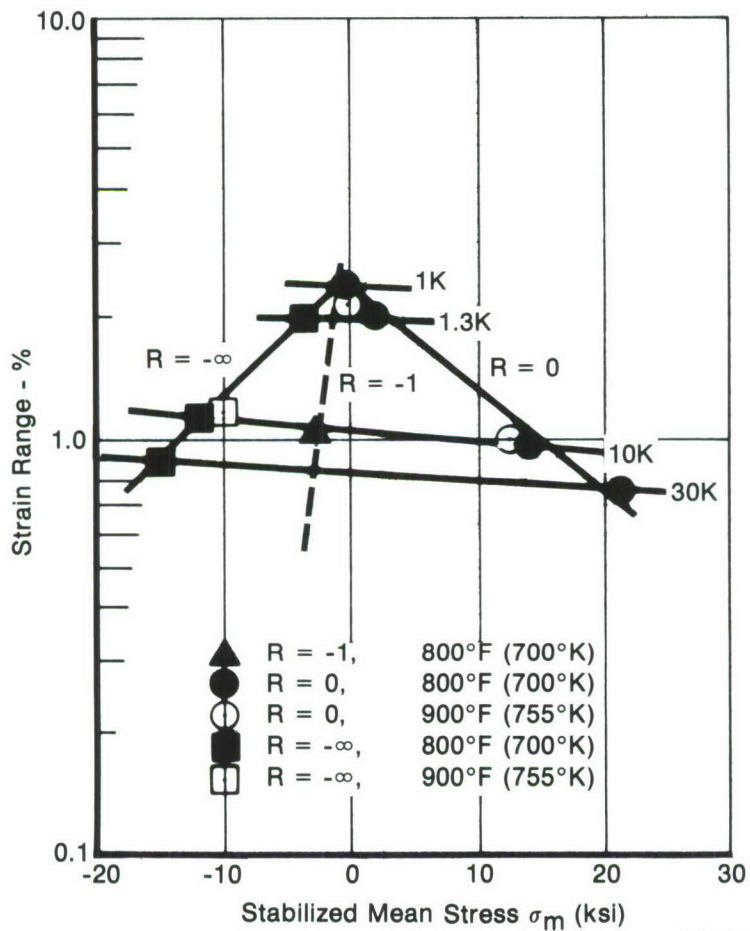

Figure 63. *Fatigue Life Curves for Different Strain Ratios (R), Constant Life Lines*
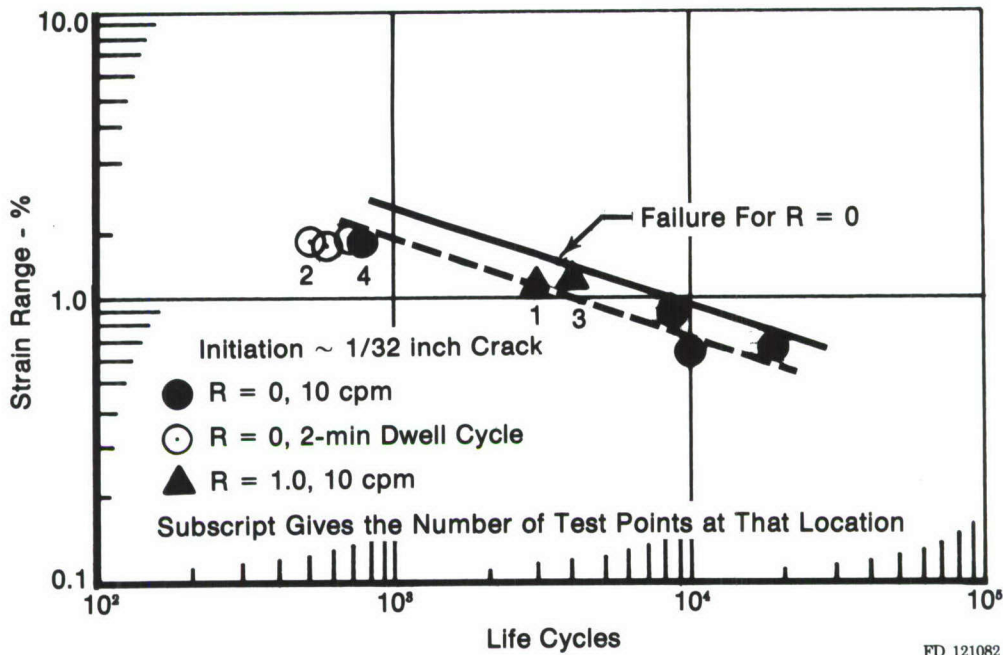
74

Figure 64. Low-Cycle Fatigue Life to Indication for Ti 8-1-1 Showing Effect of Mean Strain and Alternating Strain at 800°F (700°K)

The effect of alternating strain range on crack initiation is similar to that on failure and is shown in Figures 64 and 65 for 800 and 900°F (700 and 755°K) respectively. The initiation data, as given in Table 10, represents life to a crack length near 1/32 in. (0.0128 mm) or larger. Inspections made prior to the indicated life revealed no cracks 1/32 in. (0.0128 mm) or larger.

The 2-minute dwell cycle testing at 800°F (700°K) showed no decrease in life over the 10 cycle per minute data in Figure 61 and showed a small decrease in life to initiation in Figure 64. At 900°F (755°K) a decrease in failure life and initiation life is shown in Figures 62 and 65, respectively, due to the 2-minute dwell cycle. The mean stress in the dwell tests stabilized at a negative value due to the stress relaxation while the 10 cycle per minute test remained slightly positive.

Figures 66 and 67 show the Weibull analysis for tests conducted at a strain ratio of zero. Figure 66 shows the results for the three strain ranges tested at 800°F (700°K). Figure 67 shows a decrease in life with increasing temperature and a decrease in life with dwell time at 900°F (755°K) for tests run at 2.0% strain and a strain ratio of zero.

Figure 68 shows the stress history between tests run at three different strain ranges for a strain ratio of zero. Figure 69 is the same basic plot for a strain ratio of $-\infty$.
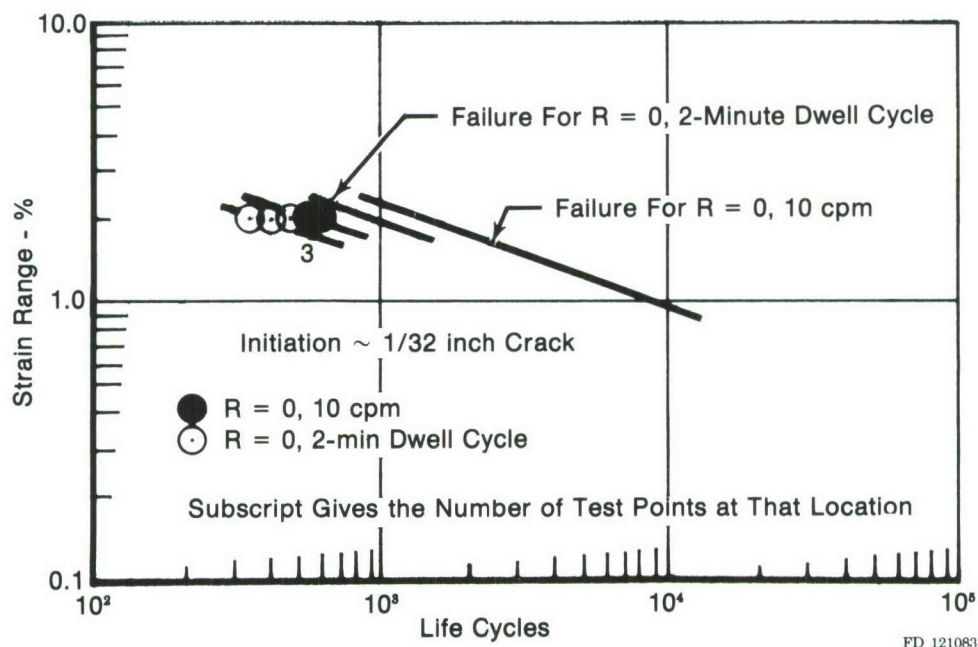
75

Figure 65. Low-Cycle Fatigue Life to Indication for Ti 8-1-1 Showing the Effect of Dwell Cycles at 900°F (755°K)
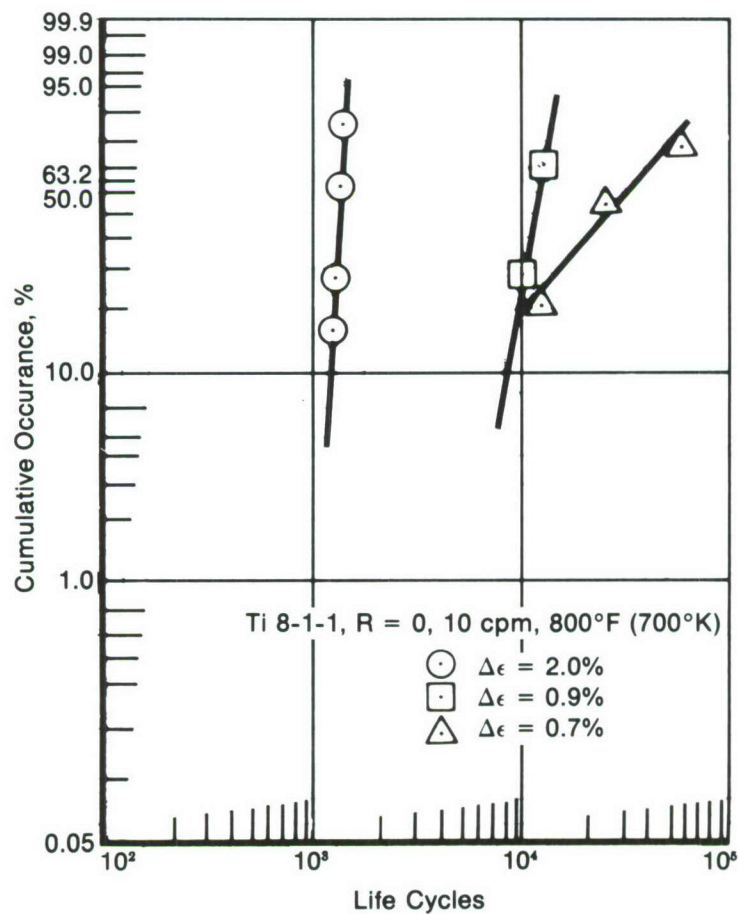

Figure 66. Weibull Distribution Analysis for Ti 8-1-1 LCF Data at 800°F, 10 cpm, Strain Ratio = 0
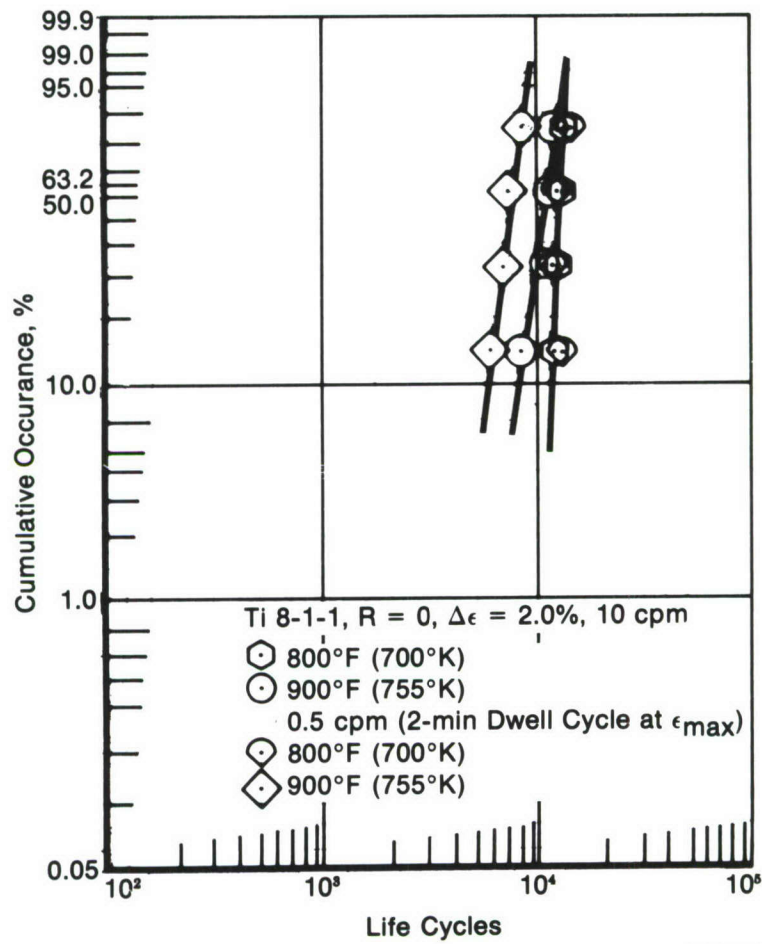
Figure 67. *Weibull Distribution Anaysis for Ti 8-1-1 LCF Data at Strain Ratio = 0*
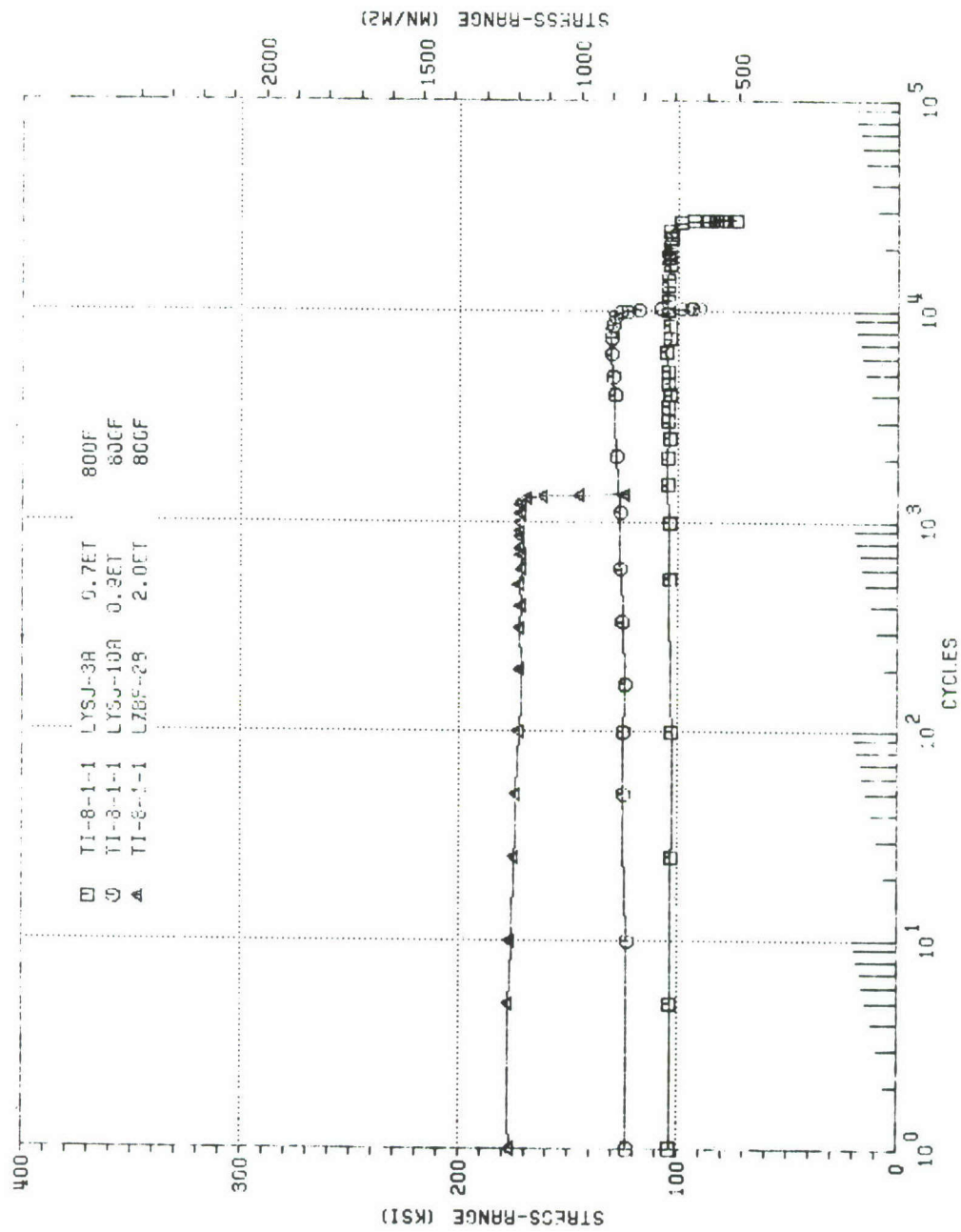
FD 121085

Figure 68. Stress Range vs Cycles to Failure for Ti 8-1-1, 800°F, Strain Ratio = 0
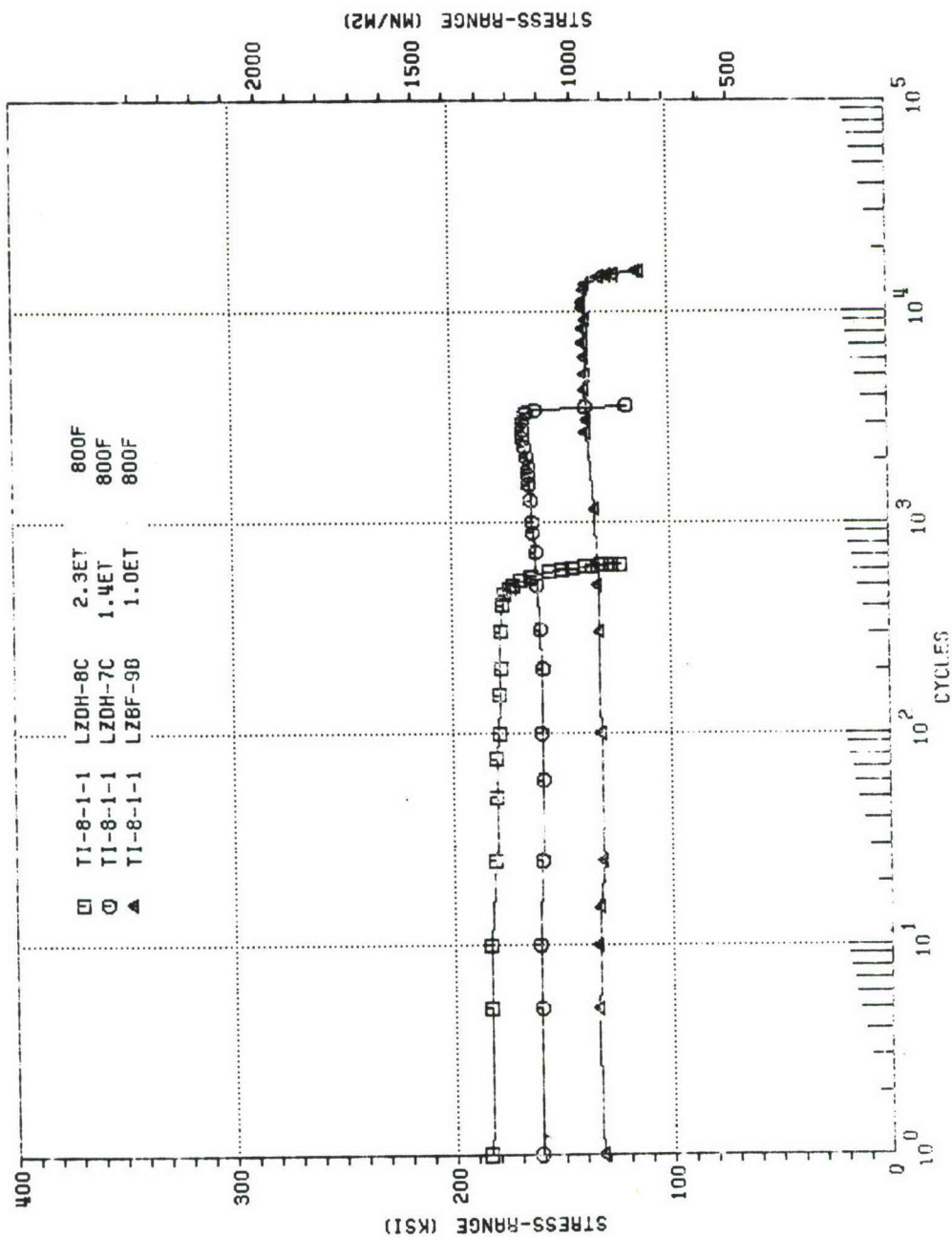
Figure 69. Stress Range vs Cycles to Failure for Ti 8-1-1, 800°F, Strain Ratio = $-\infty$

SECTION IV

CONCLUSIONS

Fracture mechanics properties for three titanium alloys, Ti 6-2-4-6, Ti 6-2-4-2, and Ti 8-1-1 were determined. Since mechanical, fatigue, and fracture properties of titanium alloys can be strong functions of microstructure, special attention should be given to Section II.

1. Basic tensile property characterization was completed. The Ti 6-2-4-6 alloy has the highest yield strength, lowest ductility, and an average modulus for the three alloys. Ti 6-2-4-2 alloy has the highest ductility, lowest yield strength, and lowest modulus. The Ti 8-1-1 alloy has the highest modulus, yield strength similar to Ti 6-2-4-2, and ductility slightly higher than Ti 6-2-4-6.

2. Stress intensity thresholds were determined on the three alloys. Ti 6-2-4-2 is superior at room temperature and Ti 8-1-1 is superior at 800°F (700°K), a common test temperature. All three alloys show a decrease in ΔK_{TH} with increasing stress ratio. Crack growth rates were determined in Region I following threshold evaluations. In general, lower crack growth rates were obtained at room temperature than at elevated temperature for each alloy. Net section creep occurred in several elevated temperature tests.

3. The effects of temperature, stress ratio, and cyclic frequency on fatigue crack propagation were established. Complicated possible mechanistic changes preclude straightforward qualitative conclusions. For example, crack growth rates can decrease at intermediate temperatures, 600°F (588°K) as compared to room temperature and 800°F+ (700°K+). In general, increases in stress ratio resulted in increased crack growth rates at equivalent ΔK's. The effects of cyclic frequency are complicated. Significant reductions in crack growth rates occurred in Region II for 1000 Hz as compared to 30 Hz+. Two-minute tensile dwells sometimes resulted in decreased growth rates possibly due to inelastic zone growth associated with creep at elevated temperatures.

4. Critical stress intensities (fracture toughnesses) were measured for three specimen thicknesses for each alloy. For Ti 8-1-1, K_c remains stable with increasing temperatures in the thin section while increasing substantially with temperature in the thick specimen. For Ti 6-2-4-2, K_c decreases with increasing temperatures in the thin sections and K_Q increases with temperature in the thick specimen. For Ti 6-2-4-6, K_c (K_Q) increases with temperature in all three thicknesses investigated.

5. Crack initiation was studied under strain-controlled conditions in Ti 8-1-1. Increases in strain range and a positive shifting of stabilized mean stress are shown to decrease fatigue life.

The data generated in this program have utilitarian value in a design life analysis to the extent they can be empirically modeled. A new interpolative model, based on the hyperbolic sine, has been developed under AFML contract F33615-75-C-5097. The effects of temperature, stress ratio, and cyclic frequency on crack propagation rate can be quantified. An example of the SINH model's ability to fit fatigue crack growth data as applied to Ti 6-2-4-6, is given in Figure 70.
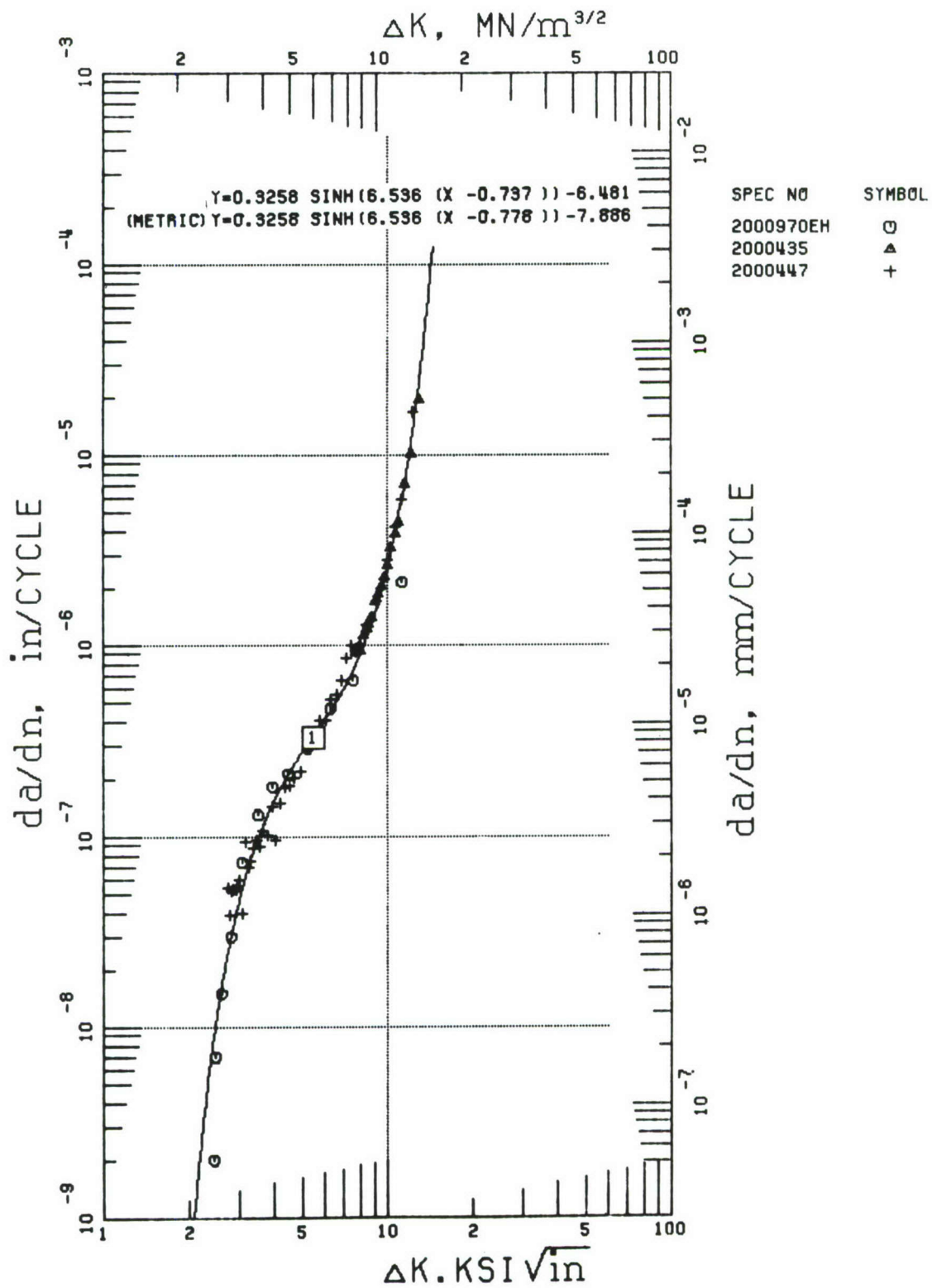
Figure 70. Sinh Model for Ti 6-2-4-6 Data

81

REFERENCES

1. Hudak, S. J. and R. J. Bucci, "Development of Standard Methods of Testing and Analyzing Fatigue Crack Growth Rate Data," Contract F33615-75-C-5064, First Semiannual Report, AFML, December 1975.

2. Erdogan F. and M. Ratwani, "Fatigue and Fracture of Cylindrical Shells Containing a Circumferential Crack," *International Journal of Fracture Mechanics,* Vol 6, No. 4, pp 379-392, December 1970

3. Yuen, A., S. W. Hopkins, G. R. Leverant, and C. A. Rau, "Correlations Between Fracture Surface Appearance and Fracture Mechanics Parameters for Stage II Fatigue Crack Propagation in Ti 6Al-4V," *Met. Trans.,* Vol 5, pp 1833-1842, 1974.

4. Wells, C. H., "Elevated Temperature Testing Methods," *Manual on Low-Cycle Fatigue Testing,* American Society for Testing and Materials, ASTM STP 465, pp 87-99, 1970.